Luby, James Craig

SIMULATION OF NONSTATIONARY MULTIBEAM SONAR REVERBERATION SEQUENCES

University of Washington PH.D. 1984

Simulation of Nonstationary Multibeam Sonar Reverberation Sequences

by

James Craig Luby

A dissertation submitted in partial fulfillment

of the requirements for the degree of

Doctor of Philosophy

University of Washington

1984

Approved by Dean W. Lytle

(Chairperson of Supervisory Committee)

Program Authorized
to Offer Degree ELECTRICAL ENGINEERING

Date 13 AUGUST 1984

Doctoral Dissertation

In presenting this dissertation in partial fullfillment of the requirements for the Doctoral degree at the University of Washington, I agree that the Library shall make its copies freely available for inspection. I further agree that extensive copying of this dissertation is allowable only for scholarly purposes, consistent with "fair use" as prescribed in the U.S. Copyright Law. Requests for copying or reproduction of this dissertation may be referred to University Microfilms, 300 North Zeeb Road, Ann Arbor, Michigan 48106, to whom the author has granted "the right to reproduce and sell (a) copies of the manuscript in microform and/or (b) printed copies of the manuscript made from microform."

Signature James C. Luby

Date August 13, 1984

University of Washington

Abstract

SIMULATION OF NONSTATIONARY MULTIBEAM SONAR REVERBERATION SEQUENCES

by James Craig Luby

Chairperson of the Supervisory Committee: Professor Dean W. Lytle
Department of Electrical Engineering

Modern sonar systems employ sophisticated signal processing methods. In order to verify system performance, data of the type expected in actual system operation is required. However, because of the prohibitively high cost of sea experiments, simulated data is often used. New methods of simulating nonstationary, Gaussian, multibeam sonar reverberation sequences are presented.

A continuous, first-order scattering model is used to relate sonar, environmental and geometrical factors to the reverberation power spectral density at a set of ranges. Then stationary, multibeam, correlated realizations of the reverberation are generated for each range by one of two methods. The two methods are called the Cholesky factor method and the autoregressive spectral factorization method. Primary emphasis is placed on the autoregressive method.

The Cholesky factor method involves factoring the power spectrum matrix at each of a set of frequencies spanning the sonar bandwidth. The resultant Cholesky factors are then used together with a random number generator to synthesize frequency domain realizations. Finally the fast Fourier transform(FFT) is used to recover the time domain realizations from the frequency domain realizations.

The autoregressive method is based on the fact that autoregressive models provide an approximate canonical factorization of the reverberation power spectrum. Regardless of the method used the next step is to window, overlap and add the stationary sequences from different ranges together. This yields a time series with time varying spectrum as is appropriate for reverberation. The final step is to apply a range(time) varying scaling to adjust the time varying mean square power of the time series.

Table of Contents

List of Figures

List of Tables

Acknowledgements

I would like to express gratitude to my commitee members and to other people who have contributed to the work presented in this dissertation. Special thanks is due my advisor, Professor Dean W. Lytle, for his guidance, encouragement and patience throughout my studies.

Also I would like to thank the University of Washington Applied Physics Laboratory staff for providing me with the financial and technical backing neccessary to undertake this work. In particular, the technical assistance provided by Dr. David W. Princehouse, Dr. Donald B. Percival, Robert T. Miyamota, the library staff and the publications department is much appreciated.

CHAPTER 1

Introduction

1.1. Introduction to Chapter 1

Recent years have brought quantum improvements in the areas of electronics, computers and signal processing theory. These improvements have in turn yielded sonar systems of ever increasing sophistication. As each new generation of sonar equipment is developed there arises the need to test the systems to ascertain actual versus predicted performance. It is in this arena, namely performance testing, that sonar signal simulation becomes important.

Sonar systems use acoustic radiation(i.e., sound pressure waves) to probe the ocean. After emitting an acoustic pulse into the ocean, a sonar system records the signals received back from the medium(i.e., the ocean) and by processing these signals attempts to infer something about the scattering structure of the medium.

When a sonar system transmits a pulse of acoustic energy into the ocean the pulse propagates outward. As the outgoing pulse encounters discontinuities in the medium acoustic impedance a certain amount of the pulse energy is reflected back towards the sonar. This reflected energy is called a "desired signal" if it reflected from an object which we are trying to locate or image with the sonar. If the reflected energy is not from the object we are trying to locate then it is considered to be an interfering noise and is called

reverberation. The three major sources of reverberation noise are from the ocean surface, bottom and volume. This dissertation is concerned with methods of modeling and simulating these three types of reverberation.

Besides the "desired signal" and reverberation other signals commonly encountered in sonar systems include ambient noise of the sea, electrical noise generated in the sonar processing electronics and flow noise resulting from the vehicle movement through the water. Reverberation differs from these latter noise types in that it is directly related to the type of signal which was transmitted(i.e., it is composed of reflected versions of the transmit pulse). The "desired signal" is also related to the transmit pulse. This fact makes reverberation a particularly difficult noise source to deal with in terms of filtering for improvement in the ratio of "desired signal" to reverberation noise.

In general the more sophisticated a sonar sytem becomes the more data required to validate its predicted performance. Ideally unlimited data of the type expected in actual sonar system operation would be available from actual "at sea" data collection expeditions. Oftentimes the cost of such expeditions precludes the gathering of requisite "at sea" data and instead computer simulated data is used for validation of system performance. This simulated data is often used in a Monte Carlo fashion to determine statistical performance bounds on the sonar detection/estimation processes.

This dissertation presents new methods of simulating nonstationary reverberation sequences for multibeam(i.e., multichannel) sonar systems. We use a continuous integral first order scattering model to compute the reverberation power spectrum with the assumption that infinitely many scatterers

contribute to the return at any time. In light of the central limit theorem[Parzen] this assumption implies that the reverberation is Gaussian.

Nonstationary reverberation is simulated by first simulating short time segments of stationary reverberation at a set of ranges which span the range interval of interest and then combining the segments with overlapping windows. The stationary segments are generated for each range by factoring the assumed quasistationary reverberation power spectrum with either autoregressive models or a method developed here termed Cholesky factorization. We emphasize the autoregressive method. We then use the spectrum factors together with a Gaussian white noise generator to realize the stationary segments. Finally, the segments are merged with the overlapped windows and a time(range) varying power scaling is applied.

1.2. Sonar Background Information

1.2.1. The Medium

The sea is an extremely complex propagation medium. Temperature and salinity gradients existing in the sea cause changes in the sound propagation velocity as a function of depth. This causes acoustic waves to follow generally curved paths. Randomly located scattering objects and the sea boundaries cause the sonar signals to be scattered and reflected in many different directions. Random motion of the scattering objects cause the scattered signals to experience time dilation/contraction effects(i.e., the doppler effect).

From a communications engineering perspective the sea may be viewed as a randomly time varying dispersive channel[Kennedy, Bello]. The sonar transmits an acoustic pulse which is the input to the channel. As the signal

travels through the channel it undergoes dispersion or spreading in both time and frequency.

Time dispersion or spreading refers to the phenomenon wherein the channel input becomes lengthened in time due to passage through the channel. In sonar systems this lengthening is primarily due to two phenomena. One, signals may propagate to any given scatterer over many different paths of unequal travel time(i.e., multipath) leading to a received signal spread over a longer time interval than the transmit signal. Two, the fact that scatterers are distributed throughout some range interval causes reflected versions of the transmit pulse to return to the sonar over a time interval proportional to the extent of scatterers in range.

Frequency dispersion or spreading is due to the fact that the scatterers have reflective properties which vary randomly with time. This random temporal variation in scatterer reflectivivity in turn modulates the signal incident on the scatterer. That is , the signal which has been scattered is a modulated version of the signal which was incident. This modulation manifests itself as a spreading of the power spectrum of the incident signal. This is termed frequency dispersion.

Since the sea is a randomly fluctuating dynamic system of scatterers it is possible to specify only statistical properties of the time and frequency dispersion of the channel. A useful characterization of the channel dispersion is provided by the channel scattering function. The scattering function is a second order statistical measure of the channel dispersion. The scattering function approach to channel description is discussed in detail in [Van Trees(1971), Ziomek]. For the present discussion suffice to say that the

randomly fluctuating nature of the sea acoustic channel directly influences the statistics of sonar signals. Hence any model developed to describe sonar signals must account for these channel characteristics.

1.2.2. Sonar Signals

Sonar systems utilize transducers of various types[Urick] to convert electrical signals to acoustic pressure and vice versa. Usually these transducers are efficient over a relatively small band of frequencies centered about some carrier frequency. The choice of a carrier frequency is based upon considerations such as frequency dependent absorption of sound in the sea, beampatterns(to be discussed) and the ambient noise spectrum. Once the carrier frequency is chosen and the transducer is designed the band of frequencies which can be efficiently converted with the transducer is fixed. All signals transmitted or received by the sonar have bandwidths limited by the transducer bandwidth.

In many current sonar systems the signal bandwidth, say BW, is small(less than 10%) compared to the carrier frequency f_c. This type of signal is termed narrowband. Narrowband signals as a function of time appear as sinusoidal oscillations at the carrier frequency with slowly varying (with respect to f_c) amplitude and phase modulations. A narrowband signal, say $x(t)$, admits the following representation

$$\begin{aligned} x(t) &= e(t)\cos[2\pi f_c t + \Phi(t)] \\ &= a(t)\cos(2\pi f_c t) + b(t)\sin(2\pi f_c t) \end{aligned} \tag{1.1}$$

where $e(t)$ and $\Phi(t)$ denote slowly varying amplitude and phase modulation functions and

$$e(t) = (a^2(t) + b^2(t))^{1/2} \tag{1.2a}$$

$$\Phi(t) = \tan^{-1}\left[\frac{b(t)}{a(t)}\right] \tag{1.2b}$$

The carrier frequency f_c is a known constant in actual sonar operation and hence the functions $e(t)$ and $\Phi(t)$ or equivalently $a(t)$ and $b(t)$ contain all the essential information in the signal $x(t)$. The functions $e(t)$ and $\Phi(t)$ are usually referred to as the signal envelope and phase, respectively. The functions $a(t)$ and $b(t)$ are usually called the in-phase and quadrature components, respectively, of the narrowband signal.

The flexibility of digital processing has made it highly advantageous for sonar systems to sample and store signals digitally. The usual sampling theorem statement specifies that the digital sampling rate(number of samples per second) exceed twice the highest frequency component of the signal being sampled. However, a careful look at the sampling problem reveals that what is really needed is that we sample at a rate commensurate with the bandwidth of the signal[Tretter]. In particular, for narrowband signals this means that the sampling rate is essentially independent of the carrier frequency and depends only upon the actual signal bandwidth or spread about the carrier frequency.

The signal bandwidth of the narrowband signal $x(t)$ is determined by $e(t)$ and $\Phi(t)$ or equivalently $a(t)$ and $b(t)$.

Consider a narrowband signal $x(t)$ with the power spectrum shown in figure 1-1a. Define the complex envelope $\tilde{x}(t)$ of the narrowband signal $x(t)$ as follows:

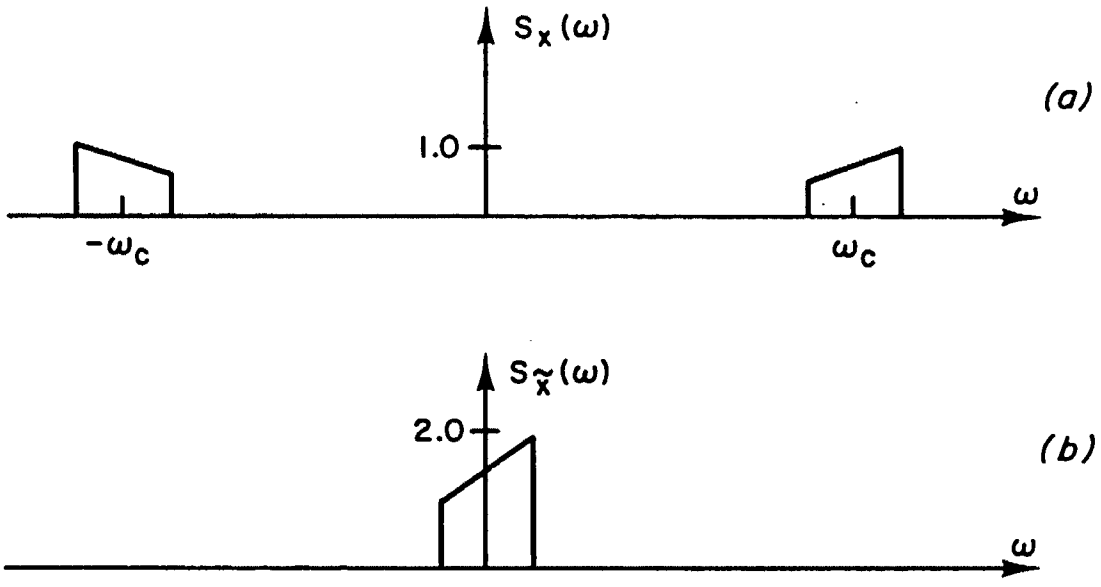

Figure 1-1) Spectra of Narrowband Signal and Complex Envelope

$$x(t) = a(t)\cos(2\pi f_c t) + b(t)\sin(2\pi f_c t)$$
$$= \mathrm{Re}\left[(a(t) - jb(t)) e^{j2\pi f_c t} \right]$$
$$= \mathrm{Re}\left[\tilde{x}(t) e^{j2\pi f_c t} \right] \qquad (1.3)$$

A tilde is used throughout this dissertation to denote the complex envelope of a time function.

The power spectrum of $\tilde{x}(t)$ is shown in figure 1-1b. Note that $\tilde{x}(t)$ is a generally complex baseband signal with spectrum which is identical to the positive frequency part of the spectrum of $x(t)$ except centered at zero frequency. Appealing to the usual sampling results the signal $\tilde{x}(t)$ need only be sampled at a sampling rate greater than or equal to twice $(BW/2)$. Hereafter we assume that all signals are sampled at the minimum permissible rate of BW complex samples per second.

Observe that if the signal $x(t)$ had been sampled directly at a high carrier frequency(i.e., $f_c \gg BW$) it would require a real sample rate in excess of $2\times[BW/2 + f_c]$. This leads to excessive data throughput and storage requirements.

The signal representation just presented is called the complex envelope representation[Van Trees(1971)]. Methods of sampling a narrowband signal to get samples of the associated complex envelope are sometimes referred to as quadrature sampling methods and are discussed in [Grace and Pitt]. The complex envelope representation may also be used to represent bandpass random processes. Bandpass random processes are random processes with power spectra concentrated in a small region of the frequency spectrum about some carrier frequency. The complex envelope of a bandpass process

$x(t)$ is also defined by 1.3 and the same sampling considerations apply as for deterministic signals. In appendix A we discuss further the complex envelope representation of bandpass processes.

This dissertation deals almost exclusively with the complex envelope of sonar signals. In particular, reverberation simulation refers to simulation of realizations of the complex envelope of reverberation. Note that the carrier frequency is important in reverberation modeling because frequency dispersion and sound absorption depend on the carrier frequency.

Sonar systems use many different types of signals to probe the ocean. The type of signal chosen at any given instant of sonar operation depends on the particular usage of the sonar at that instant. Important issues in transmit pulse choice include pulse energy, range resolution and doppler resolution.

For purposes of discussion assume the transmit pulse complex envelope is denoted as $\tilde{p}(t)$. The pulse energy is defined as

$$E = \int_{-\infty}^{+\infty} |\tilde{p}(t)|^2 dt \tag{1.4}$$

Pulse energy is an important issue in sonar system design because it places an upper bound on the detection range of a given target in an ambient noise background.

The range resolution of a sonar is the minimum separation in range between two targets which can just be discerned by the sonar. The most obvious way to get good range resolution is to transmit a very short pulse. This is because, assuming a perfect propagation medium, as long as the range spanned by the pulse in the water is less than the separation between targets

the targets will be resolvable in range. That is, the return signal will show two distinct pulses corresponding to the two targets.

A problem with short pulses however is that due to peak power constraints on the transducers(due to power supply limitations and cavitation limitations) the energy of a short pulse may be too low to allow long range detection in ambient noise limited conditions. Nevertheless short pulses are often used in sonars for accurately estimating the range to nearby targets where ambient noise is not a problem. The most common short pulse encountered in sonar systems is often referred to as a pure tone short(PTS) pulse and it is simply a short segment of pure tone oscillations at the carrier frequency.

Another way to obtain good range resolution is to use a large time-bandwidth pulse along with pulse compression processing in the receiver[Cook and Bernfield]. This type of signal is made long in time to keep pulse energy high yet when processed with a pulse compression receiver the pulse becomes compressed to a shorter duration thus restoring good range resolution. One example of this type of pulse is the linear frequency modulated(LFM) pulse. In general, range resolution is inversely proportional to the pulse bandwidth.

The doppler resolution of a sonar is the minimum difference in doppler frequency between two targets which is just discernable by the sonar. The doppler frequency of a target is related to the target velocity by the expression

$$f_d = \frac{2Vf_c}{C} \tag{1.5}$$

where f_c is the carrier frequency, C is the sound propagation velocity, V is the relative radial velocity between the sonar and the target and the factor 2 comes about due to the two way signal travel. Thus doppler resolution is equivalent to velocity resolution and is measured by examining the mean spectral shift of the spectrum of the signal received from the target.

To obtain good doppler resolution a pulse is needed which has a narrow spectrum. This is so that spectral analysis of the signal returned from two targets at the same range but with different velocities will show two distinct spectral peaks centered at the doppler frequencies corresponding to the target velocities. One obvious choice is a pure tone long(PTL) pulse. The spectrum of a PTL pulse can be made arbitrarily narrow by making the pulse arbitrarily long. In practice the pulse length is limited by the fact that the power of the reverberation signal which inevitablely accompanies the desired target return increases directly with pulse length. In general, doppler resolution is inversely proportional to the pulse duration.

It should be noted that there are other issues involved in transmit pulse choice besides those previously mentioned. In particular, the target signal to reverberation noise ratio is directly influenced by the transmit pulse choice as alluded to in the previous paragraph. This target signal to reverberation noise ratio depends on the scattering function of the reverberant channel, the joint time/frequency properties of the transmit pulse as specified by the pulse ambiguity function and the target velocity relative to the reverberant scatterer velocities. These issues are complex and are well covered in [Moose, Van Trees(1971), Baggoerer, Ziomek].

In this dissertation three types of transmit pulses are considered: pure tone long(PTL), pure tone short(PTS) and linear frequency modulated(LFM). These pulses are representative of the multitude of possible pulses used in sonar systems. The equations describing the complex envelopes of each of these pulse types are:

$$PTS \qquad \tilde{x}(t) = \begin{cases} 1 & 0 \le t \le T_1 \\ 0 & elsewhere \end{cases} \tag{1.6a}$$

$$PTL \qquad \tilde{x}(t) = \begin{cases} 1 & 0 \le t \le T_2 \\ 0 & elsewhere \end{cases} \tag{1.6b}$$

$$LFM \qquad \tilde{x}(t) = \begin{cases} e^{j2\pi\mu t^2/2} & 0 \le t \le T_3 \\ 0 & elsewhere \end{cases} \tag{1.6c}$$

In 1.6 we have $T_2 \gg T_1$ and μ is the LFM frequency sweep rate in (cycles/second/second). The approximate bandwidth of each pulse type is T_1^{-1} for the PTS, T_2^{-1} for the PTL, and μT_3 for the LFM.

It should be noted that transmit pulses may be windowed or shaded to reduce spectral sidelobes. Typical shading functions used are drawn from the class of functions commonly used as windows in spectral analyis. That is, they tend to be real functions with range [0.,1.] which go smoothly to zero at the edges of the window and which have spectra with a fairly narrow main lobe and low sidelobes.

Shading is usually applied to the PTL type pulses(i.e.,pulses used for doppler resolution) to prevent a sidelobe from the doppler spectrum of a strong target from masking the main spectral lobe of another weaker target which happens to have a doppler shift corresponding to the frequency of the sidelobe of the spectrum of the stronger target. The problem of detecting

multiple targets of different velocities is a special case of the spectral analysis problem of resolving closely spaced narrowband signals. Consequently many of the ideas from spectral estimation, such as data windowing, apply to the doppler resolution problem. In our examples we weight the PTL pulse with a Taylor weighting function[Harris] which has spectral sidelobes 50db down from the main lobe.

1.2.3. Beampatterns

Modern sonars utilize a combination of temporal and spatial filtering to enhance signal to noise ratio. The spatial filtering is usually referred to as beamforming. Beamforming refers to the techniques wherein the transmitting/receiving directionality characteristics of the sonar are adjusted so as to form a "beam" which probes only a desired region of the ocean(i.e., to filter out signals arriving from spatial regions of the ocean which are not of interest).

The physical interface between the sonar system and the medium is often referred to as the transducer face. The transducer face may consist of a single transducer of it may consist of multiple transducers working in combination. The latter configuration is called a transducer array. A derivation of the far-field, narrowband beampattern for both a single transducer and a transducer array is presented in [Burdic]. The narrowband beampattern assumption is that the beampatterns are insensitive to small frequency deviations about the carrier frequency. This assumption is valid provided that $BW \ll \frac{C}{D}$ where D is the maximum dimension of the transducer face. This condition is often met in practice.

It should be noted that an array of transducers may be used to form simultaneous multiple beams. That is, by forming appropriate combinations of the individual array transducers several different beams may be formed. These beams may or may not "look" into the same spatial region of the medium. In addition the system may form different beams for pulse transmission than those used for signal reception.

Several important issues regarding beampatterns are array gain, spatial localization of sound sources and beam to beam correlation. Array gain refers to the gain in signal to noise ration effected by using directional beams over that signal to noise ratio which would be observed using omnidirectional beams in the same signal and noise fields.

Consider a sonar array which is placed in signal and noise fields which are characterized by the functions $S(\theta,\varphi)$ and $N(\theta,\varphi)$, respectively. The functions $S(\theta,\varphi)$ and $N(\theta,\varphi)$ specify the amount of signal and noise power incident on the array per unit solid angle. Assume that the sonar array has a beampattern $b(\theta,\varphi)$ and denote an omnidirectional beampattern as $b_0(\theta,\varphi)$ where $b_0(\theta,\varphi)=1$ for all (θ,φ). With these definitions the array gain can be written as

$$AG=10\log_{10}\left[\frac{\int_{4\pi}S(\theta,\varphi)b(\theta,\varphi)d\Omega \,/\, \int_{4\pi}N(\theta,\varphi)b(\theta,\varphi)d\Omega}{\int_{4\pi}S(\theta,\varphi)b_0(\theta,\varphi)d\Omega \,/\, \int_{4\pi}N(\theta,\varphi)b_0(\theta,\varphi)d\Omega}\right] \tag{1.7}$$

where the integrations are performed over all solid angles(i.e., over 4π steradians). The denominator of the bracketed expression in 1.7 is seen to be the signal to noise ratio for the omnidirectional beam. The numerator is the sig-

nal to noise ratio for the beampattern $b(\theta,\varphi)$.

From 1.7 it can be seen that the array gain depends on the specific directionality characteristics of the signal and noise fields as well as on the beampattern. If the signal and noise arrive from the same spatial direction then spatial filtering is ineffective and the array gain is 0 db. Conversely if the noise and signal arrive from distinct spatial directions then the beampattern may increase the signal to noise ratio.

In particular, ambient noise fields observed in the ocean often impinge on the sonar array from a large number of directions(i.e., $N(\theta,\varphi)$ is angularly broad). Desired signals however are often characterized by power directionality factors $S(\theta,\varphi)$ which are angularly narrow. This situation can lead to an appreciable array gain.

The second beampattern related issue of interest is spatial localization of sound sources. Figure 1-2 depicts a sonar system with two beams which "look" into different regions of the medium. It is clear from this figure that the arrival of a backscattered return from a target in beam 1 and not in beam 2 is sufficient to localize the direction of the target at least approximately. The narrower beam 1 is the better localized is the sound source or target. Note that the system could be configured to form one broad transmit beam and several narrow receive beams to effect spatial discrimination.

In practice constraints on the choice of carrier frequency and on transducer face dimensions place limitations on the number and widths of spatially nonoverlapping beams which can be formed. This in turn constrains the accuracy of directional localization achievable by this method. However once a

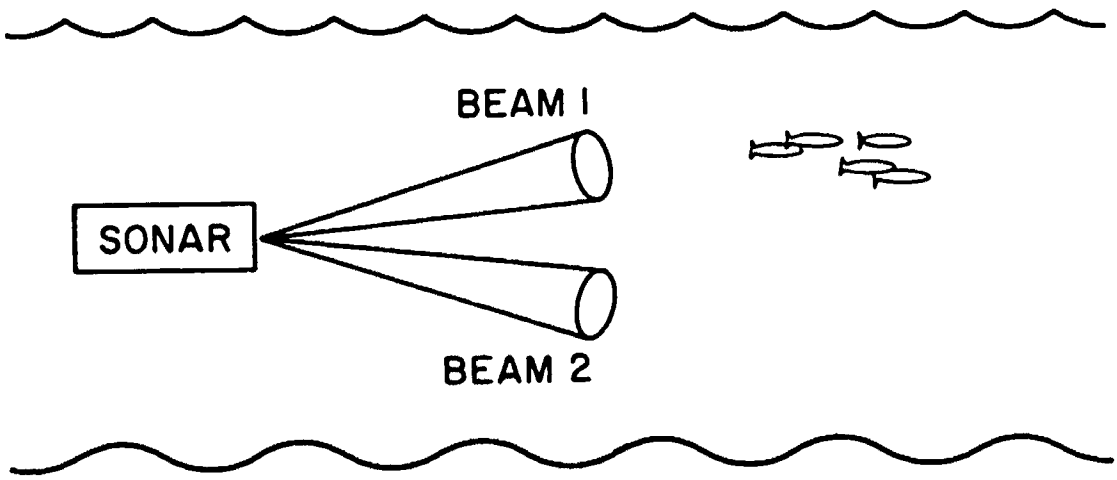

Figure 1-2) Beampattern Spatial Localization

target is detected in one of the beams the sonar can reconfigure its beampatterns to probe that area of the ocean with greater resolution.

The location of an acoustic target is specified by the target range and angles θ and φ. The range is determinable from measurement of the round trip travel time of signals propagating from the sonar to the target and back to the sonar. In order to accurately estimate the target angles so called offset phase centered beams are often used.

Figure 1-3 shows a typical offset phase centered system for measuring the elevation angle θ . In this case the two beams are formed from sets of individual transducers which have different physical locations(vertically) on the transducer face. Generally the beams have the same beampattern. Because of the phase center seperation the narrowband signals received in each beam from a scatterer at any elevation angle θ will have a well defined electrical phase difference which is proportional to $\sin\theta$. If the vertical center of the transducer face is chosen as the reference point for phase measurement then the signal in the top beam leads the reference phase and the signal in the bottom beam lags the reference phase.

Assume that a sinusoidal signal $e^{j2\pi f_c t}$ is transmitted at the carrier frequency f_c. Neglecting the phase delay and transmission losses incurred due to the round trip travel time of the signal the signals received in the top and bottom beams are given by $e^{j2\pi f_c[t+\Delta]}$ and $e^{j2\pi f_c[t-\Delta]}$, respectively. The time delay Δ corresponds to the time it takes a signal to propagate a distance $\delta R = \frac{d}{2}\sin\theta$. That is

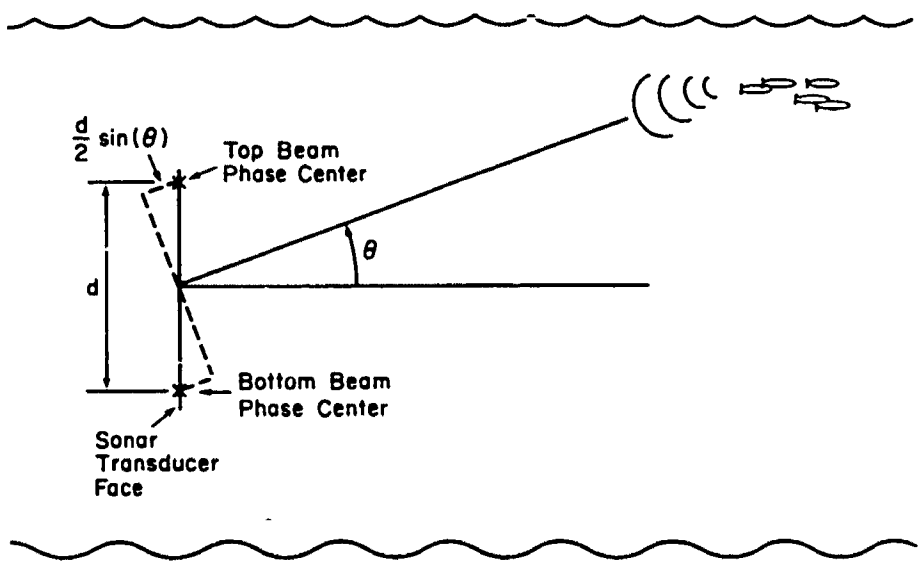

Figure 1-3) Typical Offset Phase Centered System

$$\Delta = \frac{\delta R}{C} = \frac{d\sin\theta}{2C} \tag{1.8}$$

If these signals are input to an electrical phase detector an estimate, say $\hat{\beta}$, of the electrical phase between beams signals is obtained. The estimated elevation angle $\hat{\theta}$ is related to the carrier frequency f_c, electrical phase estimate $\hat{\beta}$ and beam phase center separation d as follows:

$$\hat{\theta} = \sin^{-1}\left[\frac{C\hat{\beta}}{2\pi f_c d}\right] \tag{1.9}$$

Note that estimates of the bearing angle to the scatterers can be made by using offset phase centered beams offset in the horizontal instead of the vertical.

The third beampattern issue of interest is beam to beam correlation. Oftentimes sonars will have two or more beams which have overlapping beampatterns. The overlap may be intentional or may be the result of undesireable sidelobes from a given beam overlapping another beampattern. Whatever the case, the two beampatterns "see" a common region of scatterers and hence the signals received in the beams will be statistically correlated. The magnitude of the crosscorrelation depends on the degree of beampattern overlap, the dispersive properties of of the medium and the spatial separation between receivers. The important point here is that the signals in the two beams are correlated due to receiving returns from a common group of reverberant scatterers.

In terms of reverberation modeling and simulation the fact the the signals in different beams are correlated has several implications. One, the model for reverberation must yield correct information regarding joint random processes. That is, the model must deal with the signals received from

all beams simultaneously as a vector random process. Two, the simulation process must also be capable of generating vector random process realizations with correct auto- and cross-statistical properties.

1.3. Simulation Issues

A particularly intuitive and useful model for ocean reverberation is the point scatterer model(PSM) to be discussed in detail in chapter 2. Briefly, the PSM models reverberation as the sum of backscattered returns from point scatterers distributed randomly and densely over the scattering region. The PSM is well suited to digital computer reverberation simulation[Princehouse] because of the inherent discrete nature of the model(i.e., points in space).

Each point scatterer is assumed to reradiate a potentially doppler shifted copy of the sonar transmit pulse with time delay appropriate to scatterer range. The density of scatterers in the medium is chosen large enough to prevent a sonar signal processor from resolving the individual point scattered returns. The trend in sonar sytems has been towards using transmit pulses with ever increasing resolution. For PSM reverberation simulations this means an ever increasing density of scatterers and hence ever increasing computational load.

In the limit of an infinitely large number of scatterers the PSM reverberation return becomes a zero mean Gaussian random process in view of central limit theorem[Papoulis(1965)] considerations. In this case a sonar signal processor cannot resolve individual point scatterers using any finite resolution pulse. This dissertation is concerned with simulation of this limiting form of reverberation for multiple beam sonar systems.

The infinite point scatterer density leads naturally to a continuous integral scattering model. Such a continuous scattering model is developed in Chapter 2 and is used to compute multibeam auto- and crosspower spectra and associated correlation functions. Under the Gaussian assumption the matrix correlation function or associated matrix spectral density function is sufficient to completely specify the multivariate(i.e., multiple beams) probability density.

As an intermediate step, the simulation method developed in this dissertation generate stationary, multibeam, complex reverberation sequences for each of a set of fixed ranges which span the desired range interval. A total reverberation return(i.e., ping) is produced by windowing, overlapping and adding these stationary realizations. This technique produces multibeam Gaussian reverberation which has intensity and spectral character which vary with time(range).

Chamberlain (1983) has developed a simulation called REVSIM which also generates Gaussian reverberation. In REVSIM the stationary realizations are generated by driving noise shaping autoregressive filters, one for each beam, with a common white noise sequence. The REVSIM simulation does not control beam to beam correlation correctly except for a few particular sonar configurations. However, REVSIM is quite useful in situations where one is not concerned about beam to beam correlation. Furthermore REVSIM provided motivation for us to pursue the study of multivariate autoregressive filters for simulation of reverberation with the correct correlation between beam signals.

The problem with generating random process realizations with a desired power spectrum or covariance function is known in the literature as the spectral or covariance factorization problem[Anderson and Moore]. The spectral factorization problem is basically to find a realizeable filter which when driven by white noise generates an output sequence which has the desired power spectrum.

This dissertation discusses two methods for spectrally factoring the reverberation power spectrum. The first, Cholesky factorization, directly factors the power spectral matrices at a set of frequencies which span the processor bandwidth. The second method, and the one in which we are most interested, involves fitting multivariate complex autoregressive(AR) models to the covariance sequence specified by the reverberation power spectrum. Both of these methods are discussed in Chapter 3 with emphasis on the AR method. Finally, since the simulation technique is based on a continuous scattering model no scatterers exist to be resolved by a sonar signal processor. Hence the simulation computational load is not so directly governed by the pulse resolution as is the case with point scatterer simulations.

1.4. Dissertation Preview

Important issues concerning reverberation modeling are discussed in Chapter 2. This discussion includes the point scatterer model(PSM), development of a continuous first order scattering model, reverberation as a process reducible to stationary and reverberation as a Gaussian (i.e., normal) random process.

Chapter 3 presents the basic theory of complex multivariate Gaussian processes and spectral factorization. Both Cholesky factorization and AR modeling are discussed with emphasis on the AR method.

Chapter 4 is devoted to the development of a methodology for simulating reverberation. The reverberation is assumed to be normally distributed and quasistationary. Nonstationary reverberation is simulated by first simulating short time segments of stationary reverberation at a set of ranges and then combining the realizations with overlapping windows.

In Chapter 4 we also present simulation experiment results. The experiments show that the simulation methods developed here generate normal, nonstationary, multibeam reverberation sequences which have the desired spectrum. Examples illustrate the effects of different transmit pulses, geometry, environmental factors and beampatterns on the reverberation process.

Finally, Chapter 5 presents conclusions and future work recommendations. An appendix is included which discusses representation of bandpass random processes in the complex envelope notation.

CHAPTER 2

Characterization of the Reverberation Stochastic Process

2.1. Introduction to Chapter 2

Reverberation is a stochastic wave scattering process observed at a sonar receiver following transmission of an acoustic signal into the ocean. It is due to sound scattering by medium inhomogeneities such as fish, air bubbles, temperature gradients, boundaries or anything else which causes an abrupt change in the medium index of refraction. Reverberation appears at the receiver as a fluctuating, temporally decaying(i.e., nonstationary) noise which begins at the instant the transmit signal is emitted.

Radar clutter and light scattering in turbid media are analogous travelling wave phenomena which occur following transmission of electromagnetic waves. Besides these wave scattering processes there exist other phenomena, such as electrical shot noise, which are similar to reverberation in terms of the describing mathematics.

In practice sea reverberation is usually classified as volume or boundary reverberation depending on whether the wave scattering occurs at discontinuities located in a volume or on a boundary, respectively. The usual boundaries encountered in the sea are the sea surface and bottom.

In the remainder of this chapter we discuss the energy characteristics of reverberation, mathematical/statistical models of reverberation, reverberation as a normal(i.e., Gaussian) process and reverberation as a process

reducible to stationary(i.e., quasistationary).

2.2. Energy Characteristics of Sea Reverberation

In this section we briefly review results from the so-called energy approach to reverberation characterization. The material presented is based entirely on [Ol'shevskii]. All equations in this section use Ol'shevskii's notation. We will use a different notation throughout the remainder of the dissertation.

The energy approach to characterization of reverberation refers to the determination of the mean intensity of the reverberation signal versus time. The mean intensity is the average power crossing a unit surface per unit time and in the case of reverberation depends on the radiated power of the sonar, the transmit signal shape and duration, acoustic array characteristics, transmission losses(spreading and absorption loss) and scattering properties of the medium.

The primary assumptions made in the energy approach are isovelocity(i.e., straight line) propagation, narrowband signals, spatially uniform scattering properties in the medium and first order, independent scattering. The uniform, independent and first order scattering assumptions allow one to assume that the reverberation signal is the result of incoherent addition of signals scattered from spatially disjoint scattering regions. This in turn implies that the mean intensity of the reverberation is directly proportional to the size of the ensonified region of the medium. The ensonified region is delineated by the sonar beam patterns and the length of the transmit pulse.

The principle results of the energy or intensity study of reverberation are presented below for the cases of volume and boundary reverberation. The mean intensity for volume reverberation in ($watts/meter^2$) is given as

$$<I(t)>_V = \frac{P\sigma_V^2\delta_{eff}e^{-2aR(t)}\eta_V}{2\pi Ct^2} \tag{2.1}$$

where $<\ >$ is the statistical expectation operator, P is the radiated acoustic average power(watts), σ_V^2 is the volume scattering coefficient ($cm.^{-1}$) equal to the amount of power scattered per unit volume for a given incident intensity, α (nepers/meter) is the absorption coefficient, C is the sound propagation velocity(meters/second), δ_{eff} is the energy equivalent effective duration of the transmit pulse, $R(t)$ is the range (meters) to the scattering volume at time t (seconds) and η_V is a coefficient related to the array directivity and is given by

$$\eta_V = \frac{\int_{4\pi}\Phi_T^2(\Psi)\Phi_R^2(\Psi)d\Psi}{\int_{4\pi}\Phi_T^2(\Psi)d\Psi} \tag{2.2}$$

In expression 2.2 $\Phi_T(\Psi)$ and $\Phi_R(\Psi)$ are respectively the normalized(≤ 1.0) transmit and receive beam patterns. The variable Ψ is a solid angle(steradians).

The mean intensity for boundary reverberation is given similarly by

$$<I(t)>_B = \frac{P\sigma_B^2\delta_{eff}e^{2aR(t)}\eta_B}{2\pi Ct^2} \tag{2.3}$$

where P, δ_{eff}, α, $R(t)$ and C are as described above. The variable σ_B^2 is the boundary scattering coefficient which equals the amount of power scattered per surface area for a given incident intensity. The array directivity coefficient η_B is given as

$$\eta_B = \frac{2\int_0^{2\pi} \Phi_T^2(\alpha,\theta_B)\Phi_R^2(\alpha,\theta_B)d\alpha}{\int_{4\pi} \Phi_T^2(\Psi)d\Psi} \tag{2.4}$$

where α is the azimuthal angle to the surface scattering element and θ_B is the elevation angle to the scattering element. Note that θ_B is fixed for a constant range(i.e., time).

The main results of the energy analysis of reverberation are: one, that the mean intensity is proportional to radiated power, array directivity and energy equivalent pulse length and, two, that volume reverberation decays as t^{-2} while boundary reverberation decays as t^{-3}. Experimental results have shown that the linear dependence of reverberation intensity on energy effective pulse length is valid over a wide range of pulse durations.

2.3. Mathematical/Statistical Models of the Reverberation Process

In this section we discuss two methods of mathematically characterizing the reverberation process: the point scatterer method and the continuous scattering method. The point scatter model is discussed in detail because it it currently the most mathematically complete model, it is intuitive and it gives analytical results which are reasonably consistent with experimental observations. The concepts of quasistationary processes and reverberation as a Gaussian process are discussed along with the point scatterer model discussion. Finally a continuous first order scattering model is presented. The continuous scattering model is relatively easy to deal with analytically and includes the point scattering model as a special case. In this dissertation we use the continuous scattering model to characterize the scattered reverbera-

tion field.

2.3.1. Point Scatterer Model

The point scatterer model(hereafter PSM) is a phenomenological model which represents reverberation signals as linear superpositions of random signals returned from point scatterers distributed throughout a volume or on a surface. The point scatterers are assumed to be distributed spatially and hence temporally with a Poisson density. The Poisson density is sometimes called the distribution of complete randomness[Parzen]. The PSM is also referred to as the Faure/ Ol'shevskii/Middleton(FOM) model after the three investigators primarily responsible for its development.

In the PSM the medium is treated as infinite, homogeneous and isotropic except for the randomly distributed scatterers. Wave theory is used to determine the acoustic field incident on a given scatterer and incident on the sonar receiving aperture. The boundary conditions associated with a given scatterer are absorbed into a generally time-variant, realizable impulse response function. With this formulation an individual point scatterer can reradiate the incident wave, spread, potentially, in both time(delay) and frequency.

The earliest work with the PSM is that of [Faure]. Faure assumes a constant Poisson spatial density of scatterers and shows how this leads to a time-variant Poisson temporal density due to spreading of the wavefront. Beampattern effects are accounted for in the Poisson densities. The individual point scatterers are assumed to reradiate a copy of the transmit pulse which is delayed and doppler shifted as appropriate for the scatterer position

and relative radial velocity. The scatterer time delay, doppler shift and scattering crossection are assumed to be independent of each other. From this model Faure develops expressions for the mean, covariance and average power of reverberation. The average power result is shown to be consistent with the decay laws discussed in the previous section. For reasonably short transmit pulses($\leq$ 150 msec.) expressions are developed for a short term power spectral density. For narrowband transmit signals and small scatterer radial velocities the power spectrum is shown to be given by the convolution of the transmit pulse power spectrum with the scatterer velocity probability density function. Faure does not account for the doppler spreading induced by array platform motion.

In 1967 Ol'shevskii published a very extensive monograph dealing with reverberation point scatterer models. The reverberation signal is assumed to be formed as a sum of elementary scattered signals with stochastic perturbations. That is, the reverberation signal $r(t)$ is related to the transmit pulse $s(t)$ as

$$r(t) = \sum_{i=1}^{n} a_i s(t-\tau_i ; \underline{\xi}_i) \tag{2.5}$$

where a_i is a random variable associated with the strength of the i^{th} scatterer, τ_i is the delay associated with the ith scatterer, $\underline{\xi}_i$ is a vector of random parameters for the i^{th} scattered signal and n is a random variable equal to the number of scatterers contributing to the return at time t. Drawing upon results from the theories of superposition of stochastic perturbations as developed in the study of shot noise and related phenomena[Middleton(1960)], Ol'shevskii develops expressions for the rever-

beration process characteristic function. The logarithm of the characteristic function is then expanded in a power series where the coefficients of the power series expansion are called semi-invariants[Rice]. The k^{th} semi-invariant of the expansion is given as

$$\lambda_k(t) = \langle n(t)\rangle\langle a^k(t)\rangle\int_{-\infty}^{+\infty}\langle s^k(u;\underline{\xi})\rangle_{\underline{\xi}}du \tag{2.6}$$

In expression 2.6 the brackets < > denote statistical expectation. The factor $\langle n(t)\rangle$ is the average number of scatterers contributing to the reverberation signal at time t, $\langle a^k(t)\rangle$ is the k^{th} moment of the scatterer crossection random variable at time t, and $\langle s^k(u;\underline{\xi})\rangle_{\underline{\xi}}$ is the statistical expectation of $s^k(u;\underline{\xi})$ with respect to the random parameter vector $\underline{\xi}$. Inherent in equation 2.6 are the assumptions that $\langle n(t)\rangle$ and $\langle a^k(t)\rangle$ are essentially constant over a transmit pulse length and that the integral converges for any value of k.

Knowledge of the process semi-invariants allows one to obtain the process moments of any order k. In particular, the time-variant mean and variance of the reverberation process are given as

$$\langle r(t)\rangle = \langle n(t)\rangle\langle a(t)\rangle\int_{-\infty}^{+\infty}\langle s(u;\underline{\xi})\rangle_{\underline{\xi}}du \tag{2.7}$$

$$\sigma_r^2(t) = \langle n(t)\rangle\langle a^2(t)\rangle\int_{-\infty}^{+\infty}\langle s^2(u;\underline{\xi})\rangle_{\underline{\xi}}du \tag{2.8}$$

By generalizing the theorems on superpositions of stochastic perturbations to greater than one dimension it is also possible to derive joint process moments. A result of particular interest here is an expression for the reverberation process autocorrelation function at a fixed time t given as

$$B(\tau;t) = \langle r(t)r(t+\tau)\rangle$$

$$= \langle n(t)\rangle\langle a^2(t)\rangle \int_{-\infty}^{+\infty} \langle s(u;\underline{\xi})s(u+\tau;\underline{\xi})\rangle_{\underline{\xi}} du \tag{2.9}$$

We can define a process correlation coefficient by normalizing $B(\tau,t)$ by the variance at time t given by 2.8. The result is

$$K(\tau) = \frac{\int_{-\infty}^{+\infty} \langle s(u;\underline{\xi})s(u+\tau;\underline{\xi})\rangle_{\underline{\xi}} du}{\int_{-\infty}^{+\infty} \langle s^2(u;\underline{\xi})\rangle_{\underline{\xi}} du} \tag{2.10}$$

Note that $K(\tau)$ is not a function of time. A process $r(t)$ which can be made second order stationary by normalizing by the square root of the time varying process variance is called a quasistationary process or a process reducible to stationary[Ol'shevskii].

Ol'shevskii uses equations 2.9 and 2.10 to calculate the reverberation correlation function under the assumption of narrowband signals. The anaylsis accounts for transmit signal type, scatterer random velocity distribution and array platform motion induced scatterer velocity. The reverberation correlation function is found to factor into a product of three terms. The first term is the correlation function of the transmit signal under the assumption of no scatterer random velocity and no array platform motion. The second term accounts for scatterer random velocities and turns out to be equal to the characteristic function associated with the scatterer random velocity probability density function. The third term accounts for the doppler shifts induced by platform motion. We do not list the equations here because comparable equations will be derived in the next section using the continuous scattering model.

The fact that the reverberation process is approximately quasistationary allowed us to define a correlation function at any time t. Likewise, we may define a short term power spectrum as the Fourier transform(Wiener-Kinchine relations [Koopmans]) of this correlation function. From the discussion above regarding the correlation function factoring into a product of three functions and from elementary properties of Fourier transforms we may immediately infer that the power spectral density at any time is given as a convolution of the Fourier transforms of each of the three factors forming the overall correlation function. This result intuitively shows how scatterer motion, random and platform induced, lead to frequency spreading of the transmit signal power spectrum.

The third major reference to the point scatterer model is that of [Middleton(1967,1972)]. Middleton's work is by far the most comprehensive treatment of the PSM. Although the major results pertinent to this dissertation have been discussed above in regard to Faure and Ol'shevskii's work it seems appropriate to briefly discuss Middletons contributions.

Middletons work is available in four parts. Parts I and II develop the PSM similarly to Faure and Ol'shevskii except that the analysis is generalized to account for broadband signals, frequency dependent apertures, multiple source/receiver situations and general time-variant linear filter representations of the scatterer/wave interaction. In parts III and IV the results derived in parts I and II are further generalized to account for nonisovelocity propagation and specular reflections. The overall approach of Middleton is to develop space-time mathematical operators which linearly relate the transmit signal to the received process. These space-time operators

incorporate all pertinent factors such as apertures, geometry, scatterer density, etc...

Before discussing the continuous scattering model we discuss reverberation as a normal(i.e.,Gaussian) process. Examination of 2.5 shows that the reverberation signal is formed by summing a random number of assumed independent random variables. If the average number of signals $<n(t)>$ contributing at any time t is large the received process will be normally distributed in light of the central limit theorem. The convergence of the distribution law to normal has been investigated in several papers[Ol'shevskii,Moose]. The method generally used to show convergence is to expand the process probability density into an Edgeworth series [Middleton(1960)] and show that as the number of scatterers contributing to the series becomes infinite(i.e., $n \to \infty$) the series converges to a normal law. In this dissertation we assume that the reverberation process is normal and zero mean. Hence we are interested in developing expressions for the process correlation function as this completely specifies a normal process.

2.3.2. Continuous Scattering Model

The continuous scattering model employed here is similar in nature to general scatter communications channel models proposed in [Kennedy,Bello]. However whereas Kennedy and Bello considered scatterers continuously distributed in delay and doppler we will consider scatterers continuously distributed throughout a volume or on a boundary. Both of these approaches lead to similar results as is evident when one realizes that a differential volume or boundary element maps directly to a delay and doppler element. We prefer

to use the approach where scatterers are continuously distributed in space because it will allow us to perform integrations over spatial domains of interest to determine correlation functions and power spectral density functions associated with the reverberation returned from those spatial domains.

In this section we present the continuous scattering model and from it derive expressions for the average received power, autocorrelation function and power spectral density function for a single beam(channel) of a sonar at a fixed range. We also derive an expression for the crosscorrelation function and crossspectrum between any two beams of a multibeam sonar at a fixed range. Results are presented for both volume and boundary reverberation.

Several assumptions are required to make the analysis tractable. These assumptions include:

- scatterers are continuously distributed throughout a volume or on a boundary and are statistically independent of each other no matter how closely spaced. This is equivalent to the Poisson scattering assumption. This is also referred to as a first order uncorrelated scattering process.

- the transmit signal is narrowband.

- scatterer random velocities are small with respect to the propagation velocity and are independent and identically distributed for all volume and/or boundary differential elements.

- scatterer crossections are independent of spatial position

Because of the narrowband assumption we will use complex envelope notation throughout the remainder of this paper. In addition the transmit signal will be written in energy normalized form. That is, the actual transmit signal, $\tilde{x}_a(t)$ will be written as $\sqrt{E_t}\,\tilde{x}(t)$ where $\tilde{x}(t)$ has unit energy.

For the case of volume scattering we employ the geometry shown in figure 2-1. The sonar array platform is assumed to move in the direction of the $\hat{i}$ unit vector with a constant velocity of magnitude V_s.

Consider a differential volume element dV, located at position vector $\underline{P}$ with spherical coordinates (R,θ,ψ) which has a relative velocity such that a doppler shift f_d appears on the signal returned from this element. Also suppose that the magnitude and phase of reverberation from the element dV for a unit amplitude transmit signal is $\tilde{z}(\underline{P})$. Then

$$d\tilde{r}_1(t) = \sqrt{E_t}\,\tilde{z}(\underline{P})\tilde{x}(t-\frac{2R}{C})e^{j2\pi f_d t}\,dV \qquad (2.11)$$

is the differential reverberation($\mu pascals$) returned from differential element dV for beam 1 of the sonar. The total reverberation signal for beam 1 is then obtained by volume integration over all scatterers and is given as

$$\tilde{r}_1(t) = \sqrt{E_t}\int_V \tilde{z}(\underline{P})\tilde{x}(t-\frac{2R}{C})e^{j2\pi f_d t}\,dV \qquad (2.12)$$

The autocorrelation of the reverberation signal $\tilde{r}_1(t)$ is given as

$$B_{11}(t,s) = <\tilde{r}_1(t)\tilde{r}_1^*(s)>$$

$$= <\sqrt{E_t}\int_V \tilde{z}(\underline{P})\tilde{x}(t-\frac{2R}{C})e^{j2\pi f_d t}\,dV\ \sqrt{E_t}\int_{V'} \tilde{z}^*(\underline{P}')\tilde{x}^*(s-\frac{2R'}{C})e^{-j2\pi f_d' s}\,dV'>$$

$$= E_t\int_V\int_{V'} <\tilde{z}(\underline{P})\tilde{z}^*(\underline{P}')>\tilde{x}(t-\frac{2R}{C})\tilde{x}^*(s-\frac{2R'}{C})<e^{j2\pi[f_d t - f_d' s]}>dV dV' \qquad (2.13)$$

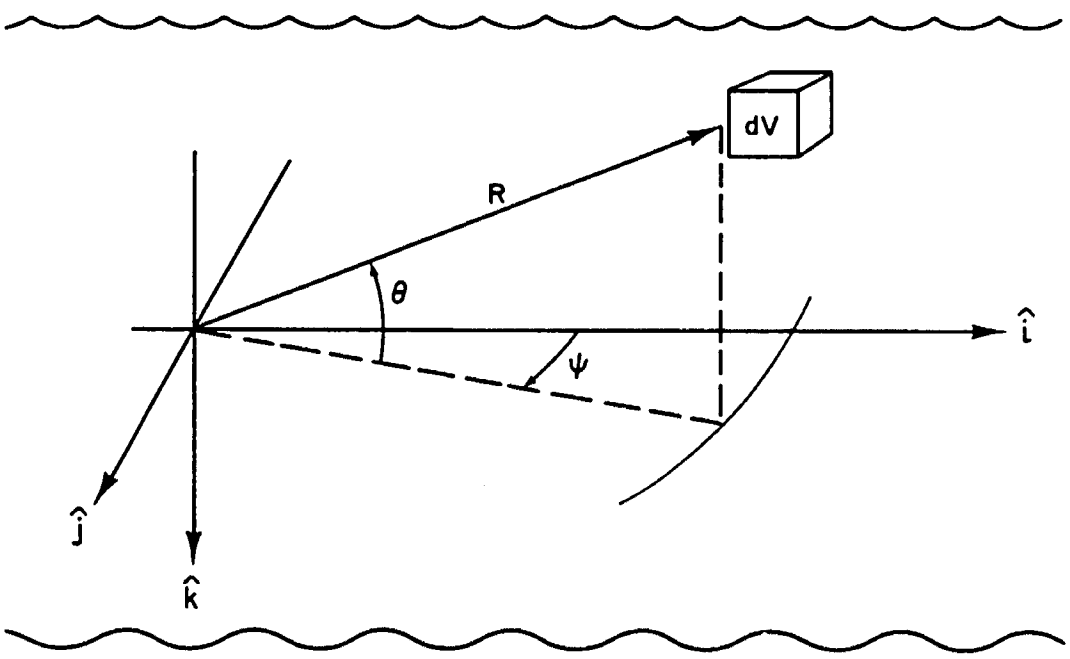

Figure 2-1) Volume Scattering Geometry

We next invoke the Poisson scattering assumption [Van Trees(1965)] which states that the signals scattered from different scatterers are statistically independent no matter how close the scatterers are to each other. This assumption allows to write

$$< \tilde{z}(\underline{P})\tilde{z}^*(\underline{P}') > = \sigma^2(\underline{P}')\delta(\underline{P}'-\underline{P}) \tag{2.14}$$

Note that $\sigma^2(\underline{P})$ is the mean square value of the signal returned from the scattering element located at $\underline{P}$ for a unit amplitude transmit pulse. Substituting 2.14 into 2.13 gives

$$B_{11}(t,s) = E_T \int_V \sigma^2(\underline{P})\tilde{x}(t-\frac{2R}{C})\tilde{x}^*(s-\frac{2R}{C})<e^{j2\pi f_d[t-s]}>dV \tag{2.15}$$

Now let $s = t + \tau$ giving

$$B_{11}(t,s) = B_{11}(t,t+\tau) \equiv B_{11}(\tau;t)$$

$$= E_t \int_V \sigma^2(\underline{P})\tilde{x}(t-\frac{2R}{C})\tilde{x}^*(t-\frac{2R}{C}+\tau)<e^{j2\pi f_d\tau}>dV \tag{2.16}$$

In order to proceed from here we need to expand the differential element dV and the doppler shift $f_d(\underline{P})$. For the coordinate system chosen the element dV is given as

$$dV = R^2\cos\theta d\theta d\psi dR \tag{2.17}$$

The doppler shift f_d is the sum of the deterministic(i.e.,non-random) platform induced doppler shift f_p and a random doppler shift f_V (V denotes volume). Thus

$$f_d(\underline{P}) = f_p + f_V \tag{2.18}$$

The platform induced doppler f_p is given as

$$f_p = \frac{2f_c V_s \cos[\gamma(\theta,\psi)]}{C} \tag{2.19}$$

where f_c is the sonar carrier frequency(hz.), V_s is the sonar speed, C is the

sound velocity and $\gamma(\theta,\psi)$ is the angle between the sonar velocity vector and a position vector drawn from the origin to the element dV. This angle is given as

$$\gamma(\theta,\psi) = \cos^{-1}[\ \cos\theta\ \cos\psi\ ] \tag{2.20}$$

Substituting 2.17, 2.18, and 2.19 into 2.16 gives

$$B_{11}(\tau;t) = E_t \int_R \int_\theta \int_\psi \sigma^2(\underline{P})\tilde{x}(t-\frac{2R}{C})\tilde{x}^*(t-\frac{2R}{C}+\tau)\ \times$$

$$<e^{j2\pi\tau[\frac{2f_c V_s \cos(\theta)\cos(\psi)}{C}+f_V]}>R^2\cos(\theta)d\theta d\psi dR \tag{2.21}$$

Because the random doppler shift is independent of position we may extract it from the integral. Also, $\sigma^2(\underline{P})$ is independent of angular position thus allowing us to express it as

$$\sigma^2(\underline{P}) = \sigma_\beta^2 \frac{e^{-2\alpha R}}{R^4} |B_T(\theta,\psi)|^2 |B_{R1}(\theta,\psi)|^2 \tag{2.22}$$

where σ_β^2 is the differential volume scattering strength, $B_T(\theta,\psi)$ is the complex transmit beam pattern and $B_{R1}(\theta,\psi)$ is the complex receive beam pattern for beam 1. Note that all beam patterns are assumed to be normalized to unity magnitude. Also , beampattern phase center offset factors are assumed to be incorporated into the complex beampattern phase. The factor R^{-4} represents spherical spreading loss and the exponential factor is the absorption loss. With these substitutions 2.21 becomes

$$B_{11}(\tau;t) = E_t \sigma_\beta^2 < e^{j2\pi f_V \tau} > \int_R \frac{e^{-2\alpha R}}{R^2} \tilde{x}(t-\frac{2R}{C}) \tilde{x}^*(t-\frac{2R}{C}+\tau) dR \times$$

$$\int_\theta \int_\psi |B_T(\theta,\psi)|^2 |B_{R1}(\theta,\psi)|^2 e^{\frac{j4\pi f_c \tau V_S \cos(\theta)\cos(\psi)}{C}} \cos(\theta) d\theta d\psi \qquad (2.23)$$

The range of integration on R is $[\frac{Ct}{2} - \frac{C\,PL}{2}, \frac{Ct}{2}]$ where PL is the transmit pulse length in seconds. For reasonably short transmit pulses ($\ll \frac{2R}{C}$) the spreading loss and absorption loss will be essentially constant over the range of integration on R. This allows us to write 2.23 as

$$B_{11}(\tau;t) = E_t \sigma_\beta^2 < e^{j2\pi f_V \tau} > \frac{e^{-\alpha Ct}}{\frac{C^2t^2}{4}} \int_R \tilde{x}(t-\frac{2R}{C}) \tilde{x}^*(t-\frac{2R}{C}+\tau) dR \times$$

$$\int_\theta \int_\psi |B_T(\theta,\psi)|^2 |B_{R1}(\theta,\psi)|^2 e^{\frac{j4\pi f_c \tau V_S \cos(\theta)\cos(\psi)}{C}} \cos(\theta) d\theta d\psi \qquad (2.24)$$

Note in 2.24 that as R spans the integral limits the argument of the function $\tilde{x}(t-\frac{2R}{C})$ takes on all possible nonzero values. This allows us to replace the integral limits by $(-\infty,+\infty)$ and with a change of variable we can write 2.24 as

$$B_{11}(\tau;t) = E_t \sigma_\beta^2 < e^{j2\pi f_V \tau} > \frac{e^{-\alpha Ct}}{\frac{Ct^2}{2}} \int_{-\infty}^{+\infty} \tilde{x}(u) \tilde{x}^*(u+\tau) du \times$$

$$\int_\theta \int_\psi |B_T(\theta,\psi)|^2 |B_{R1}(\theta,\psi)|^2 e^{\frac{j4\pi f_c \tau V_S \cos(\theta)\cos(\psi)}{C}} \cos(\theta) d\theta d\psi \qquad (2.25)$$

From 2.25 we can determine the average power at time t as

$$B_{11}(0;t) \equiv P_{11}(t)$$

$$= E_t \sigma_\beta^2 \frac{e^{-\alpha C t}}{\frac{Ct^2}{2}} \int_\theta \int_\psi |B_T(\theta,\psi)|^2 |B_{R1}(\theta,\psi)|^2 \cos(\theta) d\theta d\psi \tag{2.26}$$

If we divide $B_{11}(\tau;t)$ by the average power $B_{11}(0;t)$ we get an expression in τ only. This is an example of a nonstationary process reducible to stationary via normalization by the square root of the time varying process variance. For convenience we define the following functions:

$$Y_V(\tau) = \langle e^{j2\pi f_V \tau} \rangle \tag{2.27}$$

$$W(\tau) = \int_{-\infty}^{+\infty} \tilde{x}(u)\tilde{x}^*(u+\tau)du \tag{2.28}$$

$$Z_{V11}(\tau;t) = \frac{\int_\theta \int_\psi |B_T(\theta,\psi)|^2 |B_{R1}(\theta,\psi)|^2 e^{\frac{j4\pi f_c \tau V_S \cos(\theta)\cos(\psi)}{C}} \cos(\theta) d\theta d\psi}{\int_\theta \int_\psi |B_T(\theta,\psi)|^2 |B_{R1}(\theta,\psi)|^2 \cos(\theta) d\theta d\psi} \tag{2.29}$$

With these definitions we can write (2.25) as

$$B_{11}(\tau;t) = P_{11}(t) Y_V(\tau) W(\tau) Z_{V11}(\tau;t) \tag{2.30}$$

The function $Y_V(\tau)$ is the contribution to the overall correlation function due to the random volume scatterer velocities. The function $W(\tau)$ is the contribution due to the transmit signal. The function $Z_{V11}(\tau;t)$ is the contribution due to array platform motion, beampatterns and geometry. The dependence of $Z_{V11}(\tau;t)$ on t arises due to the fact that the limits of integration on (θ,ψ) will in general change with time du to boundary interaction.

The power spectrum associated with beam 1 is obtained at once by making use of the Wiener-Khinchine relations(ref.). That is, the power spectrum is obtained by Fourier transforming equation 2.30 with respect to the process dynamics variable τ. Thus, the power spectrum of the reverberation in beam 1 at time t is given as

$$S_{11}(f;t) = P_{11}(t)\left\{Y_V(f) * W(f) * Z_{V11}(f;t)\right\} \tag{2.31}$$

where * denotes convolution and f is frequency in hertz. We call $Z_{V11}(f;t)$ the volume motional spectrum for beam1.

As mentioned previously we are also interested in the crosscorrelation between the time series observed on different beams of a multibeam sonar system. We will assume that the two beams of interest are denoted as beam 1 and beam 2 and the reverberation signals received on each beam will be denoted $\tilde{r}_1(t)$ and $\tilde{r}_2(t)$. We employ the same geometry and use the same assumptions as in the derivation of the autocorrelaton function $B_{11}(\tau;t)$. Note that expressions analagous to 2.30 and 2.31 exist for beam 2 of the sonar and they would be be denoted as $B_{22}(\tau;t)$ and $S_{22}(f;t)$, respectively.

Derivation of the crosscorrelation proceeds exactly as in the derivation of the autocorrelation expression and consequently our discussion is less detailed. The beam to beam crosscorrelation is given as

$$\begin{aligned} B_{12}(t,s) &= \langle \tilde{r}_1(t)\tilde{r}_2^*(s)\rangle \\ &= E_t \int_V \int_{V'} \langle \tilde{z}(\underline{P})\tilde{z}^*(\underline{P}')\rangle \tilde{x}(t-\frac{2R}{C})\tilde{x}^*(s-\frac{2R'}{C})\langle e^{j2\pi[f_d t - f_d' s]}\rangle dV dV' \end{aligned} \tag{2.32}$$

From the Poisson scattering assumption 2.14 we obtain

$$B_{12}(t,s) = E_t \int_V \sigma^2(\underline{P})\tilde{x}(t-\frac{2R}{C})\tilde{x}(s-\frac{2R}{C})<e^{j2\pi f_d(t-s)}>dV \tag{2.33}$$

Expanding the differential volume element 2.17 and letting $s=t+\tau$ gives

$$B_{12}(\tau;t) = E_t \int_R \int_\theta \int_\psi \sigma^2(\underline{P})\tilde{x}(t-\frac{2R}{C})\tilde{x}^*(t-\frac{2R}{C}+\tau) \times$$

$$<e^{j2\pi f_d\tau}>R^2\cos(\theta)dR\,d\theta\,d\psi \tag{2.34}$$

Again because $\sigma^2(\underline{P})$ is independent of angular position we may write it as

$$\sigma^2(\underline{P}) = \sigma_\beta^2 \frac{e^{-2\alpha R}}{R^4}|B_T(\theta,\psi)|^2 B_{R1}(\theta,\psi)B_{R2}^*(\theta,\psi) \tag{2.35}$$

Substituting 2.35 into 2.34 and expanding the doppler shift into a random scatterer motion term plus the platform motion induced term lead to

$$B_{12}(\tau;t) = E_t\sigma_\beta^2 <e^{j2\pi f_V\tau}> \int_R \frac{e^{-2\alpha R}}{R^2}\tilde{x}(t-\frac{2R}{C})\tilde{x}^*(t-\frac{2R}{C}+\tau)dR \times$$

$$\int_\theta \int_\psi |B_T(\theta,\psi)|^2 B_{R1}(\vartheta,\psi)B_{R2}^*(\theta,\psi)e^{\frac{j4\pi f_c\tau V_S\cos(\theta)\cos(\psi)}{C}}\cos(\theta)d\theta\,d\psi \tag{2.36}$$

Proceeding as in the transition from 2.23 to 2.25 we obtain

$$B_{12}(\tau;t) = E_t\sigma_\beta^2 \frac{e^{-\alpha Ct}}{\frac{Ct^2}{2}} Y_V(\tau)W(\tau)\int_\theta \int_\psi |B_t(\theta,\psi)|^2 B_{R1}(\theta,\psi)B_{R2}^*(\theta,\psi) \times$$

$$e^{\frac{j4\pi f_c\tau V_S\cos(\theta)\cos(\psi)}{C}}\cos(\theta)d\theta\,d\psi \tag{2.37}$$

This is the desired expression for the complex beam to beam crosscorrelation function. The functions $Y_V(\tau)$ and $W(\tau)$ are defined in 2.27 and 2.28, respectively.

The average crosspower is seen to be

$$P_{12}(t) = E_t \sigma_V^2 \frac{e^{-\alpha C t}}{\frac{Ct^2}{2}} \int_\theta \int_\psi |B_T(\theta,\psi)|^2 B_{R1}(\theta,\psi) B_{R2}^*(\theta,\psi) \cos(\theta) d\theta d\psi \qquad (2.38)$$

The cross power spectrum of volume reverberation for beams 1 and 2 may be written as

$$S_{12}(f;t) = P_{12}(t)\left\{Y_V(f) * W(f) * Z_{V12}(f;t)\right\} \qquad (2.39)$$

where $Z_{V12}(f;t)$ is the Fourier transform in the variable τ of

$$Z_{V12}(\tau;t) = \frac{\int_\theta \int_\psi |B_t(\theta,\psi)|^2 B_{R1}(\theta,\psi) B_{R2}^*(\theta,\psi) e^{\frac{j4\pi f_c \tau V_S \cos(\theta)\cos(\psi)}{C}} \cos(\theta) d\theta d\psi}{\int_\theta \int_\psi |B_T(\theta,\psi)|^2 B_{R1}(\theta,\psi) B_{R2}^*(\theta,\psi) \cos(\theta) d\theta d\psi} \qquad (2.40)$$

We call $Z_{V12}(f;t)$ the cross volume motional spectrum for beams 1 and 2.

For the case of boundary scatter we employ the geometry shown in figure 2-2. We concentrate on the ocean surface boundary. The bottom boundary results are identical except that there is no random motion of the scattering elements. As in the volume scatter case the sonar is assumed to move with constant velocity $|V_s|\,\hat{i}$.

Consider a differential surface element dA, located at position vector $\underline{P}$ with spherical coordinates (R,θ,ψ), which has a relative velocity such that a doppler shift f_d appears on the signal returned from this element. Also sup-

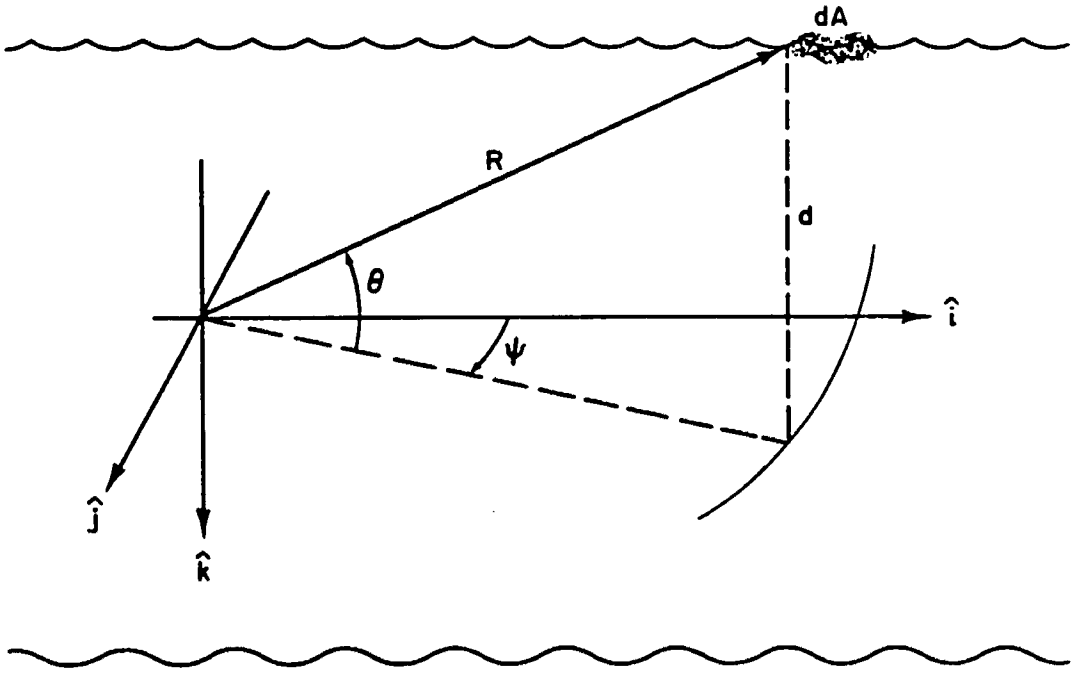

Figure 2-2) Boundary Scattering Geometry

pose that the magnitude and phase of reverberation for a unit amplitude transmit signal is $\tilde{z}(\underline{P})$. Then

$$d\tilde{r}_1(t) = \sqrt{E_t}\tilde{z}(\underline{P})\tilde{x}(t-\frac{2R}{C})e^{j2\pi f_d t}dA \tag{2.41}$$

is the differential reverberation received from element dA for beam 1 of the sonar. The total reverberation is obtained by integration as

$$\tilde{r}_1(t) = \sqrt{E_t}\int_A \tilde{z}(\underline{P})\tilde{x}(t-\frac{2R}{C})e^{j2\pi f_d t}dA \tag{2.42}$$

The autocorrelation of the surface reverberation is given as

$$B_{11}(t,s) \equiv <\tilde{r}_1(t)\tilde{r}_1^*(s)>$$

$$= E_t\int_A\int_{A'}<\tilde{z}(\underline{P})\tilde{z}^*(\underline{P}')>\tilde{x}(t-\frac{2R}{C})\tilde{x}^*(s-\frac{2R'}{C})<e^{j2\pi[f_d t - f_d' s]}>dAdA' \tag{2.43}$$

The Poisson scattering assumption allows us to write

$$<\tilde{z}(\underline{P})\tilde{z}^*(\underline{P}')> = \sigma^2(\underline{P}')\delta(\underline{P}'-\underline{P}) \tag{2.44}$$

Substituting 2.44 into 2.43 yields

$$B_{11}(t,s) = E_t\int_A \sigma^2(\underline{P})\tilde{x}(t-\frac{2R}{C})\tilde{x}^*(s-\frac{2R}{C})<e^{j2\pi f_d(t-s)}>dA \tag{2.45}$$

Proceeding analagously to the volume scatter case we now express the doppler shift f_d in terms of a deterministic platform motion induced term f_p and a random scatterer motion induced term f_s (s for surface). Thus

$$f_d = f_p + f_s \tag{2.46}$$

where

$$f_p = \frac{2f_c V_S \cos\theta\cos\psi}{C} \tag{2.47}$$

Because the integration is over a surface, only two independent variables exist. We prefer to integrate over (R,ψ). Thus the elevation variable θ is expressed in terms of R as

$$\theta(R) = \sin^{-1}(\frac{d}{R}) \tag{2.48}$$

The differential area dA hence becomes

$$dA = RdRd\psi \tag{2.49}$$

Thus 2.45 becomes

$$B_{11}(t,s)=E_t\int_R\int_\psi \sigma^2(\underline{P})\tilde{x}(t-\frac{2R}{C})\tilde{x}^*(s-\frac{2R}{C})<e^{j2\pi[f_p+f_s](t-s)}>RdRd\psi \tag{2.50}$$

Now let $s=t+\tau$ giving

$$B_{11}(\tau;t) = E_t\int_R\int_\psi \sigma^2(\underline{P})\tilde{x}(t-\frac{2R}{C})\tilde{x}^*(t-\frac{2R}{C}+\tau) \times$$

$$<e^{j2\pi[f_p+f_s]\tau}>RdRd\psi \tag{2.51}$$

Substituting 2.47 into 2.51 and assuming that the random doppler shift f_s is not a function of position allows us to write 2.51 as

$$B_{11}(\tau;t) = E_t<e^{j2\pi f_s\tau}>\int_R\int_\psi \sigma^2(\underline{P})\tilde{x}(t-\frac{2R}{C})\tilde{x}^*(t-\frac{2R}{C}+\tau) \times$$

$$e^{\frac{j4\pi f_c V_S \tau\cos(\theta(R))\cos(\psi)}{C}}RdRd\psi \tag{2.52}$$

Note that the assumption that the random doppler shift f_s is independent of position is equivalent to the assumption that the random scatterer velocity vectors are equally likely to be oriented in any direction. This assumption will not hold true for example when there exists a current in the water. We did not attempt to model this situation.

Next we express $\sigma^2(\underline{P})$ as

$$\sigma^2(\underline{P}) = \sigma_S^2(\theta(R))\frac{e^{2\alpha R}}{R^4}|B_T(\theta(R),\psi)|^2|B_{R1}(\theta(R),\psi)|^2 \tag{2.53}$$

Equation 2.53 is similar to 2.22 (i.e., the volume scatter case) except that the

term σ_S^2, the differential surface scattering strength, is dependent on the grazing angle $\theta(R)$. Substituting 2.53 into 2.52 yields

$$B_{11}(\tau;t) = E_T\langle e^{j2\pi f_c\tau}\rangle \int_R \sigma_S^2(\theta(R))\frac{e^{-2aR}}{R^4}\tilde{x}(t-\frac{2R}{C})\tilde{x}^*(t-\frac{2R}{C}+\tau) \times$$

$$\int_\psi |B_T(\theta(R),\psi)|^2|B_{R1}(\theta(R),\psi)|^2 \langle e^{\frac{j4\pi f_c V_S \tau\cos(\theta(R))\cos(\psi)}{C}}\rangle R\,dR\,d\psi \quad (2.54)$$

As was done in the volume scatter case we assume that the transmit pulse is short enough such that the transmission losses are essentially constant over the integration on R. Also we assume that $\theta(R)$ is essentially constant for the same reason. This allows us to write 2.54 as

$$B_{11}(\tau;t) = E_T\sigma_S^2(\theta(Ct/2))\frac{e^{-aCt}}{\frac{C^2t^3}{4}}W(\tau)Y_S(\tau,\theta(Ct/2))\times$$

$$\int_\psi |B_T(\theta(Ct/2),\psi)|^2|B_{R1}(\theta(Ct/2),\psi)|^2 e^{\frac{j4\pi f_c V_S \tau\cos(\theta(Ct/2))\cos(\psi)}{C}} d\psi \quad (2.55)$$

where $W(\tau)$ is defined in 2.28 and $Y_S(\tau)$ is given as

$$Y_S(\tau) = \langle e^{j2\pi f_S\tau}\rangle \quad (2.56)$$

The average power of surface reverberation is obtained as

$$B_{11}(0;t) = P_{11}(t)$$

$$= E_T\sigma_S^2(\theta)\frac{e^{-aCt}}{\frac{C^2t^3}{4}}\int_\psi |B_T(\theta,\psi)|^2|B_{R1}(\theta,\psi)|^2 d\psi \quad (2.57)$$

Note that we have dropped explicit dependence of θ on t for notational brevity. As in the volume scatter case we may define a function

$$Z_{S11}(\tau;t) = \frac{\int_{\Psi} |B_T(\theta,\psi)|^2 |B_{R1}(\theta,\psi)|^2 e^{\frac{j4\pi f_c V_S \tau \cos(\theta)\cos(\psi)}{C}} d\psi}{\int_{\Psi} |B_T(\theta,\psi)|^2 |B_{R1}(\theta,\psi)|^2 d\psi} \tag{2.58}$$

We may then write the autocorrelation for surface reverberation in beam 1 as

$$B_{11}(\tau;t) = P_{11}(t) Y_S(\tau;t) W(\tau) Z_{S11}(\tau;t) \tag{2.59}$$

As in 2.29 the dependence of $Z_{S11}(\tau;t)$ on t comes about due to time dependent limits of integration.

The power spectrum is obtained immediately via Fourier transformation of 2.59 and is given as

$$S_{11}(f;t) = P_{11}(t)\left\{Y_S(f;t) * W(f) * Z_{S11}(f;t)\right\} \tag{2.60}$$

where * denotes convolution and f is in hertz. The function $Z_{S11}(f;t)$ is called the surface motional spectrum for beam 1.

Derivation of the crosscorrelation between beam 1 and beam 2 of a multibeam sonar for surface reverberation proceeds analagously to the volume scatter case. The beam to beam crosscorrelation is given as

$$\begin{aligned} B_{12}(t,s) &= \langle \tilde{\tau}_1(t) \tilde{\tau}_2^*(s) \rangle \\ &= E_T \int_A \int_{A'} \langle \tilde{z}(\underline{P}) \tilde{z}^*(\underline{P}') \rangle \tilde{x}(t - \frac{2R}{C}) \tilde{x}^*(s - \frac{2R'}{C}) \quad \times \\ &\qquad \langle e^{j2\pi[f_d t - f_d' s]} \rangle dA dA' \end{aligned} \tag{2.61}$$

Letting $s = t+\tau$ and invoking the Poisson scattering assumption allows us to write 2.61 as

$$B_{12}(\tau;t) = E_T \int_A \sigma^2(\underline{P})\tilde{x}(t-\frac{2R}{C})\tilde{x}^*(t-\frac{2R}{C}+\tau)<e^{j2\pi f_d \tau}>dA \tag{2.62}$$

Expanding $\sigma^2(\underline{P})$, dA and f_d as in the autocorrelation case and again assuming reasonably short transmit pulses we obtain

$$B_{12}(\tau;t) = E_T \sigma_S^2(\theta)\frac{e^{-aCt}}{\frac{C^2t^3}{4}} W(\tau)Y_S(\tau,\theta)\int_\psi |B_T(\theta,\psi)|^2 B_{R1}(\theta,\psi)B_{R2}^*(\theta,\psi) \times e^{\frac{j4\pi f_c V_S \tau \cos(\theta)\cos(\psi)}{C}} d\psi \tag{2.63}$$

The functions $W(\tau)$ and $Y_S(\tau,\theta)$ are defined in 2.28 and 2.56 respectively. The average crosspower as a function of time t is seen to be

$$\begin{aligned} P_{12}(t) &= B_{12}(0;t) \\ &= E_T \sigma_S^2 \frac{e^{-aCt}}{\frac{C^2t^3}{4}} \int_\psi |B_T(\theta,\psi)|^2 B_{R1}(\theta,\psi)B_{R2}^*(\theta,\psi)d\psi \end{aligned} \tag{2.64}$$

The cross power spectrum of surface(in general boundary) reverberation for beams 1 and 2 may be written as

$$S_{12}(f;t) = P_{12}(t)\left\{Y_S(f;t)*W(f)*Z_{S12}(f;t)\right\} \tag{2.65}$$

where $Z_{S12}(f;t)$ is the Fourier transform in the variable τ of

$$Z_{S12}(\tau;t) = \frac{\int_\psi |B_T(\theta,\psi)|^2 B_{R1}(\theta,\psi)B_{R2}^*(\theta,\psi)e^{\frac{j4\pi f_c V_S \tau \cos(\theta)\cos(\psi)}{C}} d\psi}{\int_\psi |B_T(\theta,\psi)|^2 B_{R1}(\theta,\psi)B_{R2}^*(\theta,\psi)d\psi} \tag{2.66}$$

We call $Z_{S12}(f;t)$ the cross surface motional spectrum for beams 1 and 2.

We now have at our disposal the correlation equations needed to characterize the assumed Gaussian reverberation process for both boundary and volume scatter cases. These correlation equations allow us to compute the power spectrum for the multibeam sonar random process. It should be noted that all correlation functions derived are time dependent. Hence, in later sections when we consider simulation of reverberation time series we will be interested in methods which produce multibeam time series which have time dependent correlation functions.

CHAPTER 3

Spectral Factorization of Multivariate Stochastic Processes

3.1. Introduction to Chapter 3

The prior discussion of reverberation as a superposition of a large number of elementary scattered signals with random parameters provides grounds, in light of the central limit theorem, for considering reverberation to be a Gaussian stochastic process. Furthermore, because many current sonar systems are narrowband and use multiple beams we are led to the consideration of reverberation as a narrowband multivariate Gaussian stochastic process. The basic theory of multivariate stochastic processes is covered in rigorous fashion in [Hannan, Weiner and Marsani] and in a more expository manner in [Priestley].

Spectral factorization refers to the problem wherein the power spectral density function of a stationary stochastic process is given and one seeks a realizeable linear filter or algorithm which will transform a white noise sequence into a sequence which has the given power spectrum. A closely related problem is the covariance factorization problem wherein one seeks a filter or algorithm which transforms a white noise sequence into a time series which has a prescribed covariance function. These two problems are equivalent for stationary processes.

In this chapter we present theoretical background information regarding stationary Gaussian processes, covariance functions, power spectral density functions and spectral factorization. Two methods of approximately solving the spectrum factorization problem are presented. These methods are the autoregressive(AR) spectrum decomposition and the Cholesky spectrum factorization. The numerical methods used to compute these factorizations are discussed in detail in chaper 4.

Although it is well known that reverberation is a nonstationary process we will consider only stationary processes in this chapter. This is motivated by the fact that the reverberation simulation methods to be developed here generate nonstationary reverberation by windowing and adding short stationary realizations. Each stationary realization has statistical properties characteristic of the reverberation received from a fixed range. Thus, in this chapter, we are interested in the properties of stationary processes and in particular in methods of generating such realizations(i.e., the spectral factorization problem).

3.2. Gaussian Processes, Spectra and Covariance Functions

Each time a sonar system transmits an acoustic pulse into the water an assumed narrowband Gaussian stochastic reverberation return is received in each of P beams. That is, the sonar receives a multivariate realization $\{x_i(t);i=1,2,....,P\}$ of the reverberation process. Because the signals are narrowband they may be represented in complex envelope form. Thus, the signal available for processing is $\{\tilde{x}_i(t);i=1,2,....,P\}$ where $\tilde{x}_i(t)$ is the complex

envelope of $x_i(t)$. These stochastic signals are assumed to be sampled for digital processing thus giving rise to P uniformly sampled complex Gaussian random processes $\left\{\tilde{x}_i(nT_s); i=1,2,\ldots,P\right\}$. For ease of notation we assume that the sample period T_s equals one second thus allowing us to write $\tilde{x}_i(nT_s)$ simply as $\tilde{x}_i(n)$. We define a vector stochastic process $\underline{x}(n)$ for $n = 0,+-1,+-2,\ldots$ in terms of the jointly stationary processes $\tilde{x}_i(n)$ as

$$\underline{x}(n) = \begin{bmatrix} \tilde{x}_1(n) \\ \tilde{x}_2(n) \\ \vdots \\ \tilde{x}_P(n) \end{bmatrix} \tag{3.1}$$

As is well known[Parzen] a zero mean Gaussian process is completely specified statistically by knowledge of either the process covariance function or power spectral density. For a vector process $\underline{x}(n)$ the covariance is a $P \times P$ matrix function defined for lag l as

$$R_x(l) = <\underline{x}(n)\ \underline{x}^H(n-l)> \tag{3.2}$$

where H denotes the Hermitian transpose of a matrix or vector[Gantmacher] and as usual < > denotes statistical expectation. The covariance matrix satisfies

$$R_x(l) = R_x^H(-l) \tag{3.3}$$

The ij^{th} element, $R_{ij}(l)$, of the covariance matrix $R_x(l)$ is the covariance between the stochastic processes $\tilde{x}_i(n)$ and $\tilde{x}_j(n)$ for lag l.

The $P \times P$ power spectral density matrix $S_x(\omega)$ is related to the covariance function by Fourier transformation. Thus we have the transform pair

$$S_x(\omega) = \sum_{-\infty}^{+\infty} R_x(l) e^{-j\omega l}$$

$$R_x(l) = \frac{1}{2\pi} \int_{-\pi}^{+\pi} S_x(\omega) e^{j\omega l} d\omega \tag{3.4}$$

where each element of the matrix $R_x(l)$ is the Fourier transform of the corresponding element of $S_x(\omega)$. The diagonal terms of $S_x(\omega)$ are called auto power spectral densities and the off diagonal terms are termed cross-spectral densities or simply crossspectra. The spectral density functions exist provided that the associated covariance functions are absolutely summable[Priestley]. If we denote the ij^{th} element of matrix $S_x(\omega)$ by $S_{ij}(\omega)$ then the condition for existence of $S_{ij}(\omega)$ is

$$\sum_{-\infty}^{+\infty} |R_{ij}(l)| < \infty \tag{3.5}$$

Stationarity of the vector process $\underline{x}(n)$ implies that each component of the vector, say $\tilde{x}_i(n)$ admits the following representation[Koopmans]

$$\tilde{x}_i(n) = \frac{1}{2\pi} \int_{-\pi}^{+\pi} e^{j\omega n} dZ_i(\omega) \tag{3.6}$$

where $dZ_i(\omega)$ is the so-called random spectral measure of the i^{th} process at frequency ω. The spectral representation of the vector process $\underline{x}(n)$ may be written as

$$\underline{x}(n) = \frac{1}{2\pi} \int_{-\pi}^{+\pi} e^{j\omega n} \underline{dZ}(\omega) \tag{3.7}$$

where $\underline{dZ}(\omega)$ is the $P \times 1$ column vector of elements $\{ dZ_1(\omega), dZ_2(\omega), \cdots, dZ_P(\omega) \}$. The random spectral measures are, as a consequence of stationarity, crossorthogonal[Priestley] by which we mean

$$\langle dZ_i(\omega) dZ^*_j(u) \rangle = 0; \quad \omega \neq u \quad i, j = 1,2, \cdots, P \tag{3.8}$$

In words equation 3.8 says that there is no correlation between the random

spectral measures at different frequencies either within a single process ($i = j$) or between processes ($i \neq j$).

The power spectrum $S_x(\omega)$ may be defined in terms of the random spectral measures. Indeed, substituting 3.7 into 3.2 and using 3.4 and 3.8 we obtain

$$S_x(\omega)d\omega = <\underline{dZ}(\omega)\underline{dZ}^H(\omega)> \tag{3.9}$$

The ij^{th} element of $S_x(\omega)d\omega$ is then

$$S_{ij}(\omega)d\omega = <dZ_i(\omega)dZ_j^*(\omega)> \tag{3.10}$$

Letting $i = j$ in 3.10 yields the auto spectral density

$$S_{ii}(\omega)d\omega = <|dZ_i(\omega)|^2> \tag{3.11}$$

We see that $S_{ii}(\omega)$ is a real, positive quantity. Physically $S_{ii}(\omega)d\omega$ represents the average power of the i^{th} component of $\underline{x}(n)$ in a small frequency interval $d\omega$ centered about frequency ω.

The crossspectrum is obtained from 3.10 for $i \neq j$. In general the crossspectrum is complex valued and may be expressed as

$$S_{ij}(\omega) = |S_{ij}|\ e^{j\Phi_{ij}(\omega)} \tag{3.12}$$

The crossspectrum magnitude satisfies

$$|S_{ij}(\omega)| \leq (|S_{ii}(\omega)|\ |S_{jj}(\omega)|)^{1/2} \tag{3.13}$$

Thus $|S_{ij}|$ can be nonzero only if both processes $\tilde{x}_i(n)$ and $\tilde{x}_j(n)$ have nonzero power at frequency ω. The crossspectrum phase $\Phi_{ij}(\omega)$ represents the average phase difference between the spectral components of $\tilde{x}_i(n)$ and $\tilde{x}_j(n)$ at frequency ω.

An important property of the spectral density matrix $S_x(\omega)$ is that it is a nonnegative definite Hermitian matrix. The Hermitian property follows from

3.9 and is expressed as

$$S_x(\omega) = S_x^H(\omega) \tag{3.12}$$

The nonnegative definiteness can be proved as follows[Priestley]. Define a univariate process $y(n)$ as

$$y(n) = \underline{\lambda}\ \underline{x}(n) \tag{3.13}$$

where $\underline{\lambda}$ is a row vector of arbitrary complex constants. The autocovariance of $y(n)$ is then

$$R_y(l) = \langle y(n)y^H(n-l)\rangle = \underline{\lambda}R(l)\underline{\lambda}^H \tag{3.14}$$

The autospectral density of $y(n)$ is then

$$S_y(\omega) = \sum_{-\infty}^{+\infty} R_y(l)e^{-j\omega l} = \underline{\lambda}S_x(\omega)\underline{\lambda}^H \tag{3.15}$$

Since $S_y(\omega)$ is an autospectral density it is nonnegative. Thus

$$S_y(\omega) = \underline{\lambda}S_x(\omega)\underline{\lambda}^H \geq 0 \tag{3.16}$$

and therefore $S_x(\omega)$ is nonnegative definite by definition [Gantmacher].

3.3. Spectral Factorization

3.3.1. Introduction to Spectral Factorization

We begin the discussion of the spectral factorization problem by examining some properties of linear filters. For a more detailed review of multichannel filtering issues see [Treitel]. Consider a linear multivariate system described by the $P\times P$ matrix impulse response sequence $h(k)$ with $P\times 1$ input vector sequence $\underline{w}(n)$ and $P\times 1$ output sequence $\underline{x}(n)$. The output sequence $\underline{x}(n)$ is specified by the convolutional relationship

$$\underline{x}(n) = \sum_{-\infty}^{+\infty} h(k)\underline{w}(n-k) \tag{3.17}$$

The $P\times P$ matrix transfer function associated with the filter is the Fourier

transform of the impulse response sequence and is given as

$$H(\omega) = \sum_{-\infty}^{+\infty} h(k) e^{-j\omega k} \tag{3.18}$$

When a linear system is excited by a random process input the output is also a random process. Furthermore if the input process is Gaussian then the output process is also Gaussian because linear transformations of Gaussian variables are also Gaussian[Papoulis(1965)]. We now develop expressions for the power spectrum of the output process $\underline{x}(n)$ when the input process $\underline{w}(n)$ is a stationary Gaussian process.

Let $\underline{dZ_w}(\omega)$ be the $P\times 1$ random spectral measure of the input process $\underline{w}(n)$. The random spectral measure of the output process, $\underline{dZ_x}(\omega)$, is then given by [Koopmans,Priestley]

$$\underline{dZ_x}(\omega) = H(\omega)\underline{dZ_w}(\omega) \tag{3.19}$$

The output power spectrum, $S_x(\omega)$, is defined as

$$S_x(\omega)d\omega = <\underline{dZ_x}(\omega)\underline{dZ_x}^H> \tag{3.20}$$

Substituting 3.199 into 3.20 yields

$$S_x(\omega)d\omega = H(\omega)<\underline{dZ_w}(\omega)\underline{dZ_w}^H>H^H(\omega) \tag{3.21}$$

The term inside the expectation brackets in 3.21 is recognized as the input power spectrum and is given as

$$S_w(\omega)d\omega = <\underline{dZ_w}(\omega)\underline{dZ_w}^H> \tag{3.22}$$

Substituting 3.22 into 3.21 yields the desired expression relating the input and output power spectra as

$$S_x(\omega) = H(\omega)S_w(\omega)H^H(\omega) \tag{3.23}$$

The spectral factorization problem as previously mentioned, is to find a realizeable linear system or algorithm which transforms a white input sequence into an output sequence which has a specified power spectrum. In this regard let $\underline{w}(n)$ be a $P\times 1$ input vector white noise sequence. A vector white noise sequence is a zero mean sequence with covariance matrix $R_w(l)$ given as

$$R_w(l) = <\underline{w}(n)\underline{w}^H(n-l)> = Q\,\delta_l \tag{3.24}$$

where δ_l is the Kronecker delta function which equals 1 for $l = 0$ and 0 otherwise. From 3.24 we see that the white sequence $\underline{w}(n)$ is uncorrelated at different times but may have correlation between components of the vector at a given time as specified by the Hermitian nonnegative definite matrix Q.

The power spectrum $S_w(\omega)$ of the white process is obtained by Fourier transforming 3.24 to obtain

$$S_w(\omega) = \sum_{l=-\infty}^{+\infty} R_w(l)e^{-j\omega l} = \sum_{l=-\infty}^{+\infty} Q\,\delta_l e^{-j\omega l} = Q \tag{3.25}$$

Substituting 3.25 into 3.23 yields the power spectrum $S_x(\omega)$ as

$$S_x(\omega) = H(\omega)QH^H(\omega) \tag{3.26}$$

We are now in a position to discuss the spectral factorization problem. Assume we wish to find a linear filter which when excited by a white noise input sequence has a specified output power spectrum $S_x(\omega)$. We see that this problem is equivalent to finding a stable, realizeable linear filter $H(\omega)$ and matrix Q satisfying 3.26. Two methods of approximately solving this problem are now presented.

3.3.2. Autoregressive Spectral Factorization

Autoregressive (AR) time series models are a class of linear models wherein the value taken by the time series at any given time is given as a linear combination of past values of the time series plus a white noise term. AR models have found widespread use in the areas of time series prediction and spectral anaylsis. The maximum entropy method of spectral analysis[Kay and Marple] is closedly related to AR model fitting. Applications of AR models have occurred in such diverse areas as geophysics[Ionnides], radar[Bower] and automatic control[Akaike(1970)].

In this section we define the AR model and derive equations relating the model parameters to the time series' covariance sequence. The utility of AR models for prediction and spectral analysis will be discussed as will the AR approximate solution to the spectrum factorization problem.

Consider a $P\times1$ complex, stationary, Gaussian time series $\underline{x}(n)$ with associated covariance sequence $R_x(l)$ and power spectrum $S_x(\omega)$. This time series is called an AR time series of order N (denoted by AR(N)) if it is generated by the following mechanism:

$$\underline{x}(n) = -\sum_{k=1}^{N} A_k \underline{x}(n-k) + \underline{w}(n) \tag{3.27}$$

where the model parameters A_k are $P\times P$ matrices and $\underline{w}(n)$ is a $P\times1$ white sequence with $P\times P$ covariance matrix Q. The sequence $\underline{w}(n)$ is uncorrelated with the sequence $\underline{x}(n)$ in the following sense:

$$<\underline{w}(n)\underline{x}^H(l)> = 0 \quad ; \; l < n \tag{3.28}$$

This is a consequence of the whiteness of $\underline{w}(n)$ and the causal generating mechanism of 3.27. The sequence $\underline{w}(n)$ is often called the innovations

sequence because it is the part of $\underline{x}(n)$ which is unpredictable and provides in a sense a "random shock" [Koopmans] or innovation to the time series.

We now derive the equations relating the AR model parameters to the time series $\underline{x}(n)$. The covariance sequence of $\underline{x}(n)$ is defined as

$$R_x(l) = <\underline{x}(n)\underline{x}^H(n-l)> \tag{3.29}$$

Postmultiplying 3.27 by $\underline{x}^H(n-l)$ and taking expectations yields

$$R_x(l) = <-\sum_{k=1}^{N} A_k \underline{x}(n-k)\underline{x}^H(n-l)> + <\underline{w}(n)\underline{x}^H(n-l)> \tag{3.30}$$

The second term in 3.30 may be expressed as

$$<\underline{w}(n)\underline{x}^H(n-l)> = <\underline{w}(n)[-\sum_{k=1}^{N} A_k \underline{x}(n-l-k) + \underline{w}(n-l)]^H >$$

$$= <-\sum_{k=1}^{N} \underline{w}(n)\underline{x}^H(n-l-k)A_k^H> + <\underline{w}(n)\underline{w}^H(n-l)> \tag{3.31}$$

From 3.28 the first term of 3.31 is zero for $l \geq 0$. For $l = 0$ the second term of 3.31 equals Q by definition. Thus we may write 3.30 as

$$R_x(l) = -\sum_{k=1}^{N} A_k R_x(l-k) + Q\delta_l \quad ; \; l \geq 0 \tag{3.32}$$

Defining A_0 to be the $P \times P$ identity matrix(denoted as $I_{P \times P}$) we may rewrite 3.32 as

$$\sum_{k=0}^{N} A_k R_x(l-k) = Q\delta_l \quad ; \; l \geq 0 \tag{3.33}$$

Evaluating 3.33 for $l=1,...,N$ yields a set of linear equations specifying the model parameters in terms of the process covariance sequence. These are given as

$$\begin{bmatrix} A_1 A_2 \cdots A_N \end{bmatrix} \begin{bmatrix} R_x(0) & R_x(1) & \cdot\ \cdot & \cdot & R_x(N-1) \\ R_x(-1) & R_x(0) & \cdot\ \cdot & \cdot & \cdot \\ \cdot & \cdot & \cdot\ \cdot & \cdot & \cdot \\ \cdot & \cdot & \cdot\ \cdot & \cdot & \cdot \\ \cdot & \cdot & \cdot\ \cdot & \cdot & R_x(1) \\ R_x(1-N) & R_x(2-N) & \cdot\ \cdot & R_x(-1) & R_x(0) \end{bmatrix} = -\begin{bmatrix} R_x(1) R_x(2) \cdots R_{x(N)} \end{bmatrix}$$

(3.34)

This set of equations is referred to as the block normal equations. The matrix in 3.34 has equal $P \times P$ covariance matrices along any diagonal and is termed a block Toeplitz matrix. If we let $l=0$ in 3.33 we obtain an equation relating the innovation sequence covariance matrix Q to the process covariance matrices as

$$Q = \sum_{k=0}^{N} A_k R_x(-k) \tag{3.35}$$

Finally, recall that the matrices $R_x(k)$ satisfy 3.3.

Assuming that the time series under consideration is truly a stationary AR process of order N (i.e., AR(N)) with N known and assuming that the process covariance matrices $R_x(l)$ are known exactly we may solve for the model parameters via 3.34. In practice it is seldom true that we know the process order N or the exact covariance sequence or even that the process is of AR type. However, given reasonably accurate estimates of the covariance matrices AR models of increasing order can be fit until one is found which adequately models the time series of interest. The issue of order selection for AR models is discussed in [Chamberlain,Akaike].

The AR model of 3.27 may also be viewed as a multivariate all-pole digital filter. The transfer function of this filter may be obtained with the aid of the z transform[Treitel]. The z transform of 3.27 is

$$\left[\sum_{k=0}^{N} A_k z^{-k}\right]\underline{X}(z) \equiv A(z)\underline{X}(z) = \underline{W}(z) \quad ; \; A_0 = I_{P\times P} \tag{3.36}$$

The matrix polynomial $A(z)$ defined in 3.36 is called the filter characteristic polynomial. The transfer function $H(z)$ is given as

$$H(z) = \underline{X}(z)\underline{W}^{-1}(z) = A^{-1}(z) \tag{3.37}$$

In order for the filter $H(z)$ to generate a stationary process the filter must be stable. The AR filter of 3.37 will be stable provided that the zeroes of the determinant of $A(z)$ are all inside the unit circle of the complex plane[Treitel]. Provided that the block covariance matrix of 3.34 is positive definite the filter A_k will specify a stable filter[Whittle]. The block covariance matrix in turn will be positive definite if the time series with which it is associated is purely nondeterministic[Weiner and Massani]. Basically nondeterminism means that there are no exact linear dependencies amongst the time series. That is, nondeterminism implies an inability to exactly predict any value of the time series from previous values of the series. We will comment on the relationship between AR models and the prediction problem shortly.

Given the transfer function $H(z)$ of 3.37 we are now in a position to evaluate the power spectrum $S_x(\omega)$ associated with the AR(N) process $\underline{x}(n)$. Evaluating $H(z)$ on the unit circle of the complex plane(i.e., $z = e^{j\omega}$) and substituting into 3.23 we obtain

$$S_x(\omega) = A^{-1}(\omega)Q[\,A^{-1}(\omega)\,]^H \tag{3.38}$$

where Q is the power spectrum of the white noise innovation sequence $\underline{w}(n)$.

We are now in a position to examine the AR solution of the spectral factorization problem. Assume we are given the power spectrum $S_x(\omega)$ of a process $\underline{x}(n)$ and we wish to find a filter which when excited by white noise has

output power spectrum equal to $S_x(\omega)$. Since $S_x(\omega)$ is known we may at least in theory use 3.4 to compute the associated covariance sequence $R_x(l)$. Given the covariance sequence we may then fit AR(N) models by 3.34 and 3.35. If the process $\underline{x}(n)$ is an AR(N) process and $R_x(l)$ is known exactly then the spectral factorization is solved exactly. Otherwise we obtain an approximate factorization of the spectrum. In general the approximation becomes better as N is increased. In fact for a nondeterministic process the covariance sequence of the obtained AR(N) model matches the given covariance sequence up to lag N [Inouye]. Thus as N is increased we match more and more of the given covariance sequence and hence get increasingly better fits to the given power spectrum. In Chapter 4 we discuss practical issues regarding the solution of the normal equations(3.34).

Before leaving the discussion of AR models we discuss briefly the ideas behind AR spectral estimation and AR linear prediction. Figure 3.1a shows a block diagram of an AR(N) filter. The input to the filter is a white sequence $\underline{w}(n)$ and the output $\underline{x}(n)$ is related to the input by 3.27.

Now consider the configuration of figure 3-1b. The part of figure 3-1b within the dashed box represents a one-step ahead linear predictive filter of order N [Tretter]. The linear predictive filter computes a minimum mean square error(MMSE) estimate of the current sample $\underline{x}(n)$ of a time series based upon the previous N samples. We denote this estimate as $\underline{\hat{x}}(n)$ where

$$\underline{\hat{x}}(n) = -\sum_{k=1}^{N} A_k \underline{x}(n-k) \tag{3.39}$$

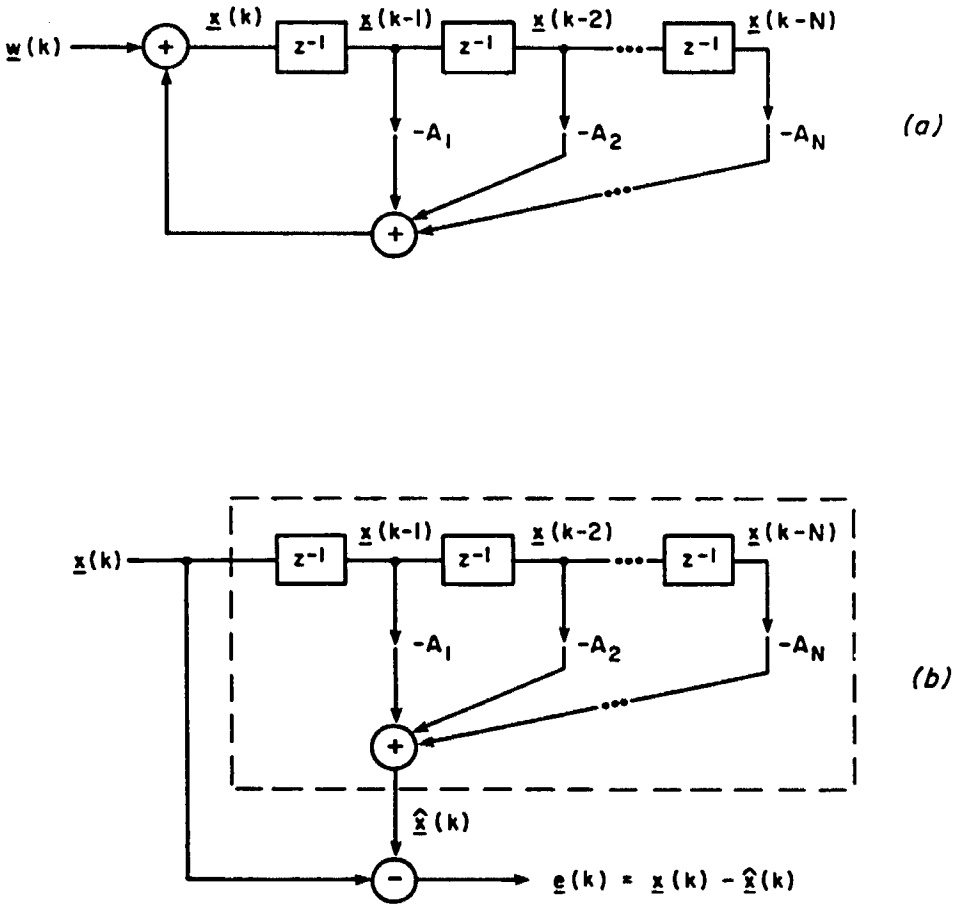

Figure 3-1) Autoregressive and Linear Predictive Filters

The coefficients A_k of 3.39 are chosen to minimize the mean square error(MSE) of prediction. The instantaneous prediction error is given as

$$\underline{e}(n) = \underline{x}(n) - \underline{\hat{x}}(n)$$

$$= \sum_{k=0}^{N} A_k \underline{x}(n-k) \quad ; \; A_0 = I_{P\times P} \tag{3.40}$$

Rewriting 3.40 as

$$\underline{x}(n) = \underline{\hat{x}}(n) + \underline{e}(n) \tag{3.41}$$

we see the similarity of the one-step prediction problem to AR model fitting(compare 3.41 and 3.27 and figures 3-1a and 3-1b).

In fact, by invoking the projection theorem in a Hilbert space of random vectors[Luenburger] the prediction filter coefficients A_k which minimize the MSE are found to satisfy the block normal equations 3.34. Thus we see that the procedure of fitting an AR(N) model to a time series and finding the MMSE linear predictive filter lead to the same set of equations(3.34). This result allows us to view an AR(N) time series as being composed of a predictable part, found by regressing over the previous N values, and an unpredictable part, the innovations sequence.

We now examine the structure of figure 3-1b assuming that $\underline{x}(n)$ is the input and $\underline{e}(n)$ is the output. We will call this filter a whitening filter for reasons to become apparent. Assume that the input sequence $\underline{x}(n)$ is truly an AR(N) time series. Furthermore assume we know the order N and the covariance $R_x(l)$ exactly. Then we can solve the MMSE prediction problem to obtain the A_k coefficients exactly. In this case we see that the output (or error) sequence $\underline{e}(n)$ corresponds to the AR innovations sequence and hence is a white sequence. Thus the whitening filter has taken a series $\underline{x}(n)$ with some

arbitrary spectrum as input and produced a sequence $\underline{e}(n)$ with a white spectrum as output. Hence the name whitening filter.

In most instances we do not know that a process which we want to predict is of order N or even that it is of AR type. In this case the whitening filter cannot completely whiten the input sequence. That is the output sequence will have nonzero temporal correlation. However, provided N is made large enough, the output sequence $\underline{e}(n)$ will be approximately white. Whitening filters find use in detection/estimation problems [Van Trees(1971),Knight,Wozencraft and Jacobs] where they are used to convert colored noise problems to a statistically equivalent white noise problems which are generally much easier to solve. Whitening filters also find use in spectral estimation problems where data are sometimes "pre-whitened" to minimize the distortions introduced by the unavoidable data windowing.

The transfer function of the whitening filter is obtained from figure 3-1b as follows. The output sequence $\underline{e}(n)$ is related to the input sequence $\underline{x}(n)$ by 3.40. Taking the z transform of 3.40 we obtain

$$\underline{E}(z) = \sum_{k=0}^{N} A_k \underline{X}(z) z^{-k}$$

$$= A(z)\underline{X}(z) \tag{3.42}$$

The whitening filter transfer function is then ($z = e^{j\omega}$)

$$H_w(\omega) = \underline{E}(\omega)\underline{X}^{-1}(\omega) = A(\omega) \tag{3.43}$$

Since the filter $H_w(\omega)$ takes a colored spectrum and shapes it into a white spectrum it makes intuitive sense in light of 3.43 that $A(\omega)$ have the inverse spectrum of $\underline{X}(\omega)$. That is, if $A(\omega)$ is an inverse of $\underline{X}(\omega)$ then the pro-

duct $\underline{E}(\omega) = \underline{A}(\omega)\underline{X}(\omega)$ will be constant(i.e., $\underline{E}(\omega)$ will be flat and hence $\underline{e}(n)$ will be white).

The use of AR models for spectral estimation can now be explained as follows. Given a set of data $\{\underline{x}(n)\}$ we estimate the covariance matrices $R_x(l)$ for lags l=0,1,2,...,N. Using 3.34 and 3.35 we then fit a whitening filter(or AR model) to this covariance. For N large enough the filter polynomial $A(\omega)$ will have a spectral shape which is approximately the inverse of the spectrum of the input data $\underline{x}(n)$. Hence an estimate of the spectrum of $\underline{x}(n)$ may be taken as the inverse of the spectrum of $A(\omega)$.

We note that so called maximum entropy methods of spectrum analysis yield estimates of the spectrum directly from the data without first estimating the covariance sequence. For information in this regard see [Haykin and Kessler].

3.3.3. Cholesky Spectral Factorization

The Cholesky spectral factorization method which we develop here is a multivariate generalization of a method proposed by Mitchell and McPherson for generating univariate stationary realizations of Gaussian processes. This discussion is brief because our primary interest is in the area of AR modeling. For univariate stationary processes the power spectrum $S(\omega)$ is nonnegative and orthogonal(3.8). For any frequency ω the value $S(\omega)d\omega$ represents the variance of the zero mean random spectral measure $dZ(\omega)$. For complex Gaussian processes the spectral measures $dZ(\omega)$ are also Gaussian. Thus, given a random number generator which generates normal, zero-mean, random phase, unit variance complex variates(i.e., N(0,1) variates) we may in

principle synthesize a realization of the spectrum $X(\omega)$ (note: this is not the power spectrum) by forming

$$X(\omega) = S(\omega)^{1/2} \times N(0,1) \tag{3.44}$$

Then in principle the process realization $x(n)$ can be obtained as the inverse Fourier transformation of 3.44.

The spectrum $S(\omega)$ is continuous for ω in the range $[-\pi,\pi]$. The aforementioned method is not realizeable in that an infinite number of N(0,1) random variates are needed(i.e., one for each ω). Thus we sample the spectrum $S(\omega)$ at M points in $[-\pi,\pi]$ and use discrete Fourier transforms(DFT) [Oppenheim and Schafer] to relate the sampled time and frequency domain realizations. The DFT relations are given as

$$X(k) \equiv X(\omega_k = \frac{2\pi k}{M}) = \frac{1}{M}\sum_{n=0}^{M-1} x(n) e^{-j\frac{2\pi}{M}kn} \quad ; \; k=0,1,\ldots,(M-1) \tag{3.45}$$

$$x(n) = \sum_{k=0}^{M-1} X(k) e^{+j\frac{2\pi}{M}kn} \quad ; \; n=0,1,\ldots,(M-1) \tag{3.46}$$

The procedure of Mitchell and McPherson is then to generate random samples of $X(\omega)$ at M points in $[-\pi,\pi]$ with

$$X(\omega_k) = \frac{S^{1/2}(\omega_k) \times N(0,1)}{M^{1/2}} \tag{3.47}$$

Then $x(n)$ is generated for $n=0,1,\ldots,(M-1)$ from 3.47 via 3.46. As pointed out in [Mitchell and McPherson] the sequence generated by this method will be periodic with period M and hence samples from the beginning of the sequence will be correlated with samples from the end of the sequence (i.e., correlation due to wraparound or circular effects). The degree of correlation, or the number of lags L_c at which this correlation is nonnegligible, is determined by the power spectrum bandwidth of the process. In practice the number of

samples M may be chosen large enough such that after discarding L_c samples from the beginning or end we obtain the requisite number of samples without the wraparound correlation problem.

The univariate realization generated by the above method has an autocorrelation function which approximates the desired autocorrelation sequence in the following sense. From 3.47 and the orthogonality of the spectrum we see that the frequency domain DFT coefficients are independent, zero mean and have variance $(\frac{1}{M})\,S(\omega_k)$. We form $x(n)$ as in 3.46 and ask the following question. Does the covariance $<x(n)x^*(n-l)>$ equal the desired covariance?

The desired covariance is given as

$$R(l) = \frac{1}{2\pi}\int_{-\pi}^{+\pi} S(\omega)e^{j\omega l}d\omega = \int_{-1/2}^{+1/2} S(f)e^{j2\pi fl}df \tag{3.48}$$

Thus

$$<x(n)x^*(n-l)> = \sum_{m=0}^{M-1}\sum_{n=0}^{M-1} <X(m)X^*(n)>e^{j\frac{2\pi}{M}[nm-(n-l)k]} \tag{3.49}$$

Because the frequency domain DFT coefficients are independent with variance $\left[\frac{1}{M}\right]S(\omega_k)$ we obtain

$$\begin{aligned} <x(n)x^*(n-l)> &= \sum_{m=0}^{M-1} <|X(m)|^2>e^{j\frac{2\pi}{M}ml} \\ &= \frac{1}{M}\sum_{m=0}^{M-1} S(\omega_k)e^{j\frac{2\pi}{M}ml} \end{aligned} \tag{3.50}$$

Because the temporal sampling period T_s is assumed equal to unity the frequency sampling increment is $\Delta f = \frac{1}{MT_s} = \frac{1}{M}$. Thus we see that 3.50

corresponds to a rectangular integration approximation to 3.48. Thus the obtained covariance function is not exact but is a good approximation for large M.

We generalize the Mitchell/McPherson method to complex multivariate Gaussian processes in the following discussion. Related results may be found in [Thompson]. The multivariate power spectrum is crossorthogonal and semipositive definite. Assume we sample the true spectrum at M points to get M $P\times P$ matrices $S_x(\omega_k)$ for $\omega_k = \frac{k2\pi}{M}$; $k=0,1,....,(M-1)$. Because each matrix is nonnegative definite there exists a lower triangular matrix $C_x(\omega_k)$, called the Cholesky factor[Golub], which satisfies

$$S_x(\omega_k) = C_x(\omega_k)C_x{}^H(\omega_k) \tag{3.51}$$

The Cholesky factorization together with the crossorthogonality of the random spectral measures provides us with a method for generating stochastic realizations of the sampled spectrum(not the power spectrum which is nonrandom) of a multivariate process $\underline{x}(n)$ with power spectrum $S_x(\omega)$.

Intuitively the Cholesky factor provides us with the linear transformation matrix neccessary to transform a $P\times 1$ vector $\underline{W}(\omega_k)$ of independent N(0,1) variates into a $P\times 1$ vector $\underline{X}(\omega_k)$ which has covariance matrix $S_x(\omega_k)$. Thus for each frequency ω_k we form

$$\underline{X}(\omega_k) = C_x(\omega_k)\underline{W}(\omega_k) \tag{3.52}$$

Then

$$\begin{aligned}\underline{<X}(\omega_k)\underline{X}^H(\omega_k)> &= C_x(\omega_k)\underline{<W}(\omega_k)\underline{W}^H(\omega_k)>C_x{}^H(\omega_k)\\ &= C_x(\omega_k)I_{P\times P}C_x{}^H(\omega_k)\end{aligned}$$

$$= C_x(\omega_k)C_x^H(\omega_k)$$

$$= S_x(\omega_k) \tag{3.53}$$

Finally we compute P inverse DFT's to obtain the time series $\underline{x}(n)$ as

$$\underline{x}(n) = \sum_{k=0}^{M-1} \underline{X}(\omega_k) e^{j\frac{2\pi}{M}kn} \tag{3.54}$$

Equation 3.54 is a vector notation to indicate that each vector component of $\underline{x}(n)$ forms a DFT pair with the corresponding component of $\underline{X}(k)$.

The time series realizations $\underline{x}(n)$ generated via the Cholesky method have the same wraparound correlation problem mentioned for the univariate case. Similarly to the univariate case the size of M can be chosen large enough to get the requisite number of samples without the undesired wraparound correlation. Likewise the Cholesky method yields a time series which has a covariance function which approximates the desired covariance function as in the univariate case(3.50). That is, the covariance function of the time series corresponds to a rectangular approximation to the Fourier integral of the desired power spectrum(i.e., multivariate version of 3.50). Implementation issues regarding the Cholesky method will be discussed in Chapter 4.

CHAPTER 4

Simulation Methodology

4.1. Introduction to Chapter 4

In this chapter we describe the computational procedures used to generate reverberation realizations and present supporting data from simulation experiments. In brief the reverberation simulation method is as follows. Given the range(or time) extent for which simulated data is desired we determine a range sampling interval at which we "sample" the reverberation power spectrum. That is, for each of a set of ranges we use the continuous scattering model of Chapter 2 to compute the power spectrum of the reverberation.

The choice of range sampling interval depends on how fast the power spectrum changes as a function of range and on the desired fidelity of the simulation. In general the spectrum of reverberation changes rapidly at short range and approaches a constant(i.e., range invariant) shape at long range. Thus, although we did not implement it here for convenience, a nonuniform range sampling scheme seems computationally efficient.

Next, utilizing either the Cholesky or AR methods discussed in Chapter 3 we generate a multivariate stationary Gaussian realization for each of the ranges. Then we window the stationary segments and add them together to form a unit mean square power nonstationary realization. Finally a range dependent intensity scaling is applied. The result is a reverberation realization which has time varying intensity and spectrum.

4.2. Computation of the Power Spectrum for a Fixed Range

In Chapter 2 we developed expressions relating the environment, geometry and sonar parameters to the power spectrum of reverberation at a fixed range. In this section we describe the computational procedures used to compute samples of this power spectrum. The sampled covariance function may then be obtained as the inverse discrete Fourier transform(DFT) of the sampled power spectrum.

The key equations from Chapter 2 are 2.31, 2.39, 2.60, and 2.65 which express the reverberation power spectrum as the convolution of the transmit pulse power spectrum, the random scatterer power spectrum and the sonar motional spectrum. For each desired type of reverberation; surface, volume or bottom, we compute the power spectrum. Then because of the assumed independence of scattering elements we add the power spectra together to give the total rverberation power spectrum at a given range.

We start by examining some sampling issues. As previously discussed the sonar is assumed to process temporally sampled complex signals. We further assume that antialiasing filters are used prior to sampling and are chosen such that the resultant filtered continuous complex signals are bandlimited to within the sonar system bandwidth. The temporal complex sampling frequency f_s is chosen equal to the sonar bandwidth. This choice satisfies the complex narrowband sampling theorem requirements stated in Chapter 1. We call f_s the complex sampling frequency to indicate that f_s complex numbers per second are obtained.

The sonar bandwidth is chosen based upon the bandwidths of the transmit signals to be employed and upon the maximum doppler shifts expected from targets. We consider the system bandwidth and hence the complex sampling frequency to be known parameters of the system.

The expressions for power spectra developed in Chapter 2 are for the continuous power spectral density. For digital computation we must sample these spectra at a finite number of points spanning the sonar bandwidth. As with temporal sampling the sampling of spectra(i.e., frequency sampling) requires that we satisfy a dual form of the sampling thereom. That is the frequency sampling period Δf is chosen to prevent time domain aliasing of the correlation functions. Note that this is the dual of the usual time domain sampling problem(i.e., we are attempting to prevent aliasing of the time domain functions instead of the frequency domain functions).

In order to choose Δf we must know the maximum expected width ("bandwidth") of the correlation function. This is equivalent to knowing the minimum signal bandwidth expected in operation. The minimum bandwidth reverberation signal which it is possible to receive is simply the transmit pulse of least bandwidth.

This is evident when one examines the convolutional form of the power spectra (see 2.31 for example). The convolution of two functions always results in a function which is broader than either of the individual functions unless one of them is an impulse function. If the sonar and scatters have zero velocity then both the motional and random scatterer spectra are impulsive and the received spectrum is of the same width as the transmit pulse spectrum.

In other words if the sonar has zero velocity and the scatterers are motionless then we receive backscattered replicas of the transmit pulse with no doppler shifts. Thus all the received energy lies at frequencies contained in the transmit pulse. If the sonar or scatterers or both are in motion however then the backscattered replicas are doppler shifted by varying degrees giving rise to a doppler spread received signal which has a spectrum broader than that of the pulse transmitted. The broader spectrum in turn implies a narrower correlation function.

In the simulation we choose Δf in a two step procedure. First we compute Δf based upon the minimum bandwidth transmit pulse. Then we reduce Δf such that we end up with N samples of the spectrum over the sonar bandwidth where N is a power of 2. This is done to allow use of a radix 2 fast Fourier transform(FFT) algorithm. We may now relate the sonar bandwidth BW, Δf, N and f_s as follows:

$$f_s = BW = N \times \Delta f \tag{4.1}$$

We now return to the problem of computing the power spectrum. Equations 2.31, 2.39, 2.60 and 2.65 are all of the same form. Hence we will discuss a general form of these equations given as

$$S_{ij}(f;t) = P_{ij}(t)\left\{Y(f) * W(f) * Z_{ij}(f;t)\right\} \tag{4.2}$$

In 4.2 the subscript ij refers to the i^{th} and j^{th} sonar beams, $P_{ij}(t)$ is the crosspower at time(range) t, $Y(f)$ is the random scatterer spectrum, $W(f)$ is the transmit pulse spectrum and $Z_{ij}(f;t)$ is the sonar motional spectrum. All of these functions except $W(f)$ depend on whether we are discussing volume or boundary reverberation. We will point out the computational procedures

appropriate to each as we proceed.

The random scatterer spectrum depends on the probablity density of the scatterer velocities. We assume that this density is zero mean Gaussian which in turn gives rise to a zero mean random scatterer spectrum $Y(f)$. The standard deviations of the scatterer velocities for volume and surface(recall that bottom scatterers are motionless) are simulation input parameters. The standard deviation of doppler frequency σ_{f_d} is related to the standard deviation of scatterer velocity σ_{sv} as

$$\sigma_{f_d} = \frac{2f_c}{C}\sigma_{sv} \tag{4.3}$$

where f_c is the carrier frequency and C is the sound velocity. Then $Y(f)$ is given as

$$Y(f) = \frac{1}{\sqrt{2\pi}\sigma_{f_d}} e^{\frac{-f^2}{2\sigma_{f_d}}} \tag{4.4}$$

Given $Y(f)$ we then sample it at $nfft$ points to get $Y(l\Delta f)$. In figure 4-1 we show a typical random scatterer spectrum. Note that this and all subsequent plots of spectra are plotted versus normalized digital frequency. Normalized digital frequency is the ratio of the actual frequency to the complex sampling frequency. The normalized digital frequency value of 0.0 corresponds to the actual frequency $\frac{-BW}{2}$ and the value 1.0 corresponds to $\frac{BW}{2}$. With this convention a signal with zero doppler shift will appear centered at a digital normalized frequency of 0.5 .

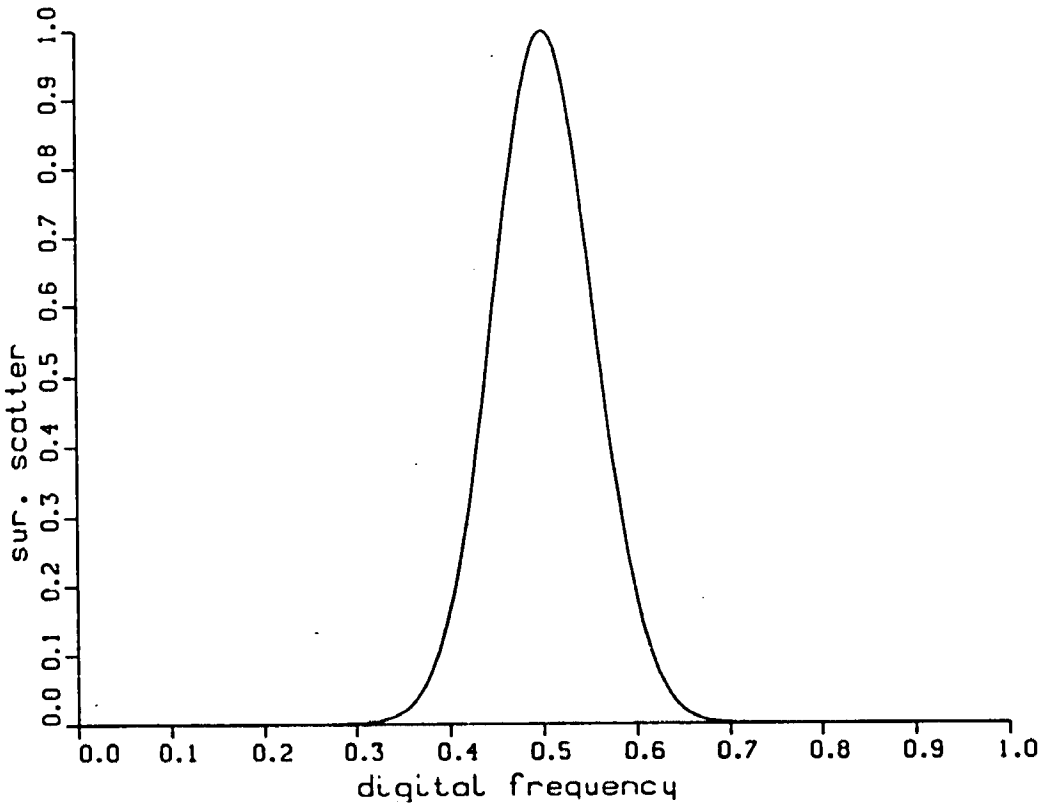

Figure 4-1) Typical Random Scatterer Spectrum

The transmit pulse spectrum $W(f)$ is the Fourier transform of the transmit pulse autocorrelation function(2.28) and is given as [Papoulis(1977)]

$$W(f) = |\tilde{X}(f)|^2 \tag{4.5}$$

where $\tilde{X}(f)$ is the Fourier transform of the transmit pulse $\tilde{x}(t)$. The transmit pulses used in the simulation are stored in sampled form $\tilde{x}(kT_s)$ on magnetic disk. Thus we use the FFT to compute samples of $W(f)$ at sampling interval Δf as

$$W(l\Delta f) = |\tilde{X}(l\Delta f)|^2 \quad ; \; l=0,1,\ldots,nfft \tag{4.6}$$

where $\tilde{X}(l)$ is the l^{th} DFT coefficient of the finite length sampled transmit pulse. In figure 4-2 we plot three transmit pulses used in simulation testing along with the associated power spectra.

The sonar motional spectrum $Z_{ij}(f;t)$ is the Fourier transform of 2.37 for volume reverberation and 2.63 for boundary reverberation. Because both $P_{ij}(t)$ and $Z_{ij}(f;t)$ are integral expressions we compute the product $P_{ij}(t)Z_{ij}(f;t)$ in one integration pass instead of computing them separately in two integration passes. We call this product the power scaled motional spectrum. We now examine computation of this quantity for the case of volume reverberation.

For volume reverberation the power scaled motional covariance is given as

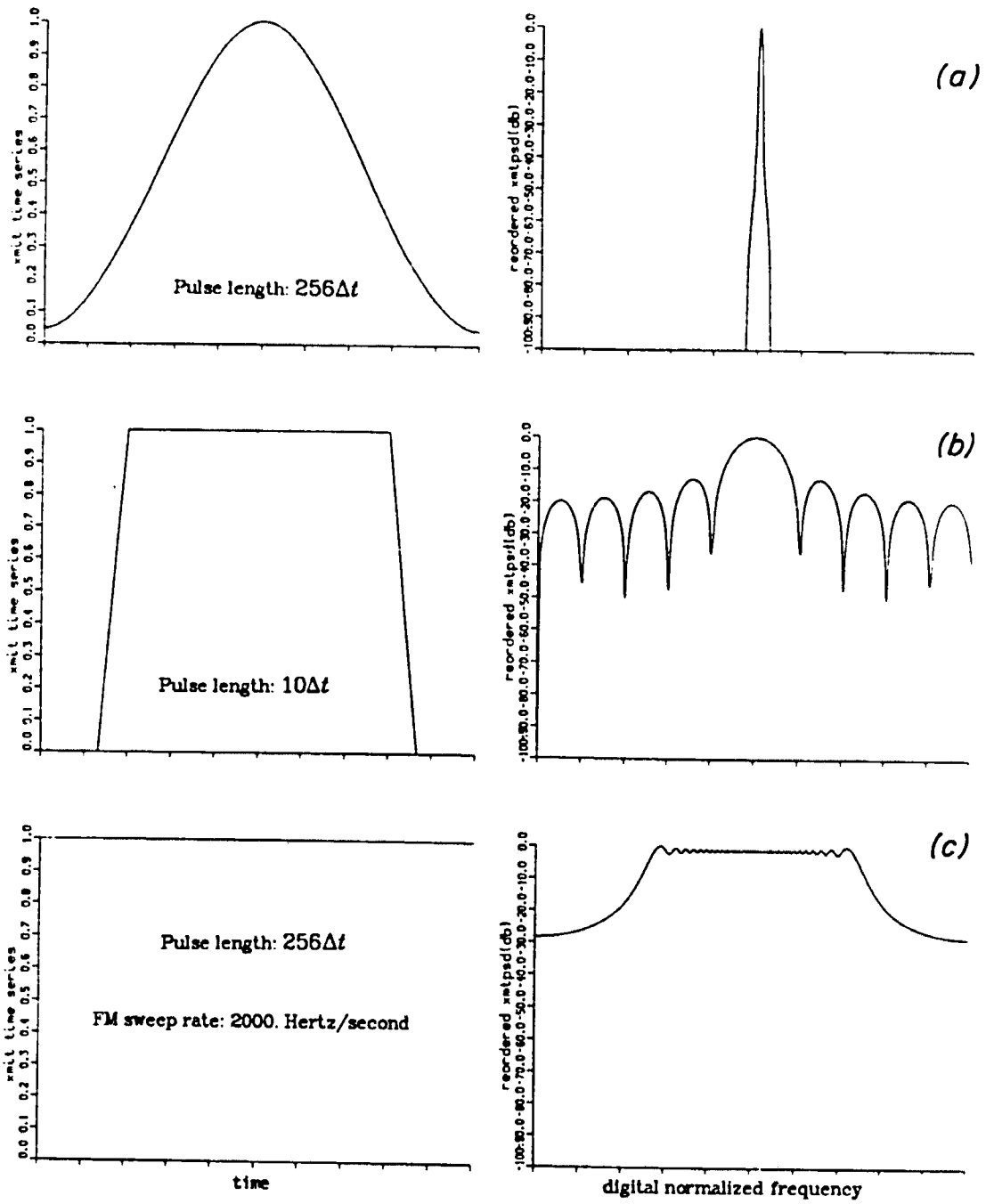

Figure 4-2) Transmit Pulses and Spectra

$$P_{ij}(t)Z_{Wij}(\tau;t) = E_t\sigma_V{}^2\frac{e^{-aCt}}{\frac{Ct^2}{2}}\int_\theta\int_\psi |B_T(\theta,\psi)|^2 B_{Ri}(\theta,\psi)B_{Rj}{}^*(\theta,\psi) \times$$

$$e^{\frac{j4\pi f_c \tau V_s \cos(\theta)\cos(\psi)}{C}}\cos(\theta)d\theta d\psi \qquad (4.7)$$

For a fixed range(i.e., fixed t) the term in front of the integral in 4.7 is a constant which may be computed from simulation input parameters as

$$K_V = \frac{E_t\sigma_V{}^2 e^{-aCt}}{\frac{Ct^2}{2}} \qquad (4.8)$$

The Fourier transform of 4.7 is the quantity which we need in order to be able to compute the power spectrum via 4.2. Taking the Fourier transform of 4.7 in the variable τ gives

$$P_{ij}(t)Z_{Wij}(f;t) = K_V\int_\theta\int_\psi |B_T(\theta,\psi)|^2 B_{Ri}(\theta,\psi)B_{Rj}{}^*(\theta,\psi) \times$$

$$\delta(f - \frac{2f_c V_s \cos(\theta)\cos(\psi)}{C})\cos(\theta)d\theta d\psi \qquad (4.9)$$

Equation 4.9 shows that a scatterer located at (θ,ψ) has a sonar platform motion induced doppler shift given by

$$f_p(\theta,\psi) = \frac{2f_c V_s \cos(\theta)\cos(\psi)}{C} \qquad (4.10)$$

We may interpret the power scaled motional spectrum(4.9) as the distribution of received reverberation crosspower as a function of doppler frequency with the influence of the transmit pulse spectrum and random scatterer spectrum removed(i.e., deconvolved).

Ultimately we require samples of the power scaled motional spectrum at frequency interval Δf. To obtain these samples we use the following scheme. First we break up the scattering volume into small rectangular elements as depicted in figure 4-3. We then compute a rectangular approximation to the double integral of 4.9. Each rectangular element corresponds to a unique (θ,ψ). This in turn implies a doppler shift $f_d(\theta,\psi)$ given by 4.10.

Note that the doppler shift $f_d(\theta,\psi)$ may not be equal to any of the frequencies $l\Delta f$ at which we sample the spectrum. Thus we use a quantizing scheme wherein we compute the crosspower for each rectangular cell as

$$K_V|B_T(\theta,\psi)|^2 B_{Ri}(\theta,\psi)B_{Rj}^*(\theta,\psi)\cos(\theta)\Delta\theta\Delta\psi \tag{4.11}$$

and then add it to the sample of the power scaled motional spectrum which lies closest in frequency to $f_d(\theta,\psi)$. In this way we account for all the received power(i.e., no power is lost due to it not returning at a frequency corresponding to one of the sampled frequencies $l\Delta f$). In 4.11 the variables $\Delta\theta$ and $\Delta\psi$ are the integration increments for each rectangular cell.

The power scaled motional spectrum for boundary reverberation is obtained in exactly the same manner as for volume reverberation except only a single integral need be computed. The resultant equation is

$$P_{ij}(t)Z_{Bij}(f;t) = K_B \int_{\psi} |B_T(\theta,\psi)|^2 B_{Ri}(\theta,\psi)B_{Rj}^*(\theta,\psi) \times \delta(f - \frac{2f_c V_s \cos(\theta)\cos(\psi)}{C})\cos(\theta)d\psi \tag{4.12}$$

where $\theta = \theta(\frac{Ct}{2})$ is a fixed range dependent constant and K_B is given as

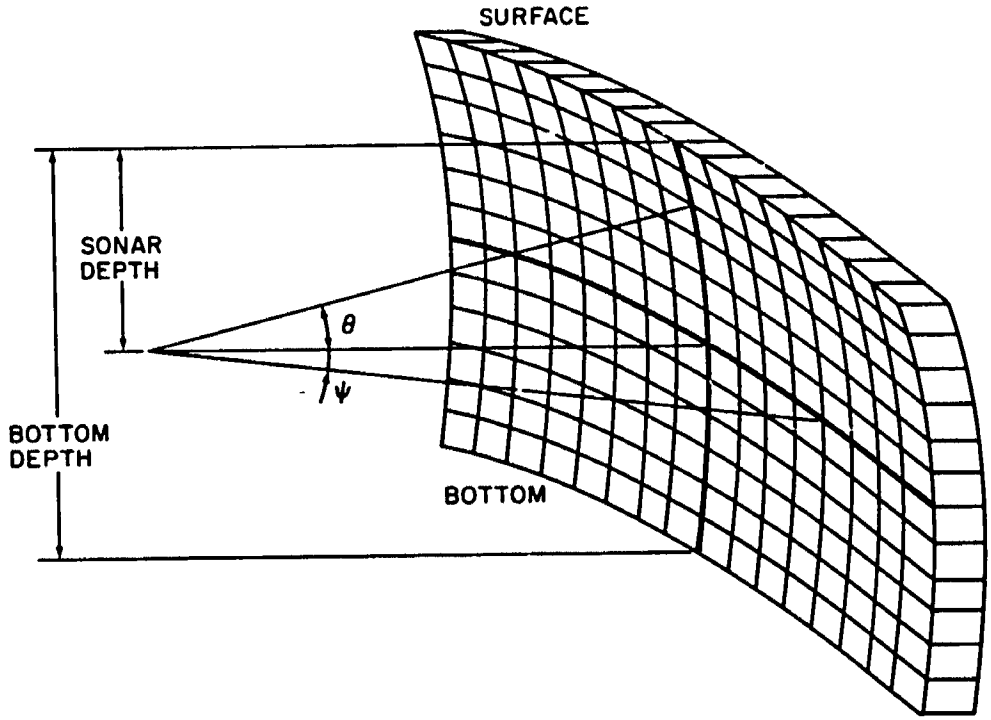

Figure 4-3) Volume Integration Grid

$$K_B = E_t \sigma_B{}^2 \frac{e^{-aCt}}{\frac{C^2 t^3}{4}} \tag{4.13}$$

In 4.13 $\sigma_B{}^2$ is the boundary scattering coefficient which generally depends on the grazing angle θ. The integration grid for boundary reverberation is shown in figure 4-4.

At this point we have at our disposal all of the functions needed to compute the power spectrum at a fixed range for either volume or boundary reverberation. The convolutions indicated in 4.2 are performed with the FFT algorithm. We append the neccessary number of zeroes to each spectrum so that the circular convolution implied by the FFT yields the desired linear convolution [Oppenheim].

We now present data from simulation experiments to demonstrate the aforementioned techniques. Figure 4-5 shows the motional spectrum of surface reverberation at a fixed range for three different beampatterns. Table 4-1 lists pertinent parameters for the experiment. In this and all subsequent experiments we use an omnidirectional transmit beam.

Parameter	*Value*	*Units*
Reverberation types	(surface)	
Pulse	Pure Tone Long	
Beampatterns	(omni,half-omni,narrow)	
Bottom depth	5000.	meters
Sonar depth	500.	meters
Sonar bandwidth	1000.	hertz
Carrier frequency	20000.	hertz
Sound speed	1500.	meters/second
Sonar speed	5.0	meters/second
Surface random scatter deviation	2.0	meters/second
Range to surface scatterers	2000.	meters

Table 4-1) Parameters for Beampattern/Motional Spectrum Experiment

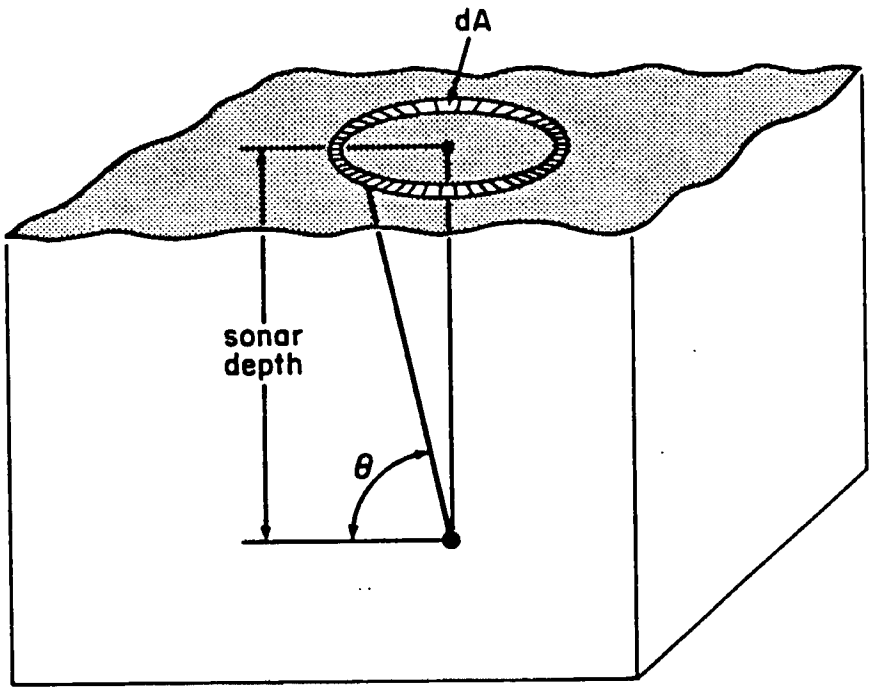

Figure 4-4) Boundary Integration Grid

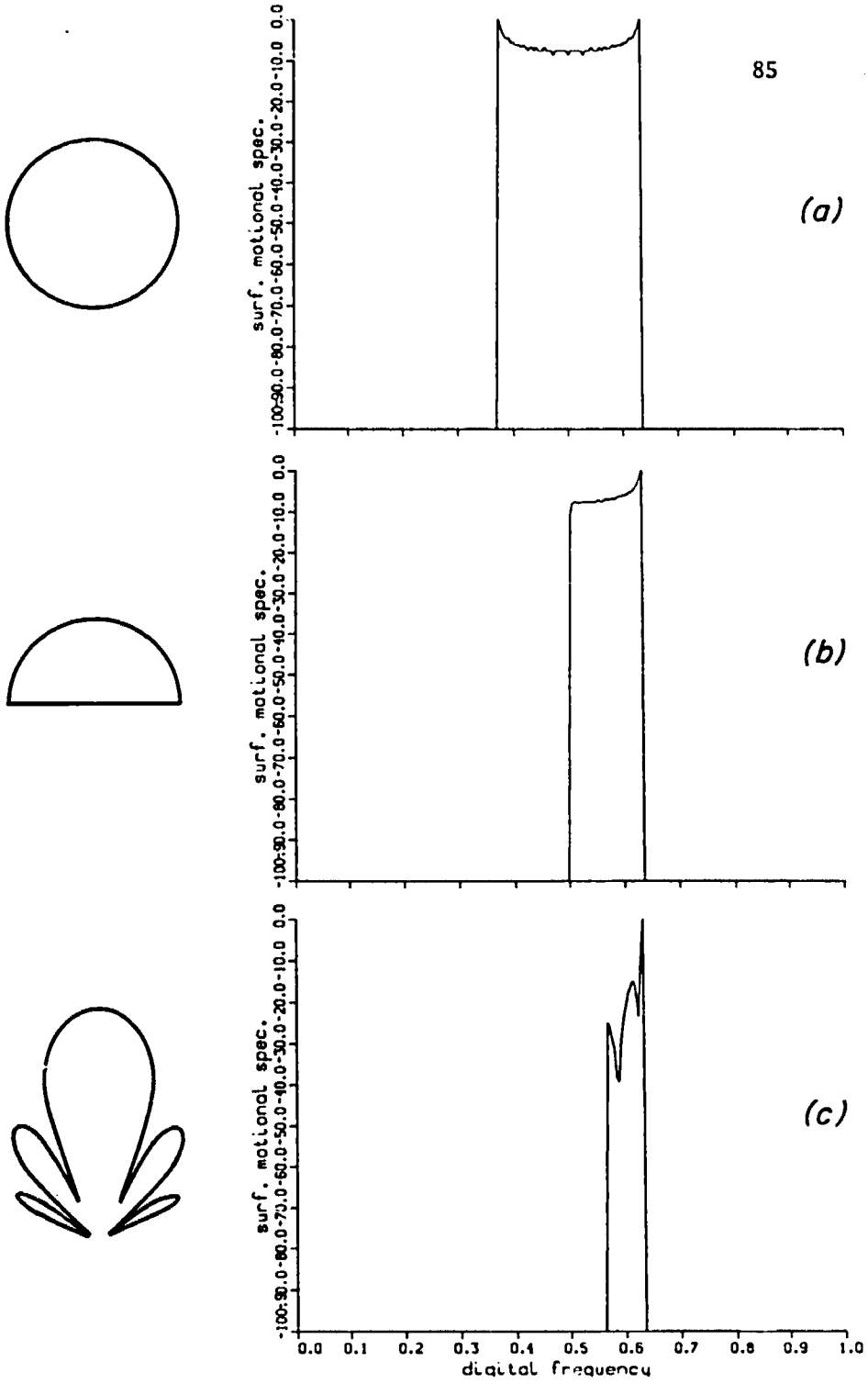

Figure 4-5) Beampatterns and Motional Spectra

In figures 4-5a, 4-5b and 4-5c we show the beampattern used on the left and the corresponding motional spectrum on the right. Note that because this example is for surface reverberation we only need plot the beampattern versus the azimuthal variable ψ.

Note in figure 4-5a that the omni beam motional spectrum is symmetric about zero hertz(i.e., 0.5 normalized digital frequency). This is because the omni beam receives an equal number of positive doppler shifted signals from scatterers in front as it does negative doppler shifted signals from scatterers behind it. Scatterers located directly in front or behind are associated with the maximum plus and minus doppler shifts respectively whereas scatterers located to either side are associated with doppler shifts close to zero hertz. The shape of the omni motional spectrum(figure 4-5a) is correct for scattering from a surface[Lacy].

Figure 4-5b shows the motional spectrum for the half omni beam. In this case the sonar receives only positive doppler shifted signals and hence the motional spectrum is simply the positive part of the omni beam spectrum(figure 4-5a).

Finally in figure 4-5c we show the motional spectrum for a narrow forward facing beam. This beampattern corresponds to an ideal piston with 10 degrees between 3db down points[Urick]. In this case the ensonified scatterers are concentrated in a small forward facing angular sector and hence the motional spectrum is concentrated in a small positive doppler shifted band of frequencies. We will use these same three beampatterns for examples throughout the remainder of this dissertation and will refer to them as the omni beam, half omni beam and narrow beam.

Next we demonstrate the effect of different transmit pulses on the power spectrum. In figure 4-6 we show the result of convolving the three different transmit pulse spectra of figure 4-2 with the motional spectrum shown in figure 4-5c. In all three cases the scatterers are assumed to be motionless and hence the random scatterer spectrum is an impulse function and does not influence the resultant power spectrum shape. The power spectra shown in figures 4-6a, 4-6b and 4-6c correspond to the PTL , PTS and LFM pulse respectively.

Figure 4-7 shows the same cases as in figure 4-6 but for the situation where the surface scatterers have Gaussian random velocities with a standard deviation of 2.0 meters/second. The random scatterer spectrum is that shown in figure 4-1. Note that the resultant spectra are wider and smoother than those of figure 4-6 due to the additional convolution with the Gaussian spectrum.

Figure 4-8 shows data for a case where the sonar has two beams(omni and narrow) with identical phase centers, the PTL transmit pulse is used, the random scatterer spectrum of figure 4-1 is used and the geometry is that shown in figure 4-5a. Figure 4-8a shows the motional spectrum, power spectrum and correlation functions for the narrow beam. Figure 4-8c shows the same for the omni beam. Figure 4-8b shows the cross motional spectrum magnitude, cross power spectrum magnitude and cross correlation function magnitude for the two beams. Note in particular that the crossspectrum is nonzero only over the band of frequencies where both beams have nonzero power and that the correlation function widths vary inversely with the widths of the corresponding spectra.

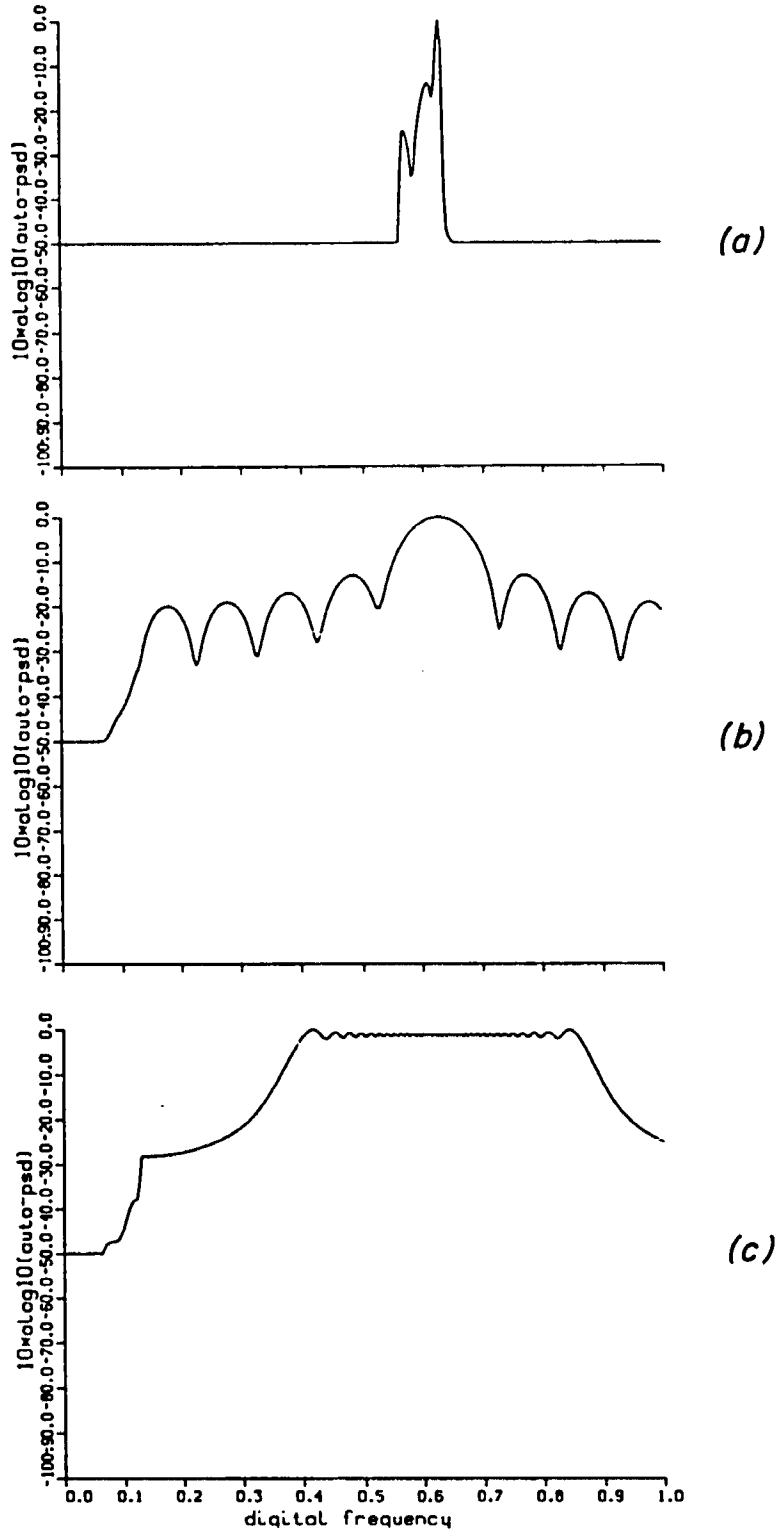

Figure 4-6) Pulse Spectra Convolved with Motional Spectrum

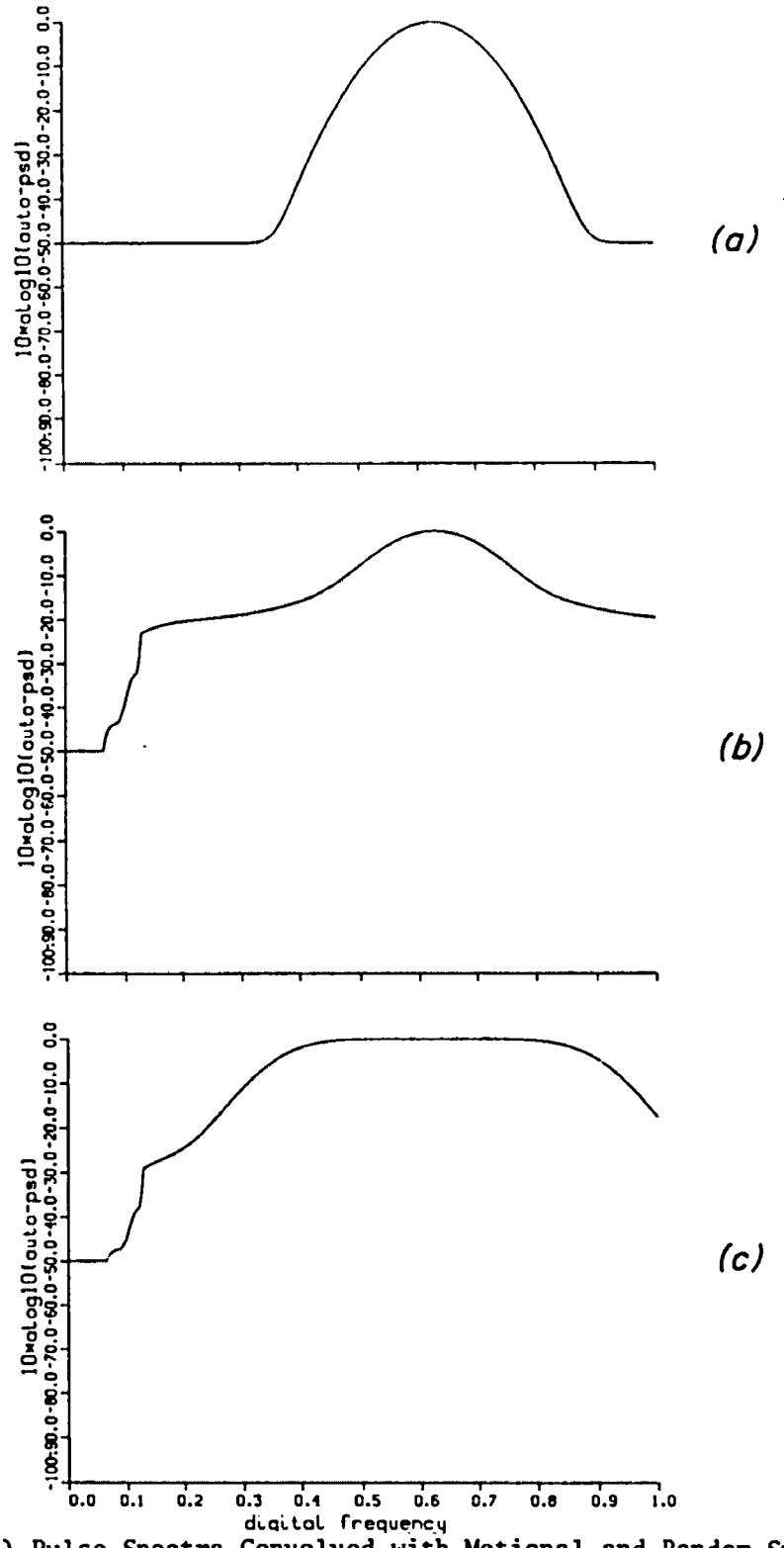

Figure 4-7) Pulse Spectra Convolved with Motional and Random Spectra

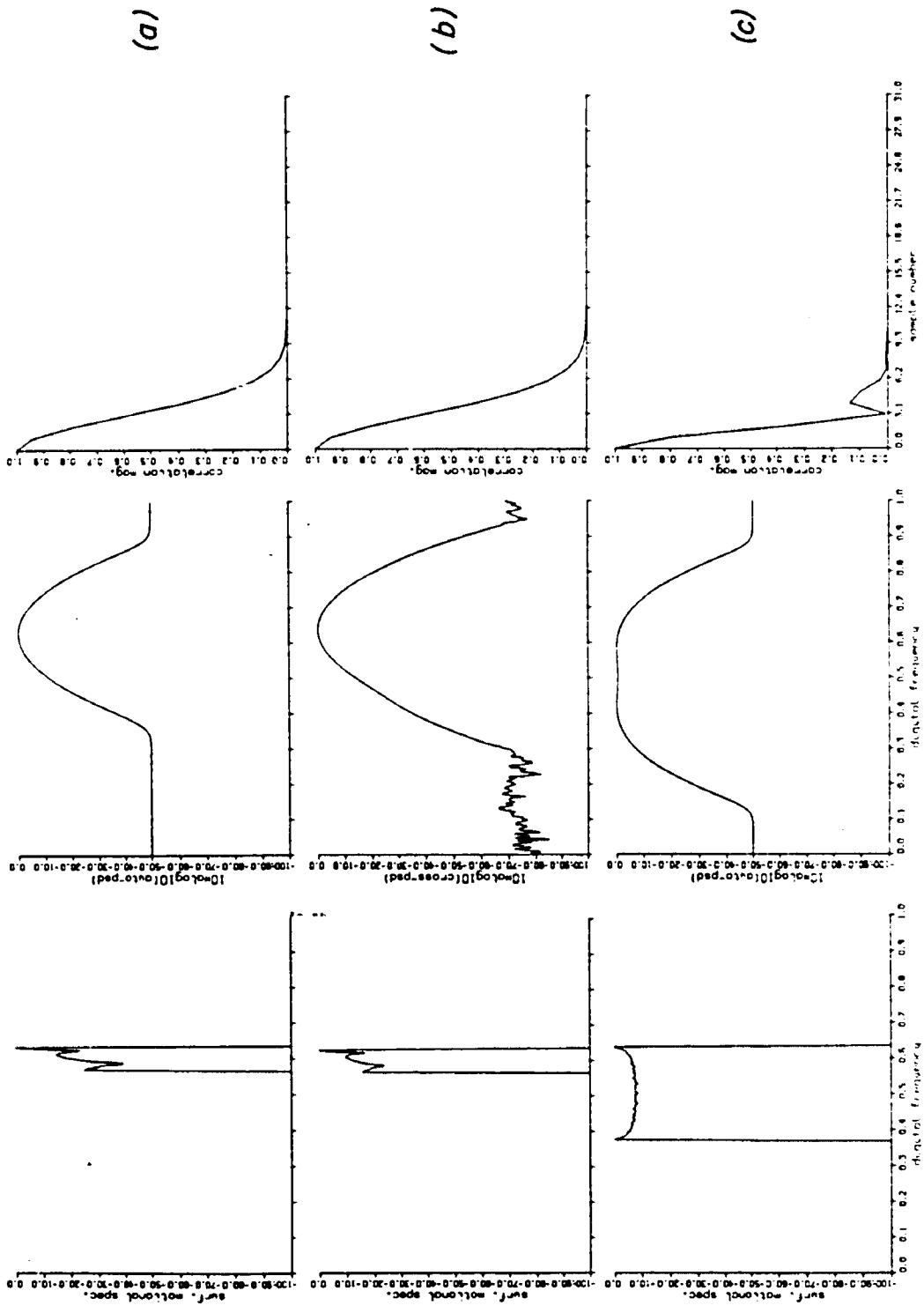

Figure 4-8) Motional/Power Spectra and Correlation Functions

4.3. Generating Stationary Sequences

In this section we describe the numerical procedures used to generate stationary sequences. Both the Cholesky and AR method are covered. We begin with a discussion of the AR method.

In section 3.3 we developed equations 3.34 and 3.35 which relate the AR model parameters to the matrix covariance function of a multivariate complex stationary process. In section 4.2 we developed the methods by which we obtain the process power spectrum and covariance for a fixed range. Given the $P \times P$ matrix covariance sequence $R_x(l)$ we may form the linear system of equation 3.34. Because the matrix in 3.34 has a special form(i.e., block Toeplitz) there exist fast order recursive algorithms [Wiggins and Robinson, Akaike(1970), Haykin and Kesler, Strand] for solving the system. By order recursive we that the N^{th} order system of 3.34 is solved by first solving the 1^{st} order block system and then using that solution to solve the 2^{nd} order block system, etc... until finally we obtain the desired N^{th} order solution in terms of the $(N-1)^{st}$ order block solution.

We programmed an order recursive algorithm to solve the system 3.34 and found that the algorithm did not yield accurate solutions. Thus we decided to abandon the order recursive algorithm and employ orthogonal matrix decomposition solution methods[Lawson and Hanson]. We examined two orthogonal decompositions, the singular value decomposition(SVD) and the Householder/Givens(QR) method.

Both the SVD and QR algorithms are available as FORTRAN algorithms in the Linpack software package[Dongarra]. As both of these methods worked

equally well in terms of accuracy and speed we discuss only one of them, the QR algorithm. First we rewrite the block normal equations(3.34) symbolically as

$$A^H \hat{R} = Z^H \tag{4.14}$$

where

$$A^H = \left[A_1 A_2 \cdots A_N\right] \tag{4.15}$$

$$Z^H = -\left[R_x(1)R_x(2) \cdots R_x(N)\right] \tag{4.16}$$

and $\hat{R}$ is the block matrix of 3.34. Noting that the matrix $\hat{R}$ is a Hermitian matrix(i.e., $\hat{R} = \hat{R}^H$) we take the Hermitian transpose of 4.14 to obtain

$$\hat{R}A = Z \tag{4.17}$$

Denote the j^{th} columns of A and Z as a_j and z_j respectively. Then we need to solve the system

$$\hat{R}a_j = z_j \tag{4.18}$$

for j=1,2,...,P. The QR decomposition expresses the matrix $\hat{R}$ as

$$\hat{R} = QR \tag{4.19}$$

where Q is a unitary matrix(i.e., $QQ^H = I$) and R is an upper triangular matrix. Then we may express 4.18 as

$$QRa_j = z_j \tag{4.20}$$

Premultiplying both sides of 4.20 by Q^H gives

$$Q^H QRa_j = Ra_j = Q^H z_j = z'_j \tag{4.21}$$

Thus we need to solve

$$Ra_j = z'_j \tag{4.22}$$

Note that the QR decomposition need only be computed once. Then we use the matrix Q to form the right hand side vectors z'_j for j=1,2,...,P as indi-

cated in 4.21.

Using the solutions a_j obtained from 4.22 we then obtain the matrix A^H of 4.15 from which we may obtain the $P\times P$ matrices A_k for $k=1,2,...,N$. The final step in obtaining the AR model is to solve 3.35 for the innovations sequence covariance matrix Q (not to be confused with the matrix Q of the QR decomposition).

In figure 4-9 we depict the AR realization scheme for P sonar beams. The $P\times 1$ vector sequence $\underline{w}(n)$ is a white sequence with covariance matrix $I_{P\times P}$. The $P\times 1$ sequence $\underline{v}(n)$ is a white sequence with the desired innovations covariance Q. We use the Cholesky factor of Q, denoted as $Q^{1/2}$(i.e., matrix square root),to form $\underline{v}(n)$. Thus we have

$$Q = Q^{1/2}\,(Q^{1/2})^H \tag{4.23}$$

$$\underline{v}(n) = Q^{1/2}\underline{w}(n) \tag{4.24}$$

$$\begin{aligned}<\underline{v}(n)\underline{v}^H(n)> &= Q^{1/2}<\underline{w}(n)\underline{w}^H(n)>(Q^{1/2})^H \\ &= Q^{1/2}I_{P\times P}(Q^{1/2})^H \\ &= Q\end{aligned} \tag{4.25}$$

Finally we drive the AR filter with the innovations sequence $\underline{v}(n)$ to obtain the output sequence $\underline{x}(n)$ with covariance sequence approximating $R_x(l)$.

We now present an example of the AR scheme. We use the two beam example associated with table 4-1 and figure 4-8. In figure 4-10 we show the desired spectrum on the left, the AR model spectrum in the center and the unwindowed periodogram spectrum estimate of a realization on the right. The top plots correspond to the wide beam spectra, the bottom plots to the narrow beam spectra and the middle plots to the cross spectra. The AR model order is 25(i.e., AR(25)). Note the close match to the desired spectrum

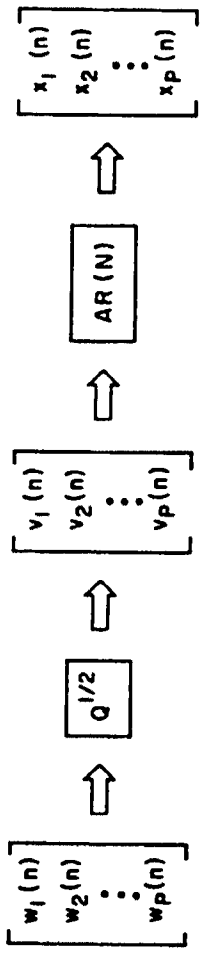

Figure 4-9) Autoregressive Realization Scheme

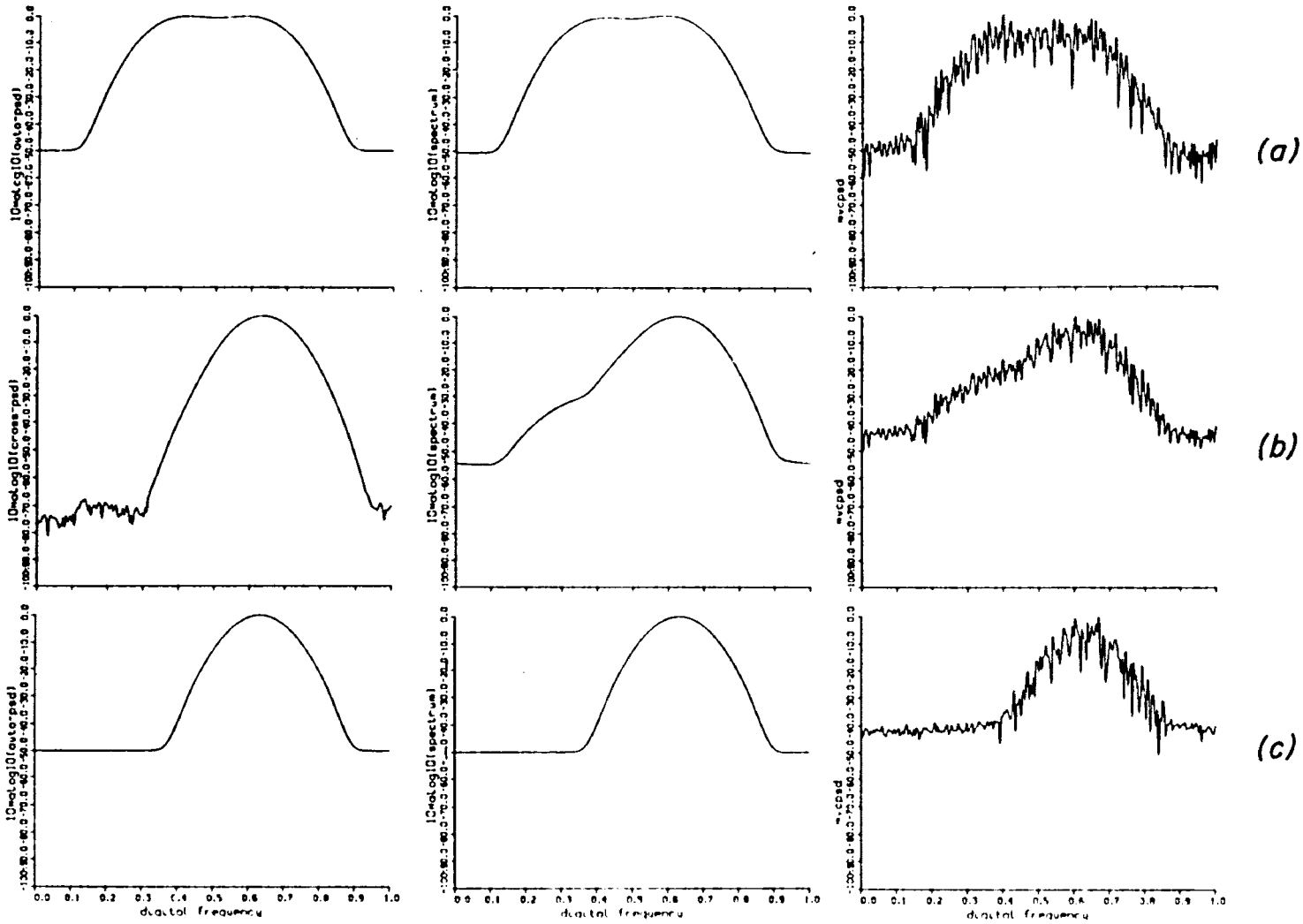

Figure 4-10) Autoregressive Transfer Functions and Realization Spectra

of figure 4-8. We note that we did not study the model order selection problem in detail. Rather we were interested in demonstrating the concept of AR model fitting in general. Chamberlain discusses various criterion which one may use to choose the order. We determined empirically that a 25^{th} order model yields a transfer function which matches the desired spectrum closely enough for demonstrative purposes.

We now briefly discuss the Cholesky spectrum factorization method of generating stationary realizations. The pertinent equations were developed in section 3.4. We assume that we desire a vector output sequence $\underline{x}(n)$ of length M where M is a power of two which has been chosen large enough to take care of the wraparound correlation problem discussed in section 3.4.

Thus in accordance with equation 3.52 we use the Cholesky factors $C_x(f_k)$ of the desired power spectrum $S_x(f_k)$ for $k=0,1,\ldots,(M-1)$ to compute frequency domain realizations $\underline{X}(f_k)$ as

$$\underline{X}(f_k) = C_x(f_k)\underline{W}(f_k) \tag{4.26}$$

Given the frequency domain realization we then use 3.54 to compute the time domain realization $\underline{x}(n)$ as the inverse DFT of $\underline{X}(f_k)$. We depict the Cholesky factor method in figure 4-11 for the case of P beams.

We now present an example of the Cholesky method. We use the same example as we did for the AR case(i.e., table 4-1 and figure 4-8). Figure 4-12 shows the resultant spectrum of the realization.

4.4. Nonstationarity

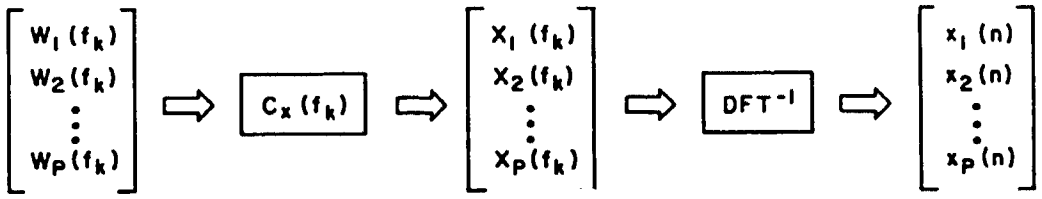

$$k = 0, 1, \cdots, (M-1)$$

$$\langle X_i(f_k)\ X_j^*(f_k) \rangle = S_{x_{ij}}(f_k)\ \delta_{ij}(f_k)$$

Figure 4-11) Cholesky Realization Scheme

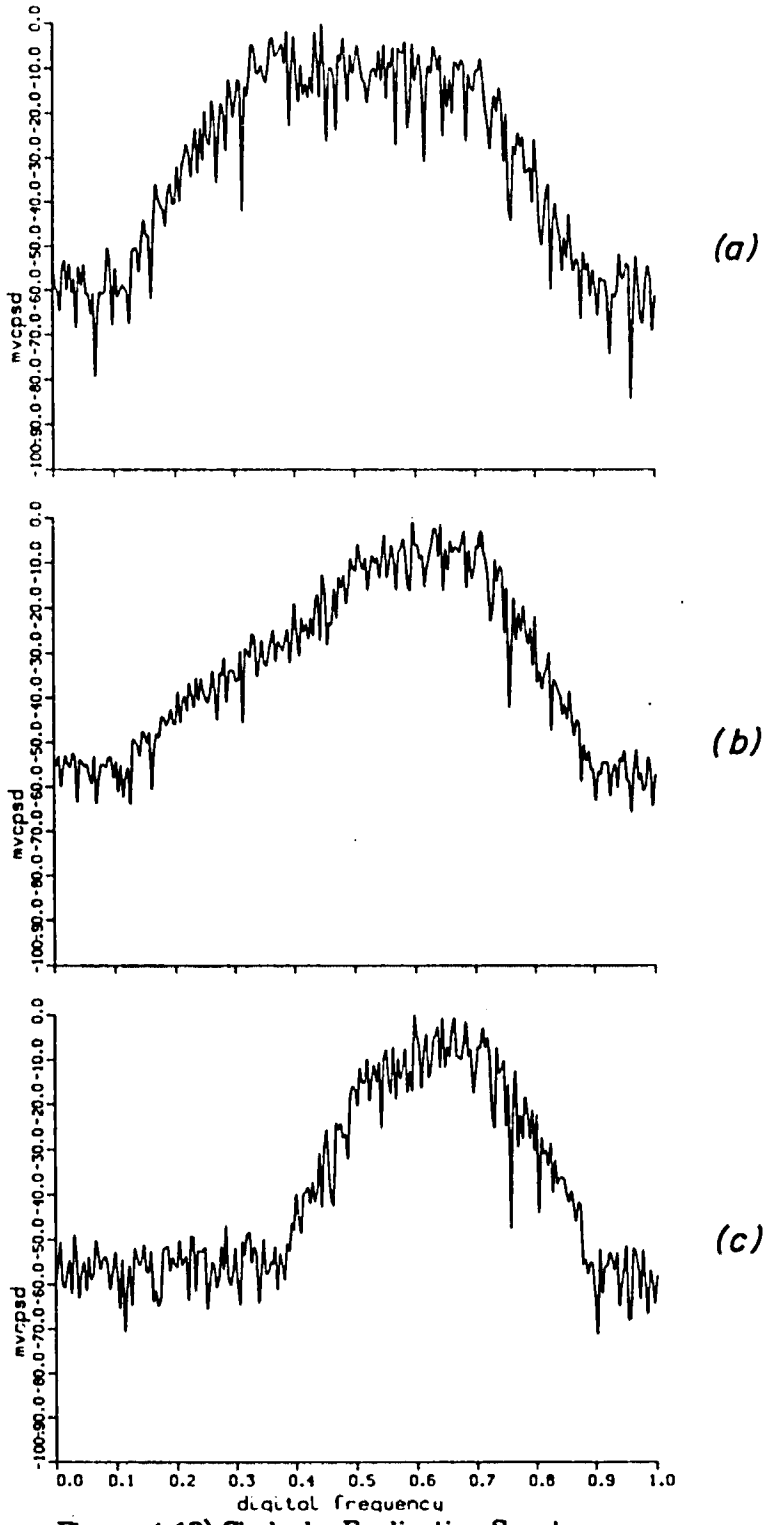

Figure 4-12) Cholesky Realization Spectrum

In this section we describe the method used to combine stationary realizations corresponding to fixed ranges such that the resultant time series has a spectral shape and average power which vary with range(time). The stationary realizations may have been generated by either the AR or Cholesky method. We assume that each stationary realization has been normed to unit mean square power initially. The weighting procedure developed by Mitchell and McPherson is used to combine the sequences. The method in brief is to apply a window to each stationary realization and to add the windowed, overlapping realizations together.

The weighting sequence, say $w(k)$, is chosen to be symmetric, to taper to zero at the ends for good spectral sidelobe performance and to conserve power in the transition region where the subsequences overlap. Mitchell and McPherson derive a family of weighting functions possessing the desired properties. From this family we chose the following window for our purposes:

$$w_k^2 = \begin{cases} .5\left(\frac{k}{N}\right)^3 & ;0 \le k \le \frac{N}{2} \\ 1-.5\left[2\left(1-\frac{k}{N}\right)\right]^3 & ;\frac{N}{2} < k \le N \end{cases} \tag{4.27}$$

In figure 4-13 we plot overlapped copies of the window to show how the subsequences overlap and to show the window shape. As previously mentioned we desire that the window have low sidelobes. That low sidelobes are desireable is evident when one realizes that each subsequence is multiplied by the window and hence the spectrum of each subsequence is convolved with the spectrum of the window. Thus undesireably high sidelibes will cause high spurious sidelobes in the spectrum of the windowed subsequence. In figure 4-14 we plot the spectrum of the window given by 4.27. Note that the first

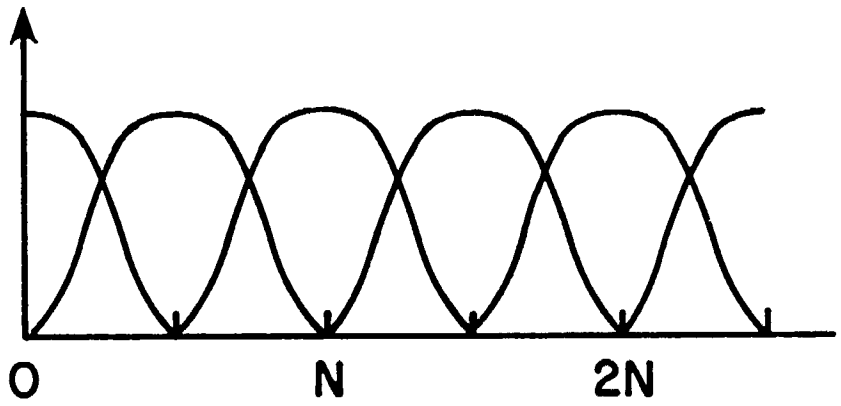

Figure 4-13) Overlapped Mitchell/McPherson Windows

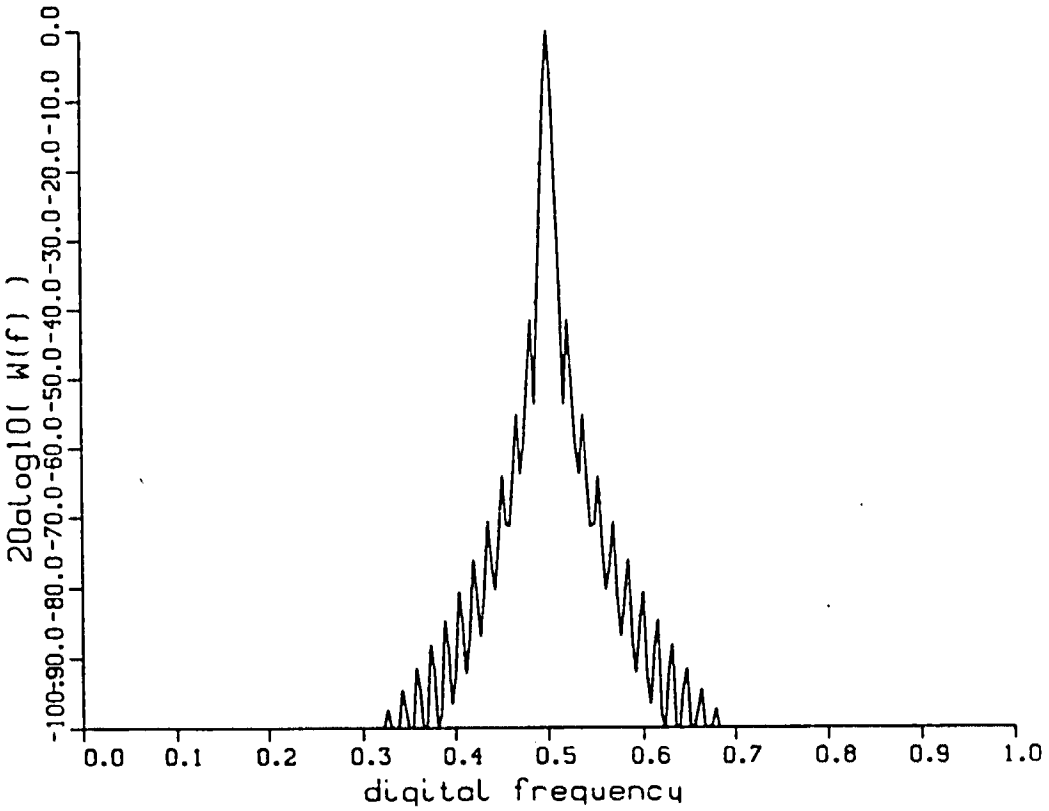

Figure 4-14) Spectrum of Mitchell/McPherson Window

sidelobe is more than 40db down from the main lobe. An additional constraint on the window spectrum is that it be much narrower than any important spectral feature of the reverberation power spectrum.

Applying the aforementioned techniques for merging the unit mean square power subsequences we obtain a unit mean square power sequence which has a time varying spectrum. The final step in dealing with the reverberation nonstationarity is to apply a time(range) dependent scaling to force the sequence to have the proper time varying mean square power. The mean square power is computed concurrently with the motional spectrum for a fixed range as discussed in section 4.4. We use a cubic spline interpolation to generate the power scaling function at ranges(times) between the range sampling points.

4.5. Simulation Experiments

In this section we present results from five simulation experiments. All five experiments use the AR spectral factorization method. In figure 4-15 we show the geometry of the first experiment. The experimental parameters are listed in Table 4-2. The chosen values of maximum range and range increment provide 8 "samples" of the reverberation power spectrum and require determination of 8 corresponding AR(25) filters. Because of the bottom depth and maximum range only volume and surface reverberation are received.

Examination of the geometry shows that the surface is not ensonified by the transmit pulse for the first 1000. meters. Thus only volume scatterers contribute initially. The standard deviation of the volume random scattering spectrum is small relative to the standard deviation of the surface random

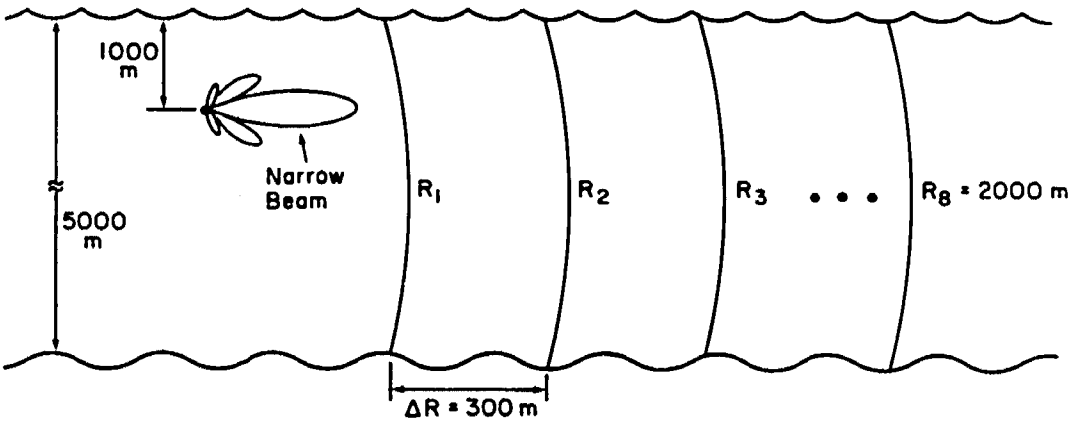

Figure 4-15) Geometry of Experiment 1

Parameter	*Value*	*Units*
Reverberation types	(surface,volume)	
Pulse	Pure Tone Long	
Beampatterns	(narrow)	
Bottom depth	5000.	meters
Sonar depth	1000.	meters
Sonar bandwidth	1000.	hertz
Carrier frequency	20000.	hertz
Sound speed	1500.	meters/second
Sonar speed	1.0	meters/second
Surface random scatter deviation	3.0	meters/second
Volume random scatter deviation	0.1	meters/second
Maximum range	2000.	meters
Range sampling increment	300.	meters

Table 4-2) Parameters for Experiment 1

scattering function so that the power spectrum would broaden considerably when the surface is ensonified. In addition the volume scattering strength is small relative to the surface scattering strength so that the surface reverberation dominates the spectral shape for ranges greater than 1000. meters.

In order to examine the spectral properties of the simulated reverberation time series we present plots of the reverberation spectrum versus range(time). We refer to these plots as spectrograms. To compute the spectrogram we first scale the reverberation sequence such that the mean square power is constant as a function of range(time). Next we break the resultant sequence up into short contiguous subsequences. The subsequences are chosen short enough that they may be considered stationary. Then a 50 db Taylor window[Harris] is applied to each subsequence and the periodogram [Oppenheim and Schafer] spectral estimate computed. Finally the subsequence spectra are plotted versus range.

In figure 4-16a we show the spectrogram computed from a reverberation sequence generated for the first experiment. The dynamic range of this and all subsequent spectrogram plots is 60 db. Because the reverberation is a random process realization the spectrogram of figure 4-16a has a jagged apppearance. In order to see the spectral shape more clearly we smooth each periodogram with a Daniell smoothing algorithm[Bloomfield]. We call the resultant plot a smoothed spectrogram. The smoothed spectrogram for this example is shown in figure 4-16b.

In both figures 4-16a and 4-16b the change from volume dominated reverberation to surface dominated reverberation is clearly visible. Note that the Mitchell/McPherson windowing scheme described in the previous section works. That is, the spectrum changes smoothly from the narrow volume dominated shape to the broader surface dominated shape and is not unduly distorted by spurious sidelobes. To further elucidate the changing spectral shape with range we plot contours of the smoothed spectrogram in figure 4-16c.

In figure 4-17 we plot the real part of the complex envelope of the reverberation time series for this example. For this and all subsequent time series plots we have not applied the final time varying power scaling. That is, the average power of the time series in the plots is constant over time. The change from the narrow volume dominated spectrum to the broader surface dominated shape is evident in this figure at about 2.0 seconds.

The second example deals with surface reverberation only. The geometry of the second example is shown in figure 4-18 and the parameters are listed in Table 4-3. The intent of this experiment is to show that the

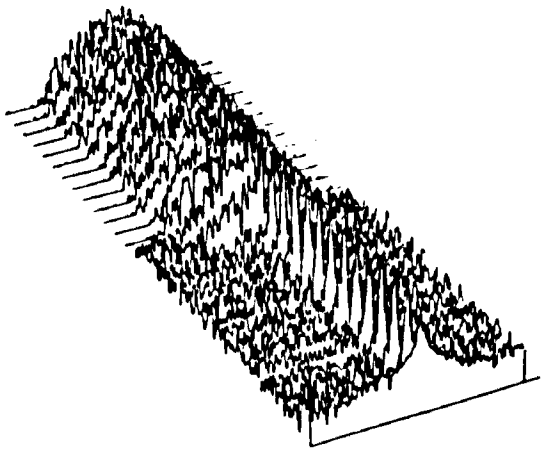

(a)

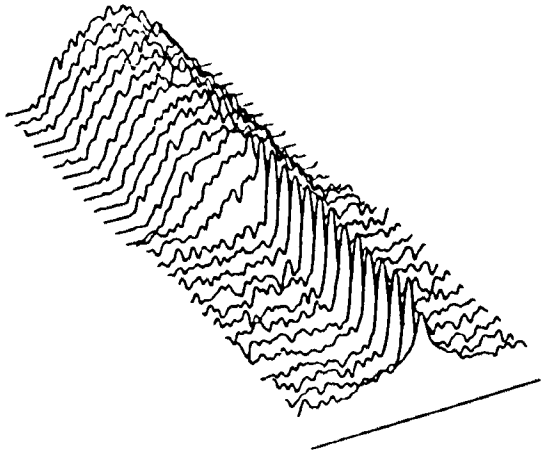

(b)

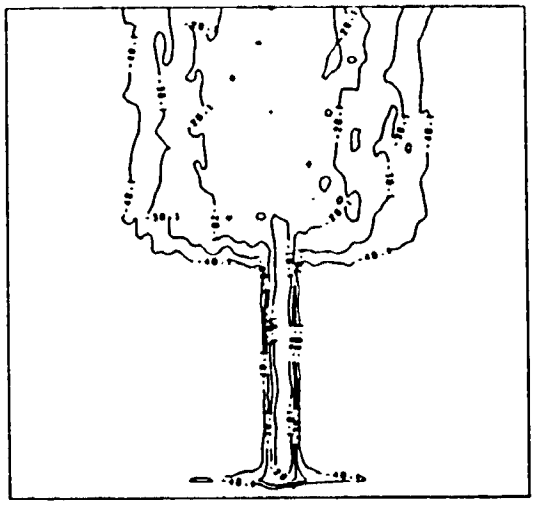

(c)

Figure 4-16) Spectrogram/Contour Maps for Experiment 1

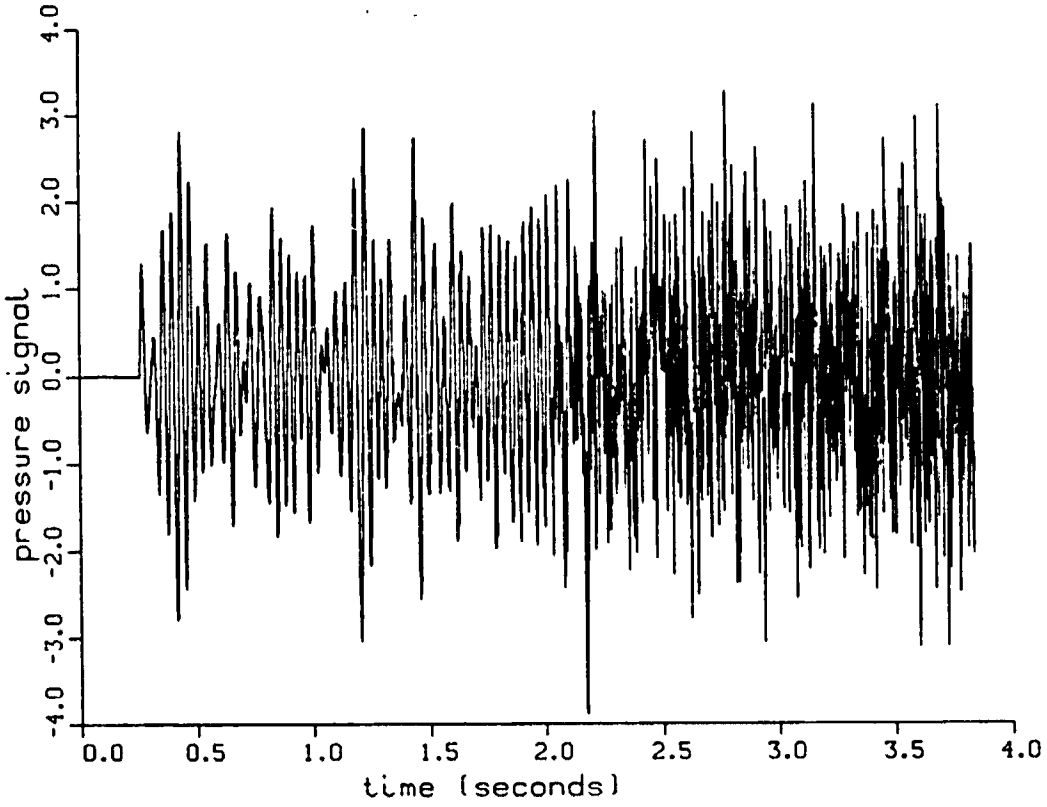

Figure 4-17) Time Series for Experiment 1

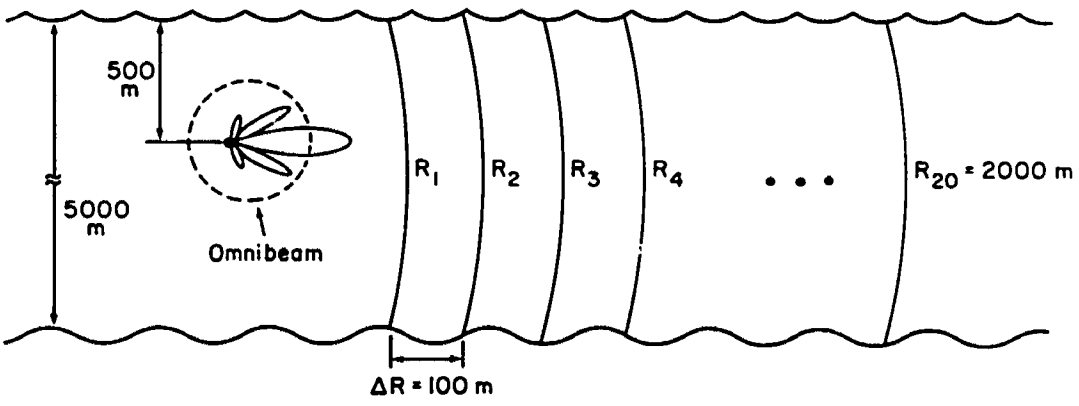

Figure 4-18) Geometry of Experiment 2

simulation method handles multiple beams with radically different spectra and that the simulation correctly models the so-called reverberation ridge phenomenom.

The reverberation ridge phenomenom is the phenomenom wherein the centroid of the reverberation power spectrum changes with range. The centroid of the spectrum is determined by the average doppler shift induced by sonar platform motion. The average doppler shift in turn depends on the average angle between the sonar platform velocity vector $\vec{V}$ and the vector $\vec{R}(t)$ connecting the sonar transducer face to the surface scattering elements at time t. In the present example we see that as time increases the angle between these vectors decreases. This leads to an increasing average doppler shift with time.

In this example the volume scattering strength is small vis-a-vis the surface scattering strength so that the centroid of the spectrum depends essentially only upon the surface after 500. meters. In addition the random

Parameter	*Value*	*Units*
Reverberation types	(surface,volume)	
Pulse	Pure Tone Long	
Beampatterns	(omni,narrow)	
Bottom depth	5000.	meters
Sonar depth	500.	meters
Sonar bandwidth	1000.	hertz
Carrier frequency	20000.	hertz
Sound speed	1500.	meters/second
Sonar speed	10.0	meters/second
Surface random scatter deviation	0.1	meters/second
Volume random scatter deviation	0.1	meters/second
Maximum range	2000.	meters
Range sampling increment	100.	meters

Table 4-3) Parameters for Experiment 2

scatterer spectrum standard deviation is small so that the spectral centroid change with range will be more easily discerned from the spectrogram plots.

In figure 4-19 we show spectrogram plots for both the narrow and omni beams of this example. The spectra of the two beams are radically different in shape yet are generated by a single bivariate AR filter driven with two independent channels of white noise.

The change of spectral centroid, although present in both beams, is most easily seen in the narrow beam smoothed spectrogram and associated contour plot. Early in the ping(<500. meters) only volume reverberation is present. Because the beampattern is narrow and facing in the forward direction the sonar platform induced doppler shifts are large. Thus the volume dominated spectrum early in the ping has centroid shifted to the right (positive doppler) in direct proportion to the sonar speed.

Next at 500 meters the surface is ensonified and becomes the dominant scattering source. Because of the high elevation angle to the surface scatterers at this point the doppler shifts are near zero. This centroid shift is apparent between the 8^{th} and 9^{th} periodogram slice of the spectrogram and in the contour plot. As the range(time) increases the surface remains the dominant scattering source but the elevation angle decreases causing the spectra to shift towards higher doppler frequencies. This tendency is also apparent in figure 4-19.

In figure 4-20 we present the time series for the two beams of this example. The wider bandwidth of the omni beam time series(4-20a) relative to that of the narrow beam time series(4-20b) is evident in the plots.

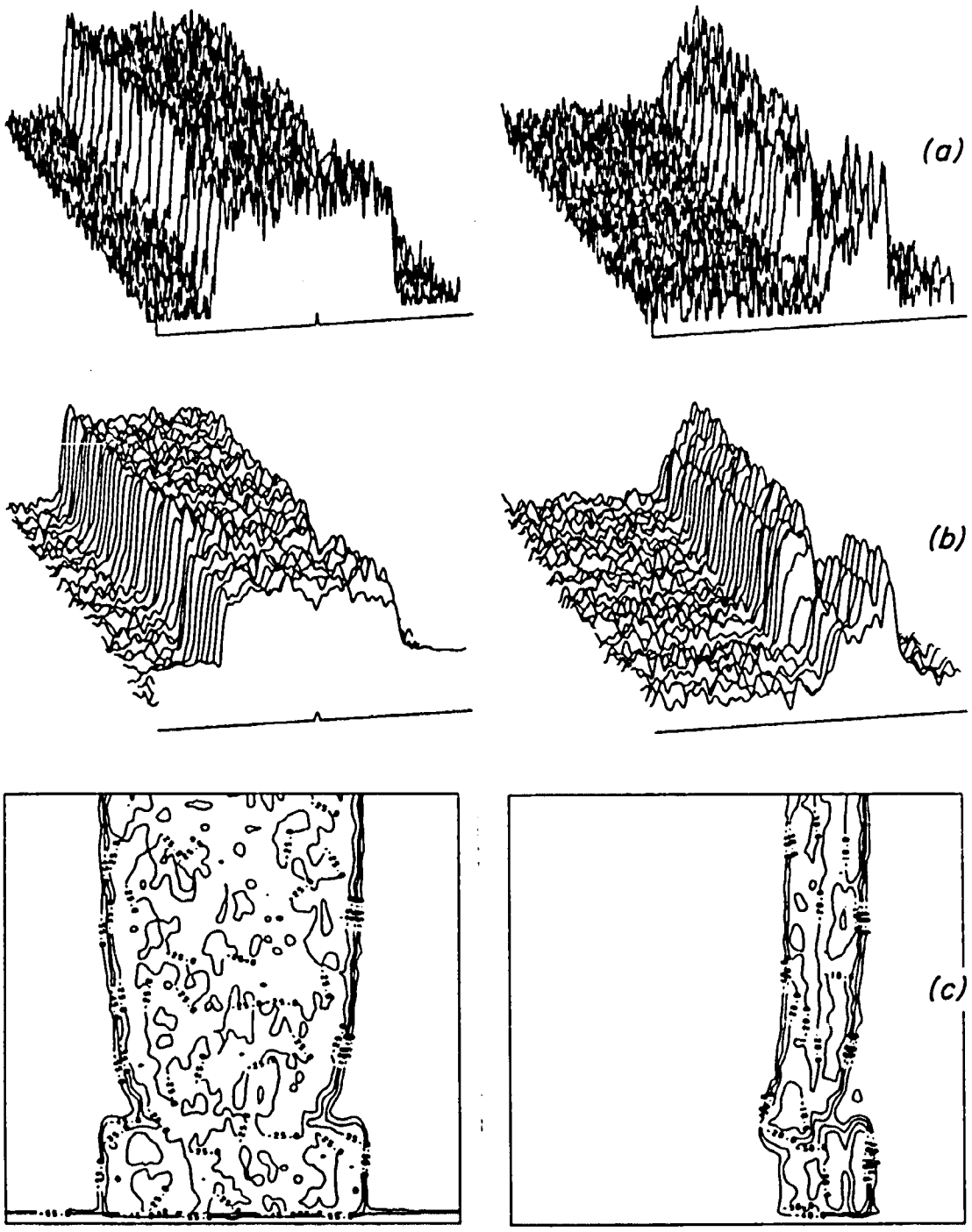

Figure 4-19) Spectrogram/Contour Maps for Experiment 2

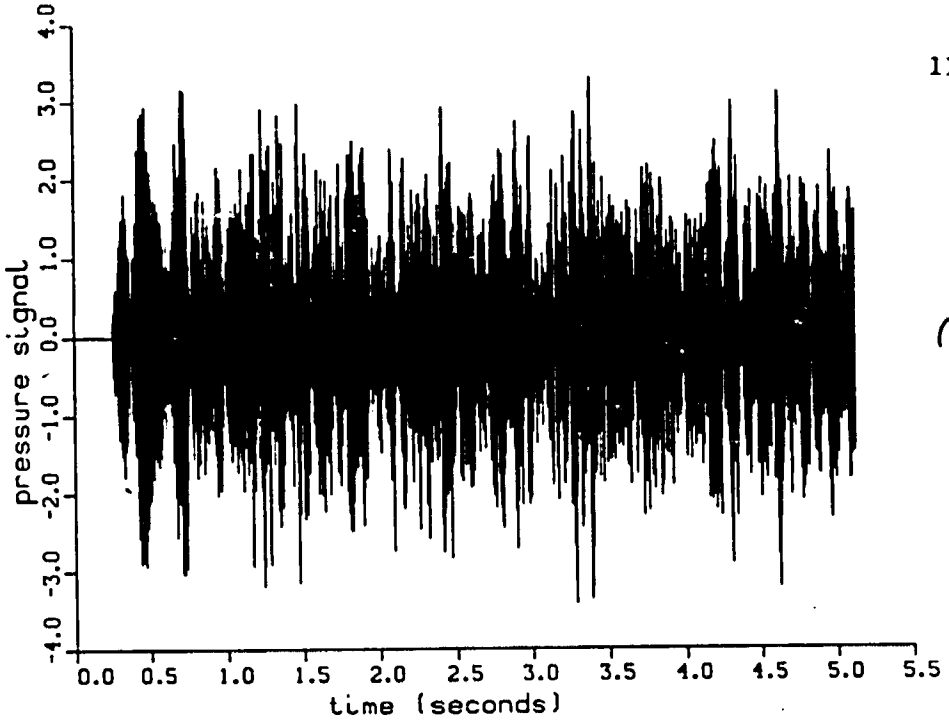

(a)

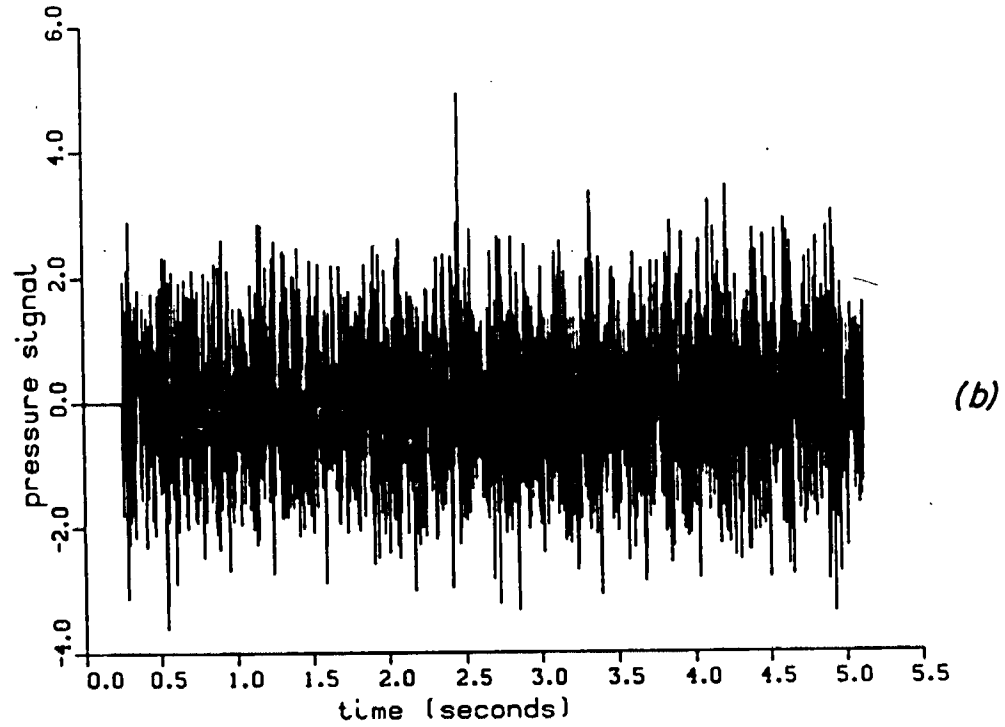

(b)

Figure 4-20) Time Series for Experiment 2

The geometry of the third experiment is shown in figure 4-21 and the parameters are listed in Table 4-4. Two beams with indentical beampatterns (i.e., that of the narrow beam) are vertically offset by half a wavelength. The intent of this experiment is to show that for surface reverberation the simulated signals for each beam are highly correlated and have an average phase difference proportional to the elevation angle θ at a given time(range). We use only surface reverberation in this example because it is a spatially localized source of radiation which leads to high beam to beam correlation and a well defined phase angle between beams.

In figure 4-22 we show spectrogram plots for only one of the two beams since the two beams have identical beampatterns and hence identical spectrogram plots. In figure 4-23a we show a plot of the instantaneous electrical phase difference between beams for this simulated ping. In figures 4-23b and 4-23c we show estimates of the average phase difference and correlation coefficient between beams. As expected the correlation coefficient magni-

Parameter	*Value*	*Units*
Reverberation types	(surface)	
Pulse	Pure Tone Long	
Beampatterns	(narrow,narrow)	
Bottom depth	5000.	meters
Sonar depth	1000.	meters
Sonar bandwidth	1000.	hertz
Carrier frequency	20000.	hertz
Sound speed	1500.	meters/second
Sonar speed	5.0	meters/second
Surface random scatter deviation	0.1	meters/second
Maximum range	2000.	meters
Range sampling increment	100.	meters

Table 4-4) Parameters for Experiment 3

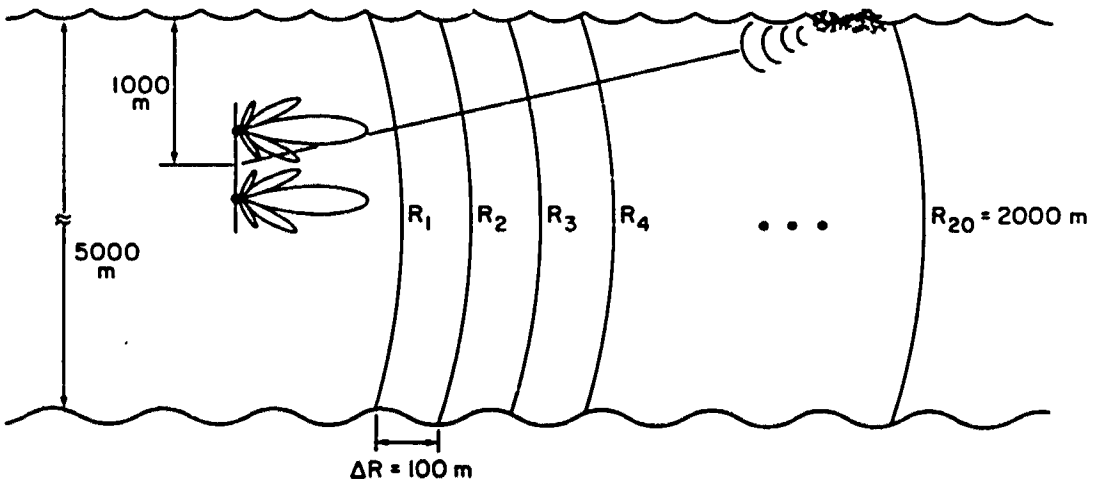

Figure 4-21) Geometry of Experiment 3

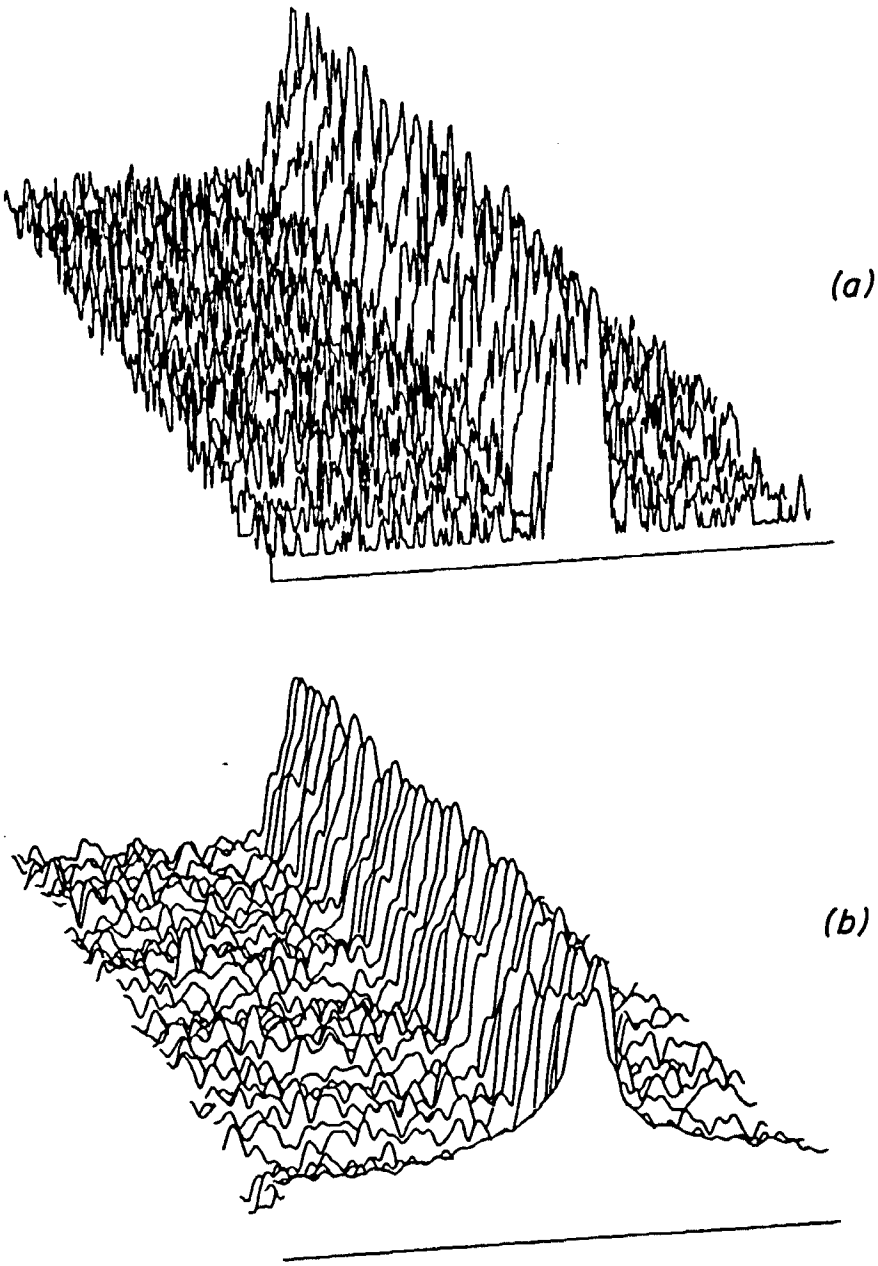

Figure 4-22) Spectrogram for Experiment 3

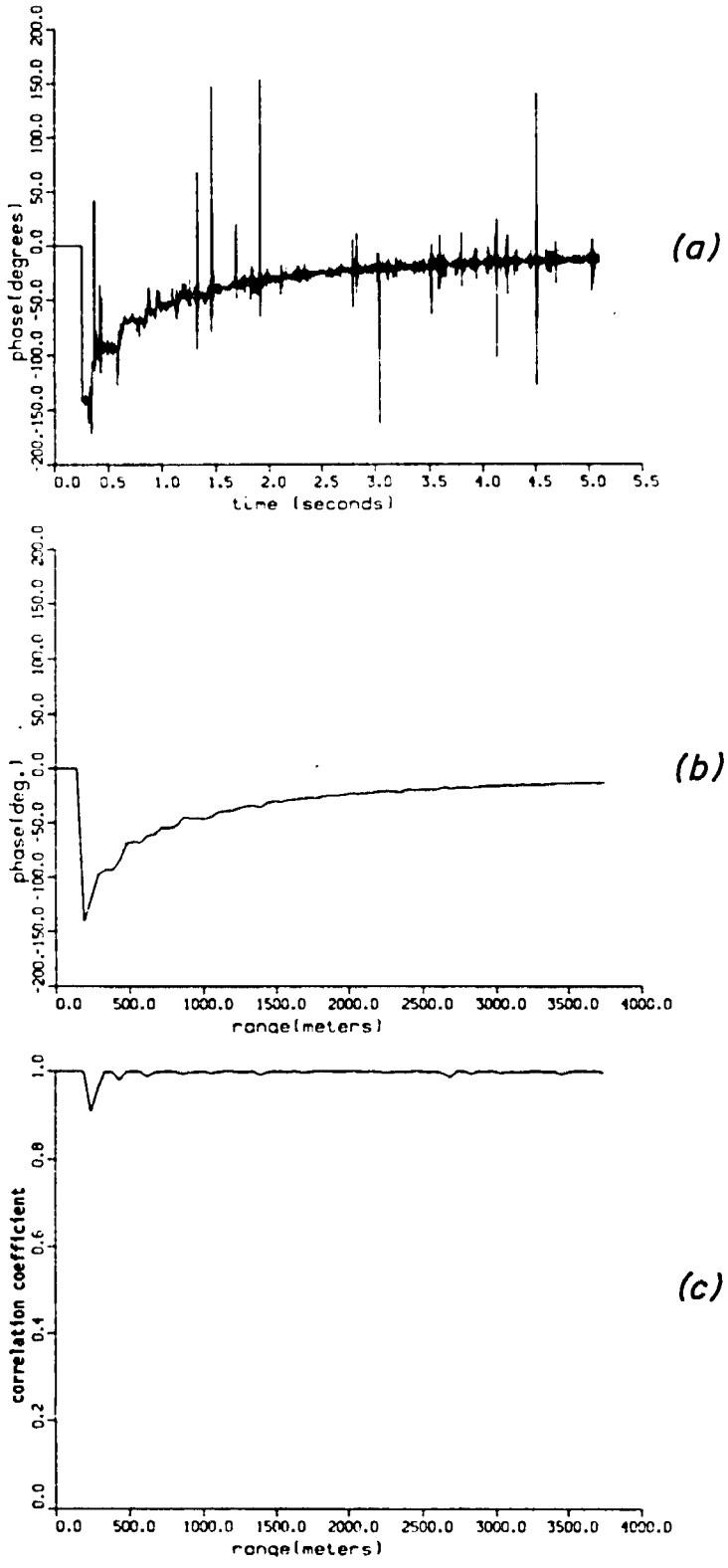

Figure 4-23) Phase and Correlation Coefficient for Experiment 3

tude remains close to 1.0 throughout the ping and the electrical phase in consistent with the time varying elevation angle and the offset phase center spacing of the beams.

Finally in figure 4-24 we show the time series realizations for each beam. Note the high degree of similarity of the two waveforms. This is expected in light of the high correlation between beams.

The final two experiments use the same geometry and parameters as the third experiment(i.e., figure 4-21 and Table 4-4) except in each case only one narrow beam is used and different transmit pulses are used. The intent of the fourth experiment is simply to show typical spectrogram and time series plots for a LFM pulse. The spectrogram plots are shown in figure 4-25 and the time series is shown in figure 4-26.

The fifth and last experiment is identical to the fourth except that a PTS transmit pulse is used. Typical spectrogram and time series plots for this case are shown in figures 4-27 and 4-28.

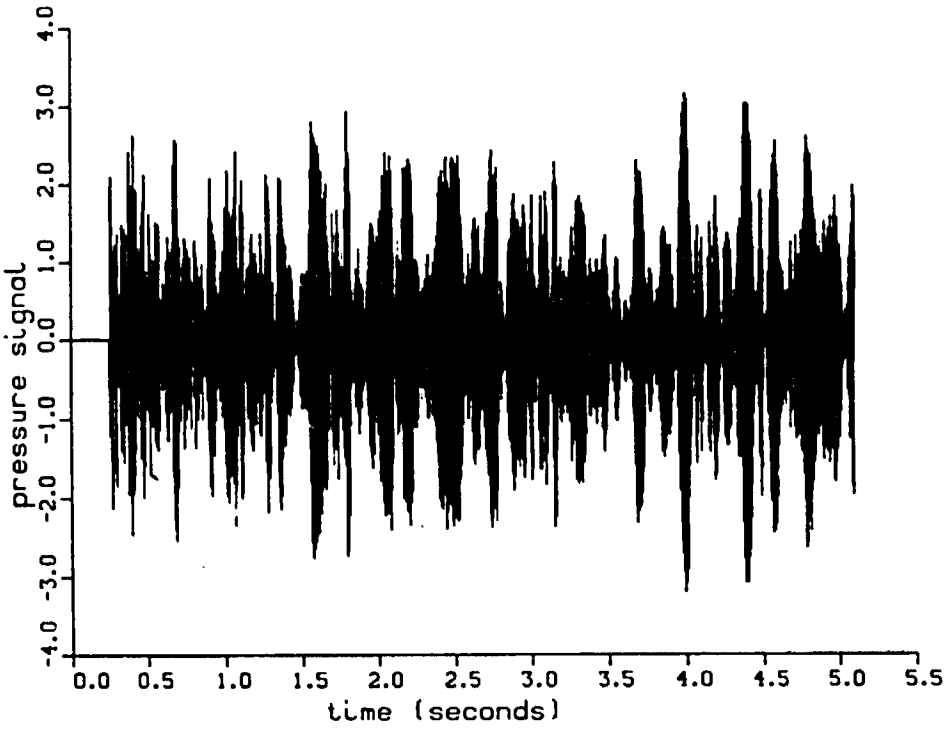

(a)

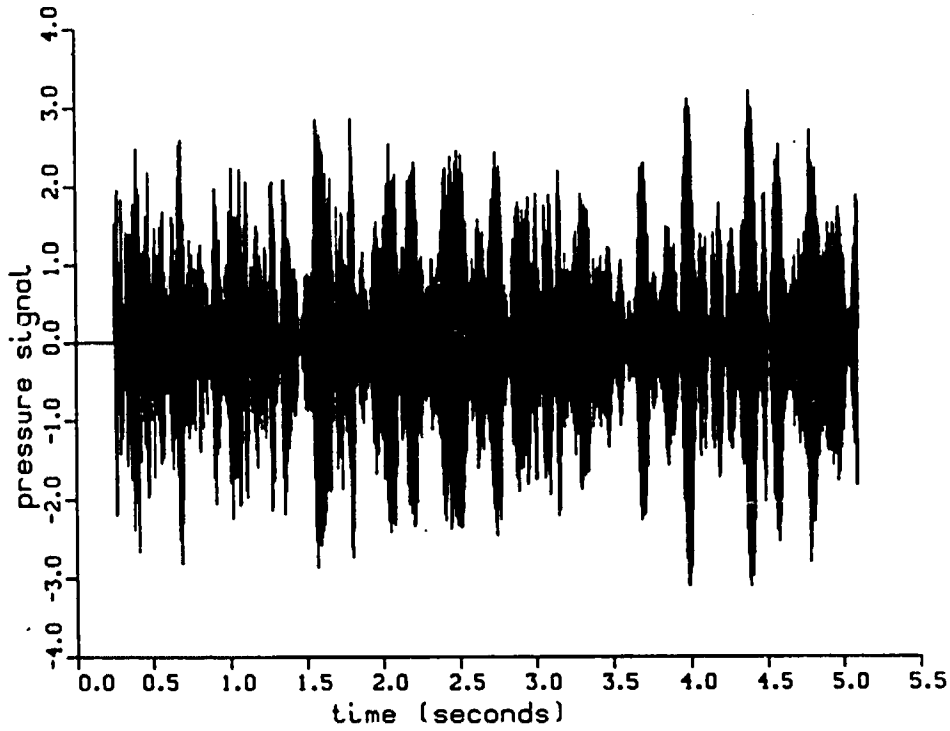

(b)

Figure 4-24) Time Series for Experiment 3

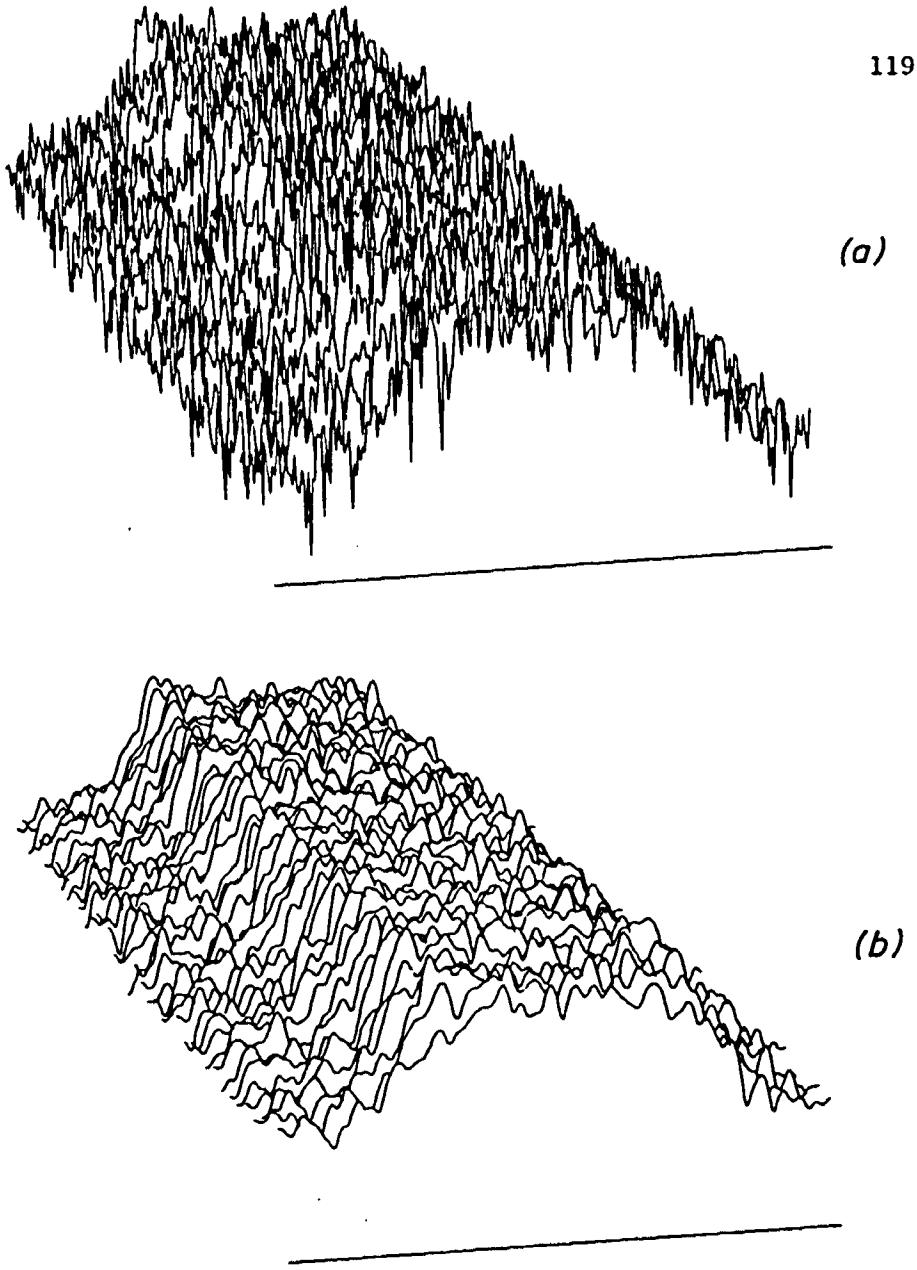

Figure 4-25) Spectrogram for Experiment 4.

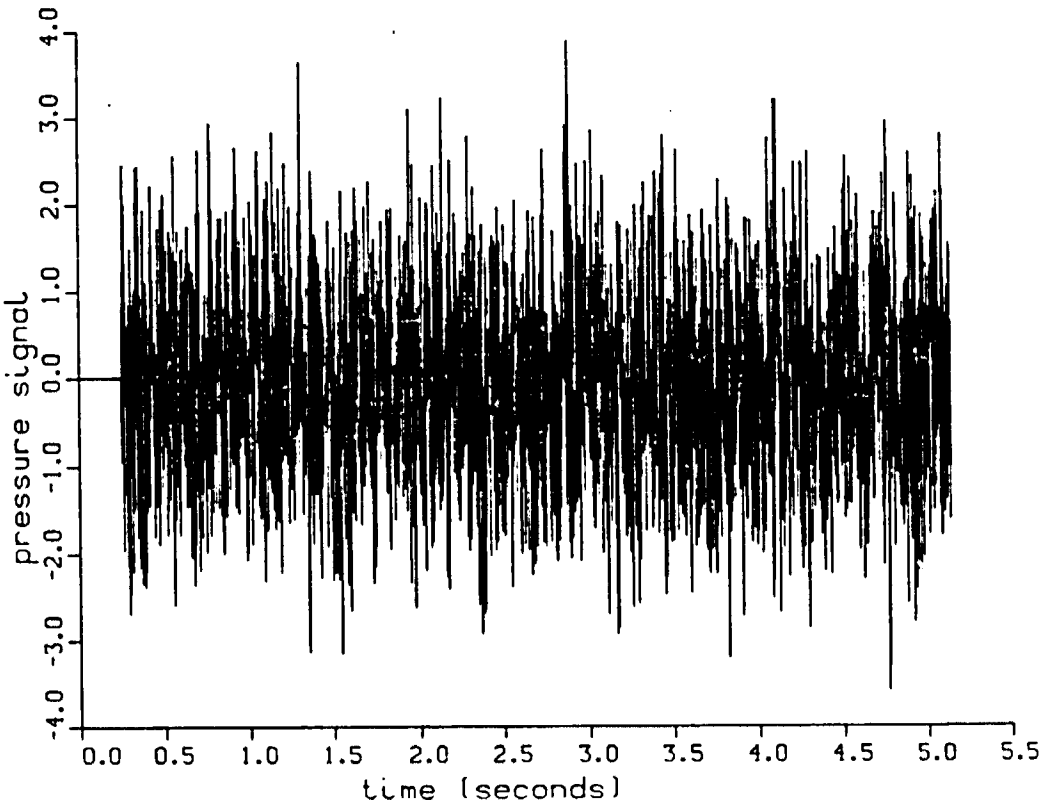

Figure 4-26) Time Series for Experiment 4

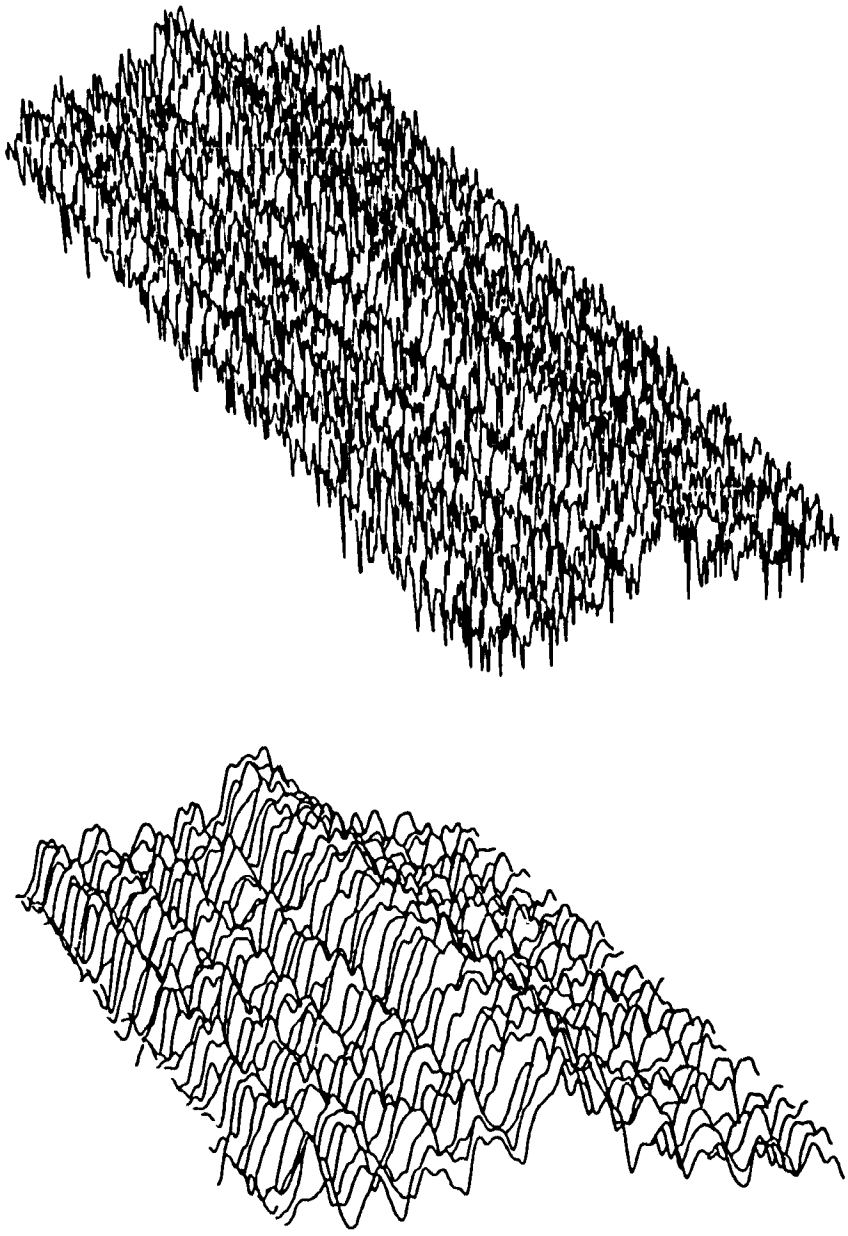

Figure 4-27) Spectrogram for Experiment 5

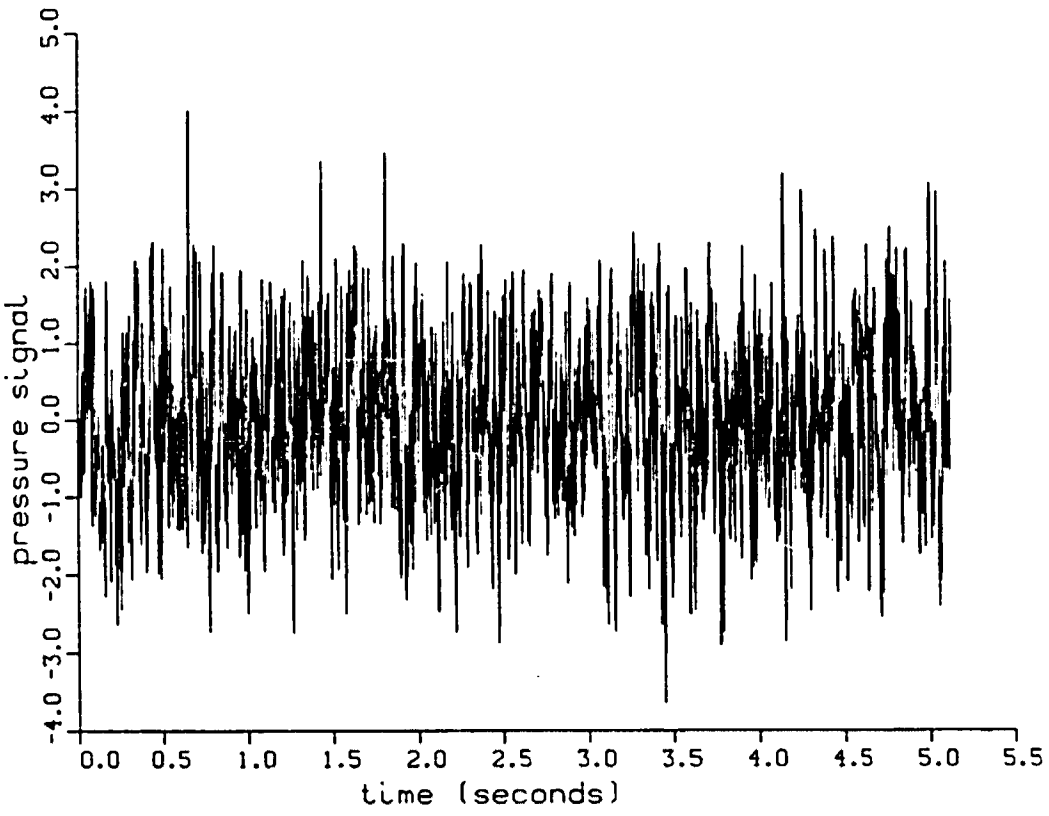

Figure 4-28) Time Series for Experiment 5

CHAPTER 5

Conclusions and Future Work Recommendations

5.1. Introduction to Chapter 5

In this dissertation we have developed a methodology for simulating nonstationary, Gaussian, multiple beam reverberation sequences. A continuous first order scattering model is used to relate the reverberation power spectrum to the geometrical, environmental and sonar parameters. Given the power spectrum for each of a set of ranges we generate stationary realizations with the desired power spectra for each range and then combine them together with a windowing scheme. The result is simulated reverberation which has time varying spectrum and intensity.

5.2. Conclusions

The methods developed in this dissertation have been programmed in FORTRAN on a VAX 11/750 computer. Tests were performed to verify the simulation. These tests included checking that the intensity and power spectra correctly reflected the pertinent sonar, environmental and geometrical factors, checking that AR and Cholesky methods generated stationary realizations with the correct power spectrum, and checking that the windowing scheme used to combine stationary realizations did realize a nonstationary time series with smoothly changing spectral shape and without undue spectral distortion.

The results of this testing process indicate that the simulation methodology yields reverberation realizations which are of high enough fidelity that they can be profitably employed in the testing of sonar systems. Furthermore, because we have employed a continuous scattering model we do not suffer from the problem associated with point scatterer model simulations where each time we employ a higher resolution transmit pulse we must concommitantly increase the number of point scatterers to prevent a sonar signal processor under test from resolving the individual scatterers. Thus we have in effect eliminated the dependence of computation time on transmit pulse resolution.

Finally, we note that the techniques developed here are applicable to mass production of simulated reverberation. Once the reverberation power spectrum is found for each of a set of ranges we may then generate as many realizations as desired provided of course that we may generate the requisite number of independent random variables. Either the AR or Cholesky method may used, both of which work and both of which are amenable to array processor implementation.

Of the two methods we tend to prefer the AR method because it provides a more parsimonious factorization of the power spectrum. Also, although we did not make extensive timing tests, the two methods seem to have comparable execution speeds.

5.3. Future Work

We envision two areas of interest for future work. The first area is propagation model enhancement. For instance, in our work we have assumed staight line propagation of sound waves. In reality temperature gradients in the ocean cause sound wave refraction and consequent curved propagation paths. By incorporating ray tracing[Urick] into the computation of power spectra one can obtain more accurate estimates of the power levels and spectra.

The second area for potential future work involves the application of innovations state variable models(i.e., minimal Markovian models) to the covariance factorization problem. [Akaike(1974), Rissanen and Kailath] These models provide a time varying factorization of the covariance function and hence are applicable to nonstationary processes. However it is not clear how to compute the covariance function for all possible times and whether these models are computationally affordable.

Bibliography

Akaike H., "Autoregressive Model Fitting for Control," Annals Inst. Statist. Math., 23,pp.163-180, 1970

Akaike H., "Stochastic Theory of Minimal Realization," IEEE Trans. on Automatic Control, Vol. AC-19, December 1974

Anderson B. D. O. and Moore J. B., *Optimal Filtering* ,Prentice-Hall, Englewood Cliffs, New Jersey, 1979

Baggeroer, A. B., "Sonar Sigal Processing," appearing in *Applications of Digital Signal Processing* (edited by Oppenheim A. V.), Prentice-Hall Inc., Englewood Cliffs, New Jersey, 1978

Bello P. A., "Characterization of Randomly Time-Variant Channels," IEEE Trans. on Communications Systems, December 1963

Bloomfield P., *Fourier Analysis of Time Series: An Introduction* , John Wiley, New York, 1976

Bower D. E., Rajasekaran P. K., and Gebhart W. W., "Adaptive Clutter Filtering Using Autoregressive Spectral Estimation,", IEEE Trans. on Aerospace and Electronic Systems, vol. AES-15, No. 4, July 1979

Burdic W. S., *Underwater Acoustic System Analysis* , Prentice-Hall, Inc., Englewood Cliffs, NJ, 1984

Chamberlain S. G. and Galli J. C., "A Model for Numerical Simulation of Nonstationary Sonar Reverberation Using Linear Spectral Prediction," IEEE J. Oceanic Engineering, OE-8, pp. 21-36, 1983

Cook C. E. and Bernfeld M., *Radar Signals* , Academic Press, New York, 1967

Dongarra J. J., et. al., *LINPACK Users Manual* , Argonne National Laboratory, August 1977

Faure P., "Theoretical Model of Reverberation Noise," J. Acoustical Society of America, Vol. 36, 1964, pp. 259-268

Faurre P. L., "Representation of Stochastic Processes," Doctoral Dissertation, Stanford University, 1967

Gantmacher F. R., *Theory of Matrices* , vols. 1-2, Chelsea, New York, 1959

Golub G. H. and Van Loan C. F., *Matrix Computations* ,The John Hopkins University Press, Baltimore, 1983

Grace O. D. and Pitt S. P.,"Sampling and Interpolation of Bandlimited Signals by Quadrature Methods," The Journal of the Acoustical Society of America, Volume 48, No. 6(Part 1), 1970

Hannan E. J., *Multiple Time Series* , John Wiley and Sons,Inc., New York 1970

Harris F. J., "On the Use of Windows for Harmonic Analysis with the Discrete Fourier Transform," Proc. of IEEE, Vol. 66, No. 1 , January 1978

Haykin S. and Kesler S., "Prediction-Error Filtering and Maximum-Entropy Spectral Analysis,"
appearing in *Nonlinear Methods of Spectral Analysis* (edited by Haykin S.) , Springer-Verlag, Berlin, 1979

Inouye Y., "Modeling of Multichannel Time Series and Extrapolation of Matrix-Valued Autocorrelation Sequences," IEEE Trans. on Acoustics, Speech and Signal Processing, Vol. ASSP-31, NO. 1, February 1983

Ioannidis G. A., "Application of multivariate autoregressive spectrum estimation to ULF waves," Radio Science, Volume 10, Number 12, pp. 1043-1054, December 1975

Kay S. M. and Marple S. L., "Spectrum Analsis-A Modern Perspective," Proceedings of the IEEE, Volume 69, No. 11, November 1981

Kennedy R. S. and Lebow I. L.,"Signal design for dispersive channels," IEEE Spectrum, March 1964

Knight W. C., Pridham R. G. and Kay S. M., "Digital Signal Processing for Sonar," Proceedings of the IEEE, Volume 69, No. 11, November 1981

Koopmans L. H., *The Spectral Analysis of Time Series* , Academic Press, New York, 1974

Lacy C. E., "Power Spectral Density of Boundary Reverberation," University of Washington Applied Physics Laboratory Internal Memorandum, December, 1983

Lawson C. L. and Hanson R. J., *Solving Least Squares Problems* , Prentice-Hall, Englewood Cliffs, New Jersey, 1974

Luenberger D. G., *Optimization by Vector Space Methods* , John Wiley and Sons,Inc., New York, 1969

Middleton D., *An Introduction to Statistical Communications Theory* , McGraw-Hill, New York, 1960

Middleton D., "A Statistical Theory of Reverberation and Similar First-Order Scattered Fields(parts I and II)," IEEE Trans. on Information Theory, Vol. IT-13, No. 3, July 1967

Middleton D., "A Statistical Theory of Reverberation and Similar First-Order Scattered Fields(parts III and IV)," IEEE Trans. on Information Theory, Vol. IT-18, No. 1, January 1972

Mitchell R. L. and McPherson D. A., "Generating Nonstationary Random Sequences," IEEE Trans. on Aerospace and Electronic Systems, Vol. AES-17, July 1981

Moose P., "On Detection of Signals in Reverberation," University of Washington Doctoral Dissertation, 1970

Ol'shevskii V. V., *Characteristics of Sea Reverberation* , Consultants Bureau, New York, 1967

Oppenheim A. V. and Schafer R. W., *Digital Signal Processing* , Prenctice Hall, New Jersey, 1975

Papoulis A., *Probability, Random Variables, and Stochastic Processes* , McGraw Hill, New York, 1965

Papoulis A., *Signal Analysis* , McGraw Hill, New York, 1977

Parzen E., *Stochastic Processes* , Holden-Day, San Fransico, 1962

Priestley M. B., *Spectral Analysis and Time Series* , Academic Press, London(1981)

Princehouse D. W., "REVGEN, A Real-Time Reverberation Generator," Applied Physics Laboratory, University of Washington, APL-UW 7511, September 1975

Princehouse D. W., "Reverberation Generator Ocean Algorithm, A Status Report," Applied Physics Laboratory, University of Washington, APL-UW 7806, February 1978

Rice S. O., "Mathematical Analysis of Random Noise," Bell System Technical Journal, July 1944, pp.282-332

Rissanen J. and Kailath T., "Partial Realization of Random Systems," Automatica, Vol. 8, pp. 389-396, 1972

Strand O. N., "Multichannel Complex Maximum Entropy(Autoregressive) Spectral Analysis," IEEE Trans. on Automatic Control, Vol. AC-22, No. 4, August 1977

Thompson, R. O. R. Y., Utilitas Mathematica, Vol. 3, 1973, pp. 127-137

Treitel S., "Principles of Digital Multichannel Filtering," Geophysics, Vol. 35, No. 5, October 1970

Tretter S. A., *Introduction to Discrete Time Signal Processing* , John Wiley and Sons Inc., 1976

Urick R. J., *Principles of Underwater Sound* , McGraw-Hill, New York, 1975

Van Trees H. L., "Optimum Signal Design and Processing for Reverberation-Limited Environments," IEEE Transactions on Military Electronics, July-October, 1965.

Van Trees H. L., *Detection, Estimation, and Modulation Theory(Part III)* , Wiley, New York, 1971

Whittle P., "On the fitting of multivariate autoregressions, and the approximate canonical factorization of a spectral density matrix," Biometrika, 50, pp. 129-134, 1963

Wiener N. and Massani P., "The Prediction Theory of Multivariate Stochastic Processes,Part I," Acta Math., 98, pp. 111-150, 1957

Wiener N. and Massani P., "The Prediction Theory of Multivariate Stochastic Processes,Part II," Acta Math., 99, pp. 93-139, 1958

Wiggins R. A. and Robinson E. A., "Recursive Solution to the Multichannel Filtering Problem," J. of Geophysical Research, Vol. 70, No. 8, April 15, 1965

Wozencraft J. M. and Jacobs I. M., *Principles of Communication Engineering* , John Wiley, 1965

Ziomek L., "Formulating Scattering Functions for Underwater Acoustic Detection," Technical Memorandum 79-218, Applied Research Laboratory, Pennsylvania State University, December, 1979

Appendix A: Stationary Bandpass Random Processes

In this appendix we summarize basic results[Van Trees] regarding the complex envelope representation of zero-mean, stationary real bandpass random processes. A bandpass random process has a spectrum which is bandlimited to a region $\pm\frac{BW}{2}$ radians per second centered about a carrier frequency ω_c.

A bandpass random process $x(t)$ may be expressed as

$$x(t) = a(t)cos(\omega_c t) + b(t)sin(\omega_c t) \tag{A.1}$$

We define the complex envelope process $\tilde{x}(t)$ as

$$\tilde{x}(t) = a(t) - j\ b(t) \tag{A.2}$$

Then $x(t)$ may be expressed as

$$x(t) = Re[\tilde{x}(t)e^{j\omega_c t}] \tag{A.3}$$

We are interested in relating statistical properties of $x(t)$ and $\tilde{x}(t)$. The covariance of $\tilde{x}(t)$ is given as

$$K_{\tilde{x}}(\tau) = <\tilde{x}(t)\tilde{x}^*(t-\tau)>$$

$$= \frac{1}{2\pi}\int_{\frac{-BW}{2}}^{\frac{BW}{2}} 2S_x(\omega+\omega_c)e^{j\omega\tau}d\omega \tag{A.4}$$

where $S_x(\omega)$ is the power spectrum of $x(t)$. In figure A-1a we show a typical bandpass process power spectrum $S_x(\omega)$. Note that the covariance $K_{\tilde{x}}(\tau)$ is dependent only upon the positive frequency components of $S_x(\omega)$. Equation A.4 implies that the power spectrum $S_{\tilde{x}}(\omega)$ of $\tilde{x}(t)$ is just the positive part of

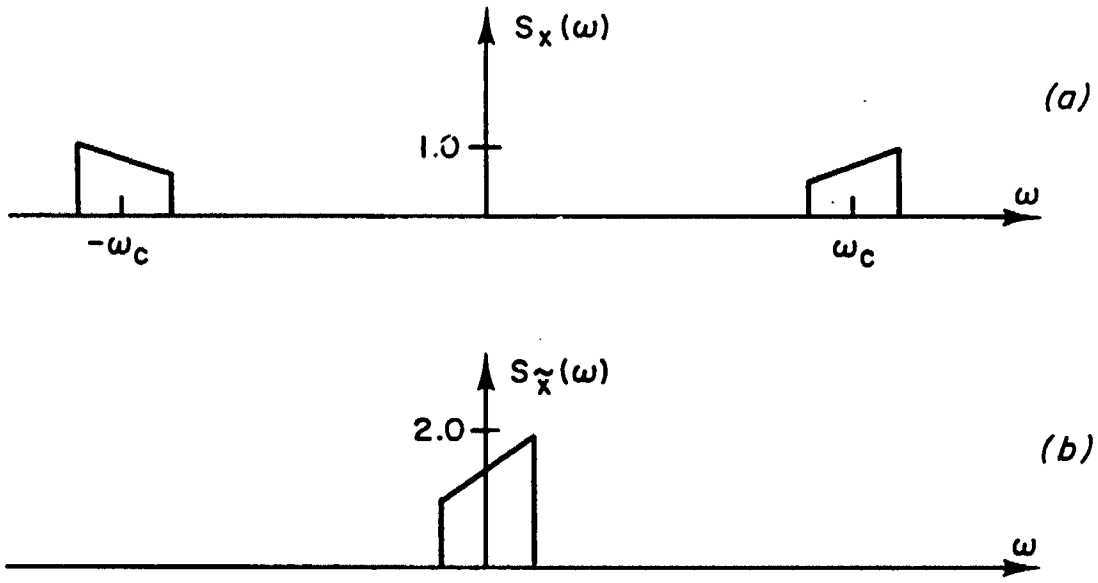

Figure A-1) Typical Bandpass Random Process Spectra

$S_x(\omega)$ multiplied by two and shifted to the origin. In figure A-1b we show the power spectrum corresponding to the complex envelope signal $\tilde{x}(t)$.

The covariance of $x(t)$ is related to that of $\tilde{x}(t)$ by

$$K_x(\tau) = Re[\, K_{\tilde{x}}(\tau) e^{j\omega_c \tau} \,] \tag{A.5}$$

The spectrum of $x(t)$ may be obtained from that of $\tilde{x}(t)$ by

$$S_x(\omega) = \frac{S_{\tilde{x}}(\omega-\omega_c) - S_{\tilde{x}}(\omega-\omega_c)}{2} \tag{A.6}$$

The covariance functions of the quadrature components $a(t)$ and $b(t)$ are related to the covariance of $\tilde{x}(t)$ as

$$K_a(\tau) = K_b(\tau) = (1/2) Re[\, K_{\tilde{x}}(\tau) \,] \tag{A.7}$$

$$K_{ba}(\tau) = -K_{ab}(\tau) = -K_{ba}(-\tau) = (1/2)\, Im[\, K_{\tilde{x}}(\tau) \,] \tag{A.8}$$

Setting τ equal to zero in A.8 yields

$$K_{ba}(0) = -K_{ab}(0) \tag{A.9}$$

which implies that $K_{ab}(0)$ is zero and hence that the quadrature components are uncorrelated at any given time instant.

VITA

James Craig Luby was born on June 10, 1953 in Hartford, Connecticut. After graduating from Windsor High School in Windsor, Connecticut in 1971 he entered the University of Connecticut where he received the B.S.S.E. in 1976. A M.S.E.E. degree was then obtained from Colorado State University in Ft. Collins, Colorado in 1978. Following completion of the M.S.E.E. degree he moved to Seattle, Washington to work for the Boeing Aerospace Company. In 1979 he accepted employment with the Applied Physics Laboratory, University of Washington, Seattle, Washington where he is currently employed.